AN EXPERIMENTAL FACILITY TO MEASURE FOULING RESISTANCE IN CONDENSERS

By

ANNAMALAI RAMESH

Bachelor of Engineering in Mechanical Engineering

ANNA UNIVERSITY

CHENNAI, TAMIL NADU, INDIA

2007

Submitted to the Faculty of the
Graduate College of the
Oklahoma State University
in partial fulfillment of
the requirements for
the Degree of
MASTER OF SCIENCE
May 2010

AN EXPERIMENTAL FACILITY TO MEASURE FOULING RESISTANCE IN CONDENSERS

Thesis Approved:

Dr. Lorenzo Cremaschi

Thesis Adviser

Dr.Jeffery Spitler

Dr. Jeremy Morton

Dr. Mark E. Payton

Dean of the Graduate College

ACKNOWLEDGMENTS

First and foremost I would like to thank my parents who are the two most important people in my life. Without their love and support none of this would have been possible and I owe it all to them and one paragraph in this section is not enough to acknowledge all that they have done for me.

I would like to thank Dr.Cremaschi for giving me the opportunity to be a part of this project, from building and running an experimental facility to writing a thesis I have learnt a lot in the two years that I worked for him. I would like to thank Dr.Spitler who was also a part of this project, I have learnt a lot by taking the courses taught by him. Finally I would like to thank Dr.Morton for being a part of my thesis committee.

Regarding this project I would like to thank Elissa Lim who worked with me during the duration of my Masters and Ozgur Aslan who designed the DAQ system.

One of the main reasons for me being able to do Masters Degree at Oklahoma State University was the excellent education I received during my Bachelors degree at Hindustan College of Engineering. I would like to thank Proferssor Ravikumr Solomon who introduced me to the field of thermal sciences and not only served as my advisor during the course of my Bachelor's degree but also as my mentor, I owe a lot to him. I would also like to thank Professor Jeyapoovan who was the Department chair during my time in Hindustan College of Engineering.

TABLE OF CONTENTS

Chapter Page

LIST OF TABLES

LIST OF FIGURES

Figure Page

CHAPTER I

INTRODUCTION

Heat exchangers are employed to transfer thermal energy between two fluids and the two fluids may or may not come in contact with each other. Some common applications of heat exchangers are heating and cooling of milk in the dairy industry, as condensers and evaporators in the refrigeration and power industries, as economizers in boilers in the power industry. The best example of a heat exchanger used in common practice would be the radiator of a car. Different types of heat exchangers available are tubular, plate and extended surface. The plate heat exchanger consists of a collection of flat thin plates sandwiched together through which the fluids pass through without making contact with each other. This thesis deals in depth with plate heat exchangers and two common kinds of plate heat exchangers available are the gasket plate heat exchangers and brazed plate heat exchangers. Enhanced heat transfer surfaces used in these types of heat exchangers provide higher heat transfer coefficients than conventional plain tubes.

1. Gasket plate heat exchangers

These heat exchangers consist of a number of thin flat plates sandwiched together. The plates are arranged in such a way the two fluids never come into contact with each other. The plates are bolted together at the ends with gaskets in between preventing leakage of fluid to the outside and preventing the two fluids from coming in contact with each other.

The plates have corrugations on them which help enhance the heat transfer. They are extremely compact and have a high heat transfer rate per unit volume of the heat exchanger. The limit of these heat exchangers is that they cannot operate at high temperatures and pressures as the gaskets may break.

Figure 1-1. Brazed plate heat exchanger

2. **Brazed plate heat exchangers**

These are similar to gasket plate heat exchangers except that there are no gaskets between the plates but the plates are brazed to each other. This allows operation at high temperatures and pressures. The disadvantage of these over gasket plate heat exchangers is that they cannot be dismantled and reassembled so cleaning or changing the number of plates is not possible. Figure 1-1 shows a brazed plate heat exchanger.

1.1 Working of plate heat exchangers

As mentioned in the previous section plate heat exchangers consist of a number of plates sandwiched together between which the two fluids pass through. Figure 1-2 (a) shows an actual picture of an individual plate, the plate is usually made of stainless steel and has corrugations or grooves on it to promote turbulence which enhances the heat transfer.

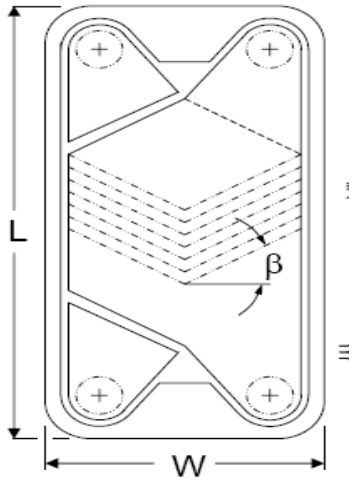

Figure 1-2. Individual Plate

Figure 1-2 shows the schematic of an individual plate, the angle between the grooves (is called the chevron angle, measured from the flow direction (chevron angle = 90- β), and the ratio of length to width of the heat exchanger (L/W) is termed as the aspect ratio.

In a plate heat exchanger one fluid enters at the top and exits at the bottom while the other enters at the bottom and exits at the top. There are holes on the top and bottom ends of the plates which form a passage for the fluids to flow through them. The hot fluid flows in between every other channel created by two plates from the top to the bottom while the cold fluid is circulated in the alternate channel and in the opposite direction. Gaskets on each plate determine which fluid is allowed to flow in the channel.

The advantages of using brazed plate heat exchangers when compared to other types of heat exchangers are a greater thermal efficiency, higher overall heat transfer coefficient, more suitable for high temperatures and pressures. Brazed plate heat exchangers are also able to achieve smaller approach temperatures with respect to the gasket type (Ayub [2003]). The corrugations on the plates create significant turbulence and mixing that further increases the heat transfer. The more even distribution of flow across these types of heat exchangers enables the entire area of the heat exchanger to be used for effective heat transfer.

1.2 Cooling towers

Cooling towers are basically heat rejection devices used to remove process heat by rejecting it to the atmosphere. This is achieved by evaporation of the circulating water or by using air to cool the circulating water or both. They are commonly used in power plants, oil refineries and buildings. Based on the cooling capacity required the size of the cooling tower varies. Figure 1-3 shows a 5 ton capacity evaporative cooling tower used for research purpose at the hybrid ground source heat pump laboratory at Oklahoma State University.

A typical schematic of a cooling tower installed in an evaporative cooling system is shown in Figure 1-4. The actual system is quite complex but the main components of the system are heat exchanger, cooling tower, and circulating pump along with a makeup water source. A make-up water source is needed because around 10% of water passing through the spray nozzles in the cooling tower evaporates and mixes with the air stream that is discharged to the environment.

Figure 1-3. Cooling Tower [Gentry, 2007]

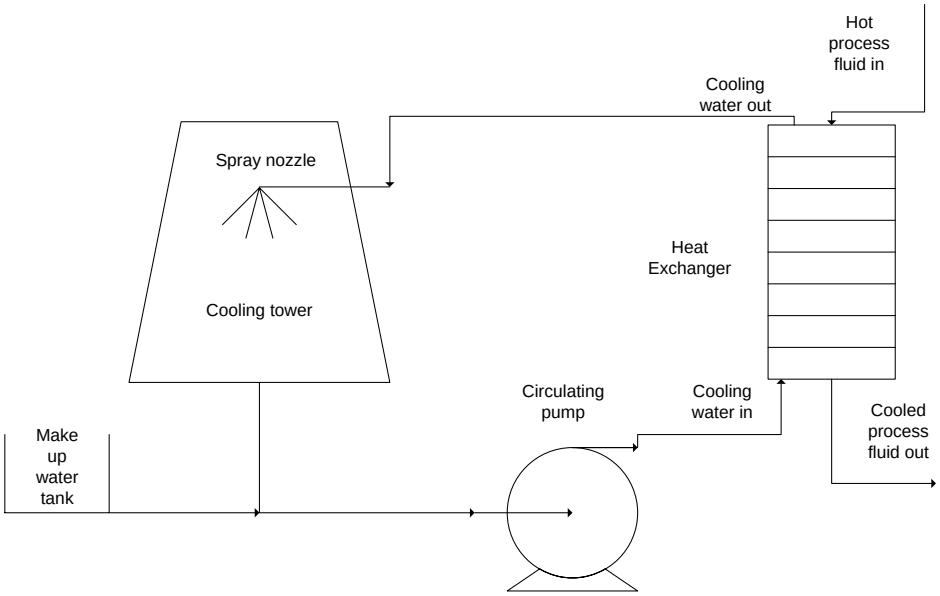

Figure 1-4. Schematic of cooling tower loop

The most significant problem encountered in systems employing evaporative cooling towers is the fouling of the heat exchanger due to the cooling water being contaminated. Circulating cooling tower water typically contains an excess of amount of mineral ions, such as calcium and magnesium, due to the evaporation of water, thus making the water hard. When the hard water is heated inside compact plate heat exchangers (PHEs), the calcium and bicarbonate ions precipitate because a drop in solubility occurs. The extent of the fouling problem depends upon the water quality, operating conditions, monitoring system, and maintenance practice. Users of this type of equipment have typically applied the same fouling factors that are recommended for tube-type heat exchangers, which are summarized in the AHRI guideline E [1997]. Guidance to the industry has also been provided by AHRI standard 450 [2007] and from recommendations by the Tubular Exchanger Manufacturers' Association (TEMA). It has also been determined that significant precipitation and particulate fouling occurs for internally enhanced tubes [Li and Web, 2000] but, unfortunately, fouling characteristics cannot be easily generalized for all applications.

Enhanced heat transfer surfaces used in PHEs provide higher heat transfer coefficients than conventional plain tubes but they are usually more sensitive to fouling [Li and Web, 2002]. Brazed PHEs performances under clean conditions are well known but their long-term thermal and hydraulic performances under fouling conditions have not been systematically investigated.

In spite of their long use, few calculation methods have been proposed for predicting the heat transfer and pressure drops during fouling conditions and actual operating service conditions

1.3 Fouling

Fouling is defined as the accumulation of deposits on the heat transfer surface which provide a resistance to the heat transfer, thereby decreasing the heat transfer capacity of the surface. The deposits are usually present in the fluid and adhere to the heat transfer surface causing fouling. The accumulation of deposits on the heat transfer surface decreases the area available for fluid flow thereby causing an increase in pressure drop across the surface which results in an increase in pumping power. Fouling usually occurs in heat exchangers when water is being heated, in most cases the water is used for cooling purpose. Fouling depends on the geometry, surface temperature and material of the heat transfer surface along with the velocity of fluid flow and the chemical nature of the fluid that is causing the fouling.

1.3.1 Categories of Fouling

In order to better understand the process of fouling it is necessary to review the different aspects of fouling, some of the most common types of fouling encountered in daily use are listed below.

a. Particulate fouling

It is basically the deposition of solid particles suspended in the fluid stream onto the heat transfer surface. Particulate fouling consists of three major processes, the transport of particles from the fluid to the heat transfer surface, the attachment of these particles to the heat transfer surface and finally the re-entrainment of previously deposited particles back into the fluid. The other processes that are likely to occur that influence particulate fouling are the growth of deposited particles, loosely bound particles becoming tightly bound, agglomeration of suspended particles, etc. Particulate fouling will be discussed in detail in chapter 2.

b. Precipitation fouling

This type of fouling is common in condensers and cooling tower applications which is the focus of this thesis. The water used on cooling systems has salts that include sulfates, carbonates, phosphates, etc of calcium and magnesium. These salts are inversely soluble in the water, i.e. they precipitate on the heat transfer surface when the temperature of the water increases. In cooling towers there is a continuous evaporation of water, this causes the concentration of these salts to increase which result in precipitation. The precipitation is likely to occur on the hottest part of the fluid path which is the heat transfer surface. This type of fouling will also be discussed in detail in chapter 2.

c. Corrosion fouling

It is a well-known fact that almost all surfaces subject to a fluid flow on them are susceptible to corrosion. Corrosion fouling refers to the removal of material from parts on the flow path and heat transfer surface due to corrosion. This largely depends on the properties of the material used to constitute the pipes, heat exchangers, etc on the flow path and the chemical properties of the process fluid. Use of corrosion resistant materials like alloys of copper, brass and stainless steel minimize the effects of corrosion fouling, also the use of certain additives with the process fluid will reduce the fouling. Corrosion products from the rest of the system add to the particulate fouling, but the more serious problem is the corrosion of the heat transfer surface itself which can lead to breakdown.

d. Biological fouling

It is defined as the accumulation of living matter on the heat transfer surface; this not only causes a decrease in heat transfer but also has the potential to infect humans that work in the same environment. The living matter usually refers to bacteria, algae, molds, etc that are likely to be found on the heat transfer surface which involve cooling towers, marine and power plant condensers using untreated sea or freshwater. One of the most common and dangerous bacteria that can be found in systems using cooling towers is legionella. It is responsible for legionnaires disease in humans when they inhale the mist from cooling towers, it can prove to fatal at times. All cooling tower manufacturers and industries

employing cooling towers have enforced standards regarding the use of biocides to control the growth of legionella.

1.3.2 **Costs of fouling**

It is well known that fouling causes a decrease in heat transfer, hence the heat exchangers must be oversized in order to compensate this loss, this leads to an increase in capital cost of the heat exchangers. Severe fouling causes a large pressure drop leading to high velocities of fluid which could lead to stress on joints and fittings on other parts of the system causing a break down and an increase in pumping power which increases the operating cost.

The air conditioning industry has been under pressure to improve the efficiency of systems by adopting enhanced heat exchangers. Several plate heat exchanger used in today applications now have leaving temperature difference of 2°F (1.1°C) instead of 5° to 6°F (2.7° to 3.3°C). With these small leaving temperature differences the field fouling allowance of 2.5×10^{-4} hr-ft^2-°F/Btu (4.4×10^{-5} m^2-°C/W) is now more of the total heat transfer resistance than it was when designs were based on 5° to 6°F (2.7° to 3.3°C) leaving temperature difference (AHRI guideline E [1997]. Thus, the selected equipment might not work efficiently in the field because the fouling allowances are based on higher leaving temperature difference than the one in the actual service conditions.

The manufacturers for brazed-plate heat exchangers that are in the process of fully adopting this technology have a market for more than $350M worldwide and about $30M in North America only. Therefore, it appears a critical need to quantify the fouling rates and field allowances of brazed plate heat exchangers (PHEs) used in today cooling towers.

1.4 Objective

The current thesis aims to experimentally measure the thermal and hydraulic performances of brazed plate heat exchangers (PHEs) under controlled fouling conditions. The specific objectives of my thesis are as follows:

- To design and construct a test facility for studying brazed plate heat exchangers functioning as condensers at pressures up to 200 psi.

- To demonstrate the feasibility of conducting accelerated-type fouling experiments on PHEs under controlled operating conditions and water quality that are similar of the ones in cooling tower applications.
- To design, construct and run a small scale cooling tower cycle that concentrates water directly on line with the PHE and maintains the water saturated in minerals at all time.
- To conduct fouling tests on three different heat exchangers, two having the same chevron angle but different aspect ratios, while two have same aspect ratios but different chevron angles and identify the differences or similarities in fouling resistance.
- To compare similarities and differences, if any, between the fouling behaviors of PHEs with the one of tube-and-tube heat exchangers and verify or upgrade the semi-empirical correlations used to predict the fouling resistance and pressure drop.

1.5 Overview of thesis

The thesis is organized as follows:

- Chapter one deals with the introduction to the three main components of this project, heat exchangers, cooling towers and the fouling process.
- Chapter two provides a literature review which consists of three parts:
  a. Plate heat exchanger theory and operation along with their thermal and hydraulic performance and the parameters affecting them.
  b. Understanding the theory of the fouling process, the different types of fouling and their causes.
  c. Review of previous work done on the fouling of heat transfer surfaces.
- Chapter three deals with the design and construction of the test facility and description of all components used.
- Chapter four describes the calibration of the test facility, data acquisition system, measurement instrumentation, uncertainty analysis, testing methodology and the control of the facility.
- Chapter five includes the data analysis of all the fouling tests conducted.
- Chapter six comprises of the conclusion and recommendations for future work.

CHAPTER II
REVIEW OF LITERATURE

2.1 Review of plate heat exchanger design

The first part of this literature review deal with the previous work done on plate heat exchangers. In order to have a better understanding of the thermal (heat transfer) and hydraulic (frictional pressure drop) performance of plate heat exchangers it is necessary to identify the parameters that influence them.

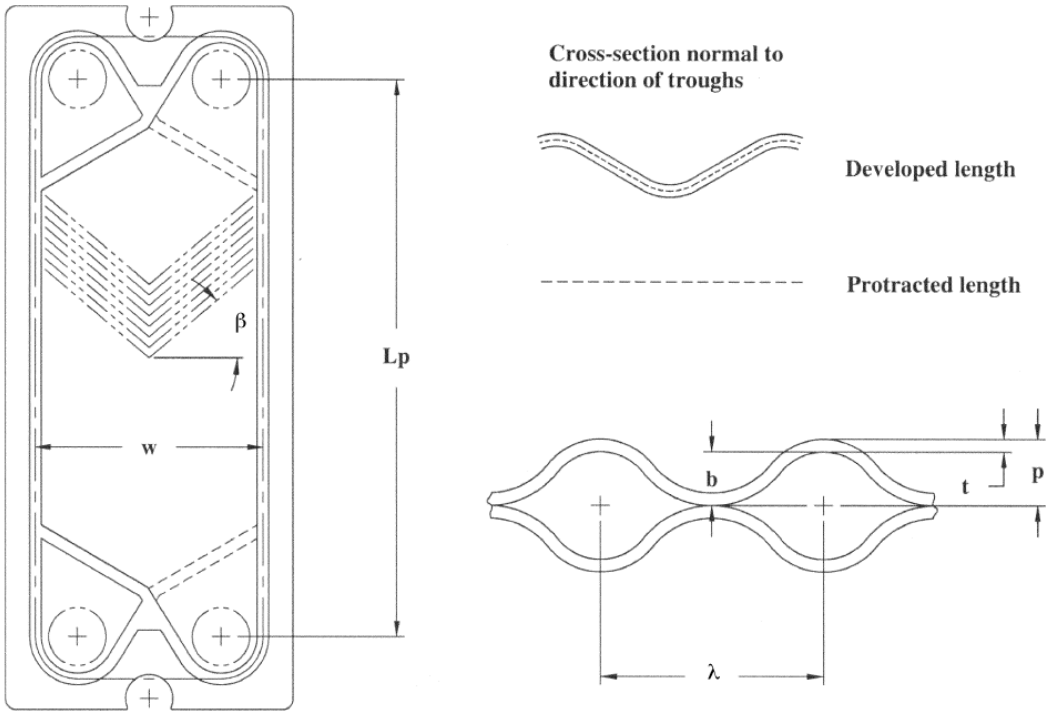

Figure 2-1. Plate Geometry as described by Ayub [2003]

The key geometric parameters listed by Ayub [2003] are shown in Figure 2-1.

Chevron Angle (90 - β): It is the angle of inclination of the grooves or corrugations measured from the direction of the flow, present on the heat transfer surface to increase the turbulence of the fluid thereby aiding the heat transfer; it usually varies between 20^0- 65^0.

Enlargement Factor (φ): It is defined as the ratio of developed length to the protracted length. In mathematical form $\varphi = L_d/L_p$.

Mean Flow Channel Gap (b): This is the actual gap available for the flow as shown in Figure 2-1.

$$b = p - t \tag{2.1}$$

Channel Flow area (A_x): This is the actual flow area, it is defined as

$$A_X = b \times w \tag{2.2}$$

Where w is the width of the heat exchanger and b is the mean flow channel gap shown in figure 2-1.

Channel equivalent diameter (d_e): This diameter is used in calculation of Reynolds number, it is defined as

$$d_e = \frac{4A_x}{P} \tag{2.3}$$

Where,

$$P = 2 * (b + \varphi w) = 2\varphi w \tag{2.4}$$

Since b <<w

Hence,

$$d_e = \frac{2b}{\varphi} \tag{2.5}$$

There are no general correlations available to determine the thermal and hydraulic characteristics of plate heat exchangers, but a few correlations are available for heat exchangers of specific geometry and operating ranges in terms of the Reynolds number (Re) and Prandtl number (Pr). The heat transfer characteristics are usually represented by the Nusselt number (Nu) and the hydraulic characteristics are represented by the frictional pressure drop (f) across the heat exchanger.

Troupe et al. [1960] proposed the following correlation for Nusselt number:

$$\mathrm{Nu} = \left(0.383 - 0.505^{\frac{\mathrm{Lp}}{\mathrm{b}}}\right) \mathrm{Re}^{0.65}\mathrm{Pr}^{0.4} \tag{2.6}$$

Equation 1 is valid when the working fluid is water and the Reynolds number (Re) is greater than the critical Reynolds number ($Re_{cr)}$ which lies between 10 and 400 depending on the heat exchanger.

Muley and Manglik [1999] provide the following correlations of Nusselt number and pressure drop:

$$\mathrm{Nu} = [0.2668 - 0.006967(90 - \beta)\beta + 7.244 \times 10^{-5}(90 - \beta^2)] \times [20.98 - 50.94\varphi + 41.16\varphi^2 - 10.51\varphi^3] \times \mathrm{Re}^{\left[0.728+0.0543\sin\left[\frac{\pi(90-\beta)}{45}\right]+3.7\right]}\mathrm{Pr}^{\frac{1}{3}}\left(\frac{\mu}{\mu_w}\right)^{0.14} \quad (2.7)$$

$$\mathrm{f} = [2.917 - 0.1277(90 - \beta) + 2.016 \times 10^{-3}(90 - \beta^2)] \times [5.474 - 19.02\varphi + 18.93\varphi^2 - 5.431\varphi\text{^}3] \times \mathrm{Re}^{-[0.2+0.0577\sin\left(\frac{\pi(90-\beta)}{45}\right)+2.1]} \quad (2.8)$$

Where,

μ is the dynamic viscosity of the fluid (determined from bulk mean temperature)

μ_w is the dynamic viscosity of the fluid at the wall(determined from the wall temperature).

Equations 2 and 3 are valid for Reynolds numbers (Re) greater than 1000, chevron angles (β) between 30^0 and 60^0 and enlargement ratios (φ) between 1 and 1.5.

Wanniarachchi et al. [1995] suggest a correlation to calculate the friction factor (f) and the heat transfer group (j_{NU}) which can be used for flows in the laminar, transition and turbulent regions since for plate heat exchangers the ranges of laminar and turbulent flows is not well defined.

$$f = (f_l^3 + f_t^3)^{1/3} \quad (2.9)$$

$$j_{NU} = \left(j_{Nu,l}^3 + j_{Nu,t}^3\right)^{1/3} \quad (2.10)$$

$$f_l = 1774/(\beta\text{^}1.026\, Re) \quad (2.11)$$

$$f_t = \frac{46.6}{\beta^{1.08} Re^{0.00423\beta - 0.0000223\beta^2}} \quad (2.12)$$

$$j_{Nu,l} = \frac{3.65}{\beta^{0.65} Re^{0.339}} \quad (2.13)$$

$$j_{Nu,t} = \frac{12.6}{\beta^{1.142}} Re^{0.646+0.0011\beta} \quad (2.14)$$

$$j_{Nu} = j\,Re \tag{2.15}$$

Where,

j is the colburn factor

Suffix l and t indicate laminar and turbulent regions respectively.

Focke et al. [1995] performed flow visualization as well as evaluating the thermal and hydraulic performance of plate heat exchangers having different chevron angles (90 - β) measured from the direction of flow. Heat exchangers with chevron angles of 0º, 30º, 45º, 60 º, 72 º, 80 º and 90 º were tested. The heat transfer and pressure drop were found to increase with β up to 60 º at an increasing rate then increase at a decreasing rate from 60 º to 80 º with a maximum at 80 º and at 90 º was found to be considerably lower approximately the same magnitude as at 60 º. The flow visualization process showed different types of flows, at 0 º a two dimensional channel flow was observed, between 30 º and 60 º sets of criss-crossing streams flowing along the furrows on either side of the flow passage were observed on either side of the flow passage inducing secondary flow motions that determine the heat transfer enhancement process, furrows are the channels formed in between the corrugations on the plate. At 80 º the flow consisted of parallel zigzag patterns and at 90 º separated flow regions across the flow passage were observed.

Dovic and Svaic [2007] studied the effect of chevron angle (90 - β) measured from the direction of the flow and aspect ratio (W/L) on plate heat exchangers along with performing a flow visualization on two plate heat exchangers with identical aspect ratio but chevron angles of 28º and 61 º. Two flow components were found to exist simultaneously a longitudinal flow and a criss-crossing furrow flow. The longitudinal component refers to the part of the fluid flowing alternatively along adjacent plate through respective furrows and the furrow component denotes the fluid flowing through the furrow on one plate without change of direction until it reaches the edge of the plate or the center line where the furrows change direction. The longitudinal flow was found to be dominating the heat exchanger with a chevron angle of 61 º and the furrow flow dominates the other one. In general it was found that plates with larger chevron angles and aspect ratios were characterized by more intense heat transfer and pressure drop, probably due to more mixing of the flow streams and longer flow paths. These conclusions seem to be in accordance with the work of Focke et al. [1995].

All of the work mentioned previously focused predominantly only on heat exchangers using liquids and involving no phase change and do not hold good for condensers and evaporators. Little research has been done on evaporators but not reviewed here as condensers are the subject of interest in this project. The information available on condensers is sparse and most of it is held confidential by the companies that manufacture the heat exchangers.

Yan et al. [1998] conducted experiments to determine the condensation heat transfer coefficient and pressure drop of refrigerant R134a in a brazed plate heat exchanger. The heat exchanger consisted of 3 stainless steel plates 500 mm long and 120 mm wide with a chevron angle of 60 º. Tests were conducted at mass fluxes ranging from 60 – 120 kg/m^{2}s and inlet vapor qualities ranging from 0.08 to 0.86 at 3 different system pressures of 0.7, 0.8 and 0.9 MPa. It was found that at a given mass flux the condensation heat transfer coefficient (CHTC) increased linearly with vapor quality, for example at a constant mass flux of 60 kg/m^{2}s the CHTC was 70 % larger at a quality of 0.8 than at 0.1. At the same time a rise in the refrigerant mass flux did not produce a comparable rise in the CHTC. The effect of system pressure is not significant on the CHTC, the CHTC at 0.9 MPa is about 5-10% smaller than at 0.7 Mpa. The frictional pressure drop of the refrigerant across the heat exchanger was found to vary similar to the CHTC but the variation is much larger. Investigations into the effect of vapor super heating on the CHTC were not reported in this paper.

The objectives of this research is to determine the fouling potential of R134a brazed plate condensers at one saturation temperature and a vapor superheat of 65 ^{0}F. It is helpful to understand the sensitivity of the CHTC on the refrigerant side with respect to the degree of superheat and refrigerant flow rate or mass flux since they do not factor in the expression used to calculate the overall heat transfer coefficient of the heat exchanger (see Table 4-1). The effects of vapor superheating and saturation temperature on the CHTC and the pressure drop in R134a brazed plate condensers were experimentally analyzed by Longo [2008]. A brazed plate heat exchanger consisting of 10 plates, 72 mm long and 310 mm wide with a chevron angle of 65 º. Tests were carried out at 4 different saturations temperatures. Two distinct sets of tests were carried out, the first set had a refrigerant inlet vapor quality of 0.96-1 while the second set had a vapor super heat of 10K. It was found that the refrigerant side CHTC had a weak sensitivity to the saturation temperature which is in accordance with the results of Yan el al. [1998], the CHTC of superheated vapor was found to be 8-10% larger than that of saturated or near saturated vapor.

Two types of condensation processes were found to occur in the brazed plate condenser for R134a based on the refrigerant mass flux. Gravity controlled condensation was found to occur for low refrigerant mass fluxes and the CHTC was not dependent on the mass flux but at high mass fluxes forced convection condensation occurs, in this type of condensation the mass flux is a significant factor affecting the CHTC, doubling of mass flux leads to a 30% increase in CHTC.

2.2 The fouling process

The second part of the literature review deals with the fouling process and the previous work done on fouling of heat transfer surfaces. Only the work done on precipitation and particulate fouling is reviewed here as biological and corrosion types of fouling are not the subject of this work. Addition of bleach to the cooling tower water eliminated the growth of microorganisms leading to biological fouling. The corrosion fouling was kept to a minimum by mixing small quantities azole, which acts as a corrosion inhibitor with the water. For every 100 gallons (378.5 liters) of water about 2.4 ounces (71.4 milliliters) of azole were mixed. The amount of azole to be mixed was estimated form personal communications with NALCO water treatment company. About 2.4 ounces significantly reduces the corrosion fouling and small changes in this volume do not have a significant impact. By eliminating the biological and corrosion fouling, the remaining fouling phenomena is mainly reduce to scaling effects, which could be then isolated and possibly quantified.

Though there are many types of fouling and a large number of variables that affect it, Kakac [2002] states that the fundamental process of fouling can be divided into 5 stages which are initiation, transport, attachment, removal and aging. According to the author during the initiation state the heat transfer surface is conditioned for the fouling that will occur later, the temperature of the surface starts to increase which decreases the super saturation of salts in the process fluid causing fouling in the case of precipitation fouling. During the transport phase the fouling substances from the fluid are brought to the heat transfer surface due to the process of diffusion, sedimentation (movement of particles in the fluid to a horizontal or inclined surface due to gravity) and thermophoresis (movement of small particles in a fluid stream when a temperature gradient is present). In the attachment stage the fouling particles transported attach to the surface, this depends on the forces acting on the particles, temperature of surface and the properties of the material of the surface. The removal phase involves the removal of some of the

particles deposited on the heat transfer surface due to shear forces between the fluid and the particles deposited on the heat transfer surface depending on the fluid velocity and roughness of the surface. The final stage is that of ageing that occurs once the fouling particles or deposits settle on the heat transfer surface, the mechanical properties of these fouling deposits changes due to change in crystal or chemical structure.

The basic fouling model is that given by Kern and Seaton [1959] which defines the fouling rate as:

Fouling rate = deposition rate – removal rate (2.16)

Sommerscales [1979] stated that the deposition rate is affected by process in the body of the fluid, transport of particles to the heat transfer surface and the attachment/formation of the deposit while the removal rate depends on dissolution where material leaves in molecular or ionic form, erosion or re-entrainment where material leaves in particulate form and spalling or sloughing where material leaves as a large mass.

Based on the deposition and removal rate on the fouling resistance, 3 kinds of fouling curves are possible as shown in Fig 2-2.

a. Linear – it is obtained when the removal rate is small in comparison to the deposition rate.
b. Falling – it is obtained when after a period of time the removal rate exceeds the deposition rate
c. Asymptotic – it is observed when after a period of time the deposition and removal rates are equal.

The fouling process does not start immediately there is an initiation period or delay time where it is possible to have a negative fouling resistance.

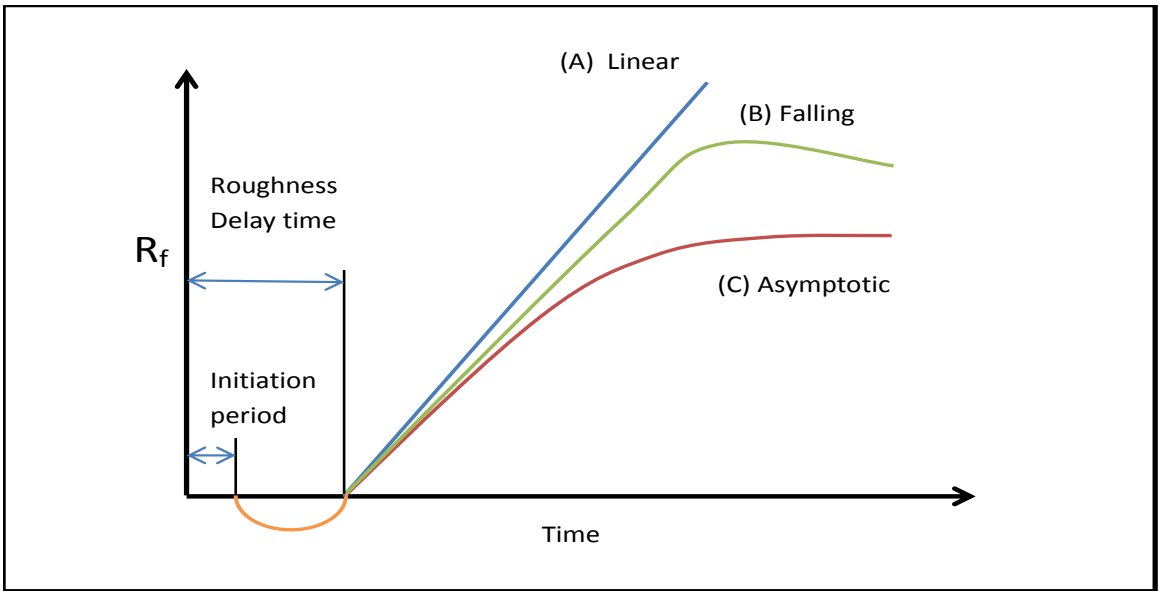

Figure 2-2. Typical trends of resistance curves

A few of the terminologies commonly associated with precipitation fouling or scaling are listed below.

Langalier Stability Index (LSI):

It is used to determine if certain water will tend to precipitate or dissolve calcium carbonate. If the water dissolves calcium carbonate it is corrosive in nature and if it precipitates then scaling will occur. The LSI is defined as the difference between the actual PH of water and the calculated PH of water saturated in calcium carbonate. If the LSI is positive then the water is expected to be noncorrosive but scale forming, if it is negative then it will dissolve calcium carbonate and no scale formation will occur, if it is zero then the water is said to be stable but sudden changes in temperature or evaporation rate can change the index. The LSI is calculated using the following equations:

$$LSI = pH_a - pH_s \tag{2.17}$$

Where

pHa = pH of water sample measured

pHs = pH of water saturated in calcium carbonate defined as :

$$pH_s = (9.3 + A + B) - (C + D) \quad (2.18)$$

Where

A = $(Log_{10}[TDS] - 1)/10$

B = -13.12 x Log_{10} (^oC + 273) + 34.55

C = Log_{10} [Ca^{2+} as $CaCO_3$] - 0.4

D = Log_{10} [alkalinity as $CaCO_3$]

All units are in parts per million (ppm); TDS – total dissolved solids

Supersaturation

A supersaturated solution is one which contains more of the dissolved substance than what can be dissolved by the solution at the present conditions. In fouling or scaling experiments the term bulk concentration (c_b) refers to the concentration of calcium salt present in the solution at room temperature and saturation solution concentration (c_s) refers to the saturation concentration at the temperature of the heat transfer surface. For example consider a solution of calcium sulfate at 20 ^{0}C (68 ^{0}F) which has a concentration of 900 mg/kg referred to as the bulk concentration (c_b), at 20 ^{0}C (68 ^{0}F) the solubility if calcium is of 997 mg/kg, hence it is not saturated, now when the same solution comes in contact with the heat transfer surface at 80 ^{0}C (176 ^{0}F) the solubility of calcium is 280 mg/kg termed as saturation solution concentration (c_s) which is less than the bulk concentration causing the fluid to be supersaturated resulting in precipitation. Hence it can be concluded that precipitation (scaling) will occur when $c_b > c_s$ indicating the fluid is supersaturated.

An important aspect of the fouling process is the re-entrainment of the particles in the heat transfer fluid. Cleaver and Yates [1974, 1975] analyzed the effect of re-entrainment on particle deposition. In practical applications not all particles present in the fluid adhere to the heat transfer surface, some of them are still re-entrained in the fluid itself. It is assumed that all particles are convected into a sub layer by a cohesive down sweep or subsequent down or are transported back into the flow by an outward burst. The position of down sweep and bursts are said to vary in a stochastic manner so deposited particles may experience a burst at a later stage causing it to be detached and re-entrained in the flow. It was found that the wall shear stress is a key factor in determining detachment; there is a certain critical wall of wall shear stress below

which detachment will not occur. Two kinds of mechanisms were said to exist for deposition of particles, for small particles it is diffusion controlled and large particles it is inertia controlled.

In order to have a better understanding of the fouling process it is necessary to study the different forces involved in adhesion or detachment of particles to the heat transfer surface. Oliviera [1997] states that particles of colloidal size (dimension < 1μm) absorb on to the surface whereas larger particles do not adhere as gravitational and hydrodynamic forces remove them. The principle attractive force between colloidal particles is due to Wan der waal's interactions which depend upon the geometry of the surface along with the physical and chemical properties of the liquid. Electro static double layer forces are the other predominant forces acting on the particles, when solid bodies are immersed in a liquid medium like water they tend to acquire an electrical charge due to preferential absorption of ions; at neutral PH most of the particles tend to acquire a negative charge. The surface immersed in the liquid also tends to acquire a charge which promotes a redistribution of ions in the solution; ions of opposite charge are attracted to the surface while those with the same charge are repelled. Usually the Wan der waal's forces are attractive while the electrostatic double layer forces are repulsive in nature.

The concentration effect caused due to cooling towers on the fouling of heat exchangers was studied by Hasson [1979]. It is found that the potential for precipitation fouling in cooling water systems is magnified due to the concentration effect. The major parameters involved can be analyzed by taking the specific heat of water as unity and latent heat of water vapor as 1000 btu/lb, then the makeup water M, expressed in lb/hr required to discharge 1000 btu/hr to the surroundings is:

$$M = \frac{CF}{CF-1} \tag{2.19}$$

Where the concentration factor or cycles of concentration CF represents the ratio of dissolved solids concentration in the bleed of stream to the dissolved solids in the makeup. The significance of the expression for makeup water (M) is that it reduces rapidly as CF increases but the heat transfer surface is exposed to a more concentrated solution of potentially precipitating species, this helps in determining a trade of between the rate of evaporation and the heat transfer, since a larger evaporation rate will not only increase the heat transfer but also the potential for fouling.

The effect of PH, ionic strength and the electrical charge of particles on the heat transfer surface were analyzed by Oliveira [1997]. Tests were conducted to determine the thickness of

deposits on copper surfaces using Kaolin particles as a function of PH, the deposit was found to be thicker when the PH was kept constant using sodium carbonate than using sodium hydroxide because sodium carbonate is a weaker base and a larger quantity is needed to maintain the PH. The deposit thickness was found to decrease as the PH was raised. Hematite particles [Fe_2O_3] or hydrous Alumina when mixed in the fluid were found to adhere to the heat transfer surface at neutral PH since they carry a positive charge, forming a positively charged coating on the surface ready to attract negatively charged particles and are difficult to remove due to electrostatic interactions.

2.3 Fouling on heat transfer surfaces

One of the first investigations into the fouling of plate heat exchangers was done by Cooper et al. [1980]. Each plate used had a length of 1.14m and width of 0.45m, a total of 7 plates comprised the heat exchanger. The fouling tests were conducted at a petrochemical plant in Houston, TX, where hot steam condensate was cooled, the cooling water used came from different sources and was treated to prevent corrosion and biological fouling. It was found that fouling resistances establish a stable asymptotic value after about 600-900 (~ 25 – 38 days) hours of operation. The asymptotic fouling resistance at a flow velocity of 0.85 m/s was found to be half of that at a velocity of 0.45 m/s. On dismantling of the heat exchanger after the tests it was found that fouling occurred only on the upper third of the plates where the hot condensate entered, based on the water chemistry it was determined that precipitation is expected only at wall temperatures greater than 346 K (~163°F) and it corresponds closely to the fouled region. In a similar test conducted by Kho and Muller-Steinhagen [1999] the same distribution of fouling deposits on the plates was observed.

Karabelas et al. [1997] analyzed the effect of chevron angle of plate heat exchangers and flow velocity had on the fouling resistance. Two heat exchangers with identical geometries and number of plates but with chevron angles of 30^0 and 60^0 were tested. The fouling fluid was prepared by adding calcium carbonate particles to de-mineralized water, the mean particles size was around 5μm and each test lasted between 100 and 300 (~ 4 – 13 days) hours till the asymptotic fouling resistance was reached. At high velocities (1.35 m/s) the fouling resistance of the PHE with 60^0 chevron angle was found to be negligible, at a lower velocity (0.35m/s) the asymptotic fouling resistance was 7 times higher. The plate heat exchanger with a 30^0 chevron

angle was found to have a much higher value of fouling resistance that that with 60^0. It was concluded that the zigzag flow pattern associated with the 60^0 chevron plate led to better heat transfer performance and lower fouling resistance than the furrow flow pattern associated with the 30^0 chevron plate.

Grandgeorge et al. [1998] experimentally studied the effect of chevron angle and flow velocity on particulate fouling of plate heat exchangers. The fouling fluid used for tests was obtained by mixing anatase $Ti0_2$ particles (4-5 μm size) in deionized water. The plate heat exchangers used were identical expect for the chevron angles of 30^0 and 60^0. The tests were runs for periods up to 440 hours (~ 18 days); the asymptotic fouling resistance at a low velocity of 0.3 m/s was found to about 6 times higher than that at 1m/s. Also the plate with 30^0 chevron angle showed a higher fouling resistance than the plate with 60^0 chevron angle which is in accordance with that of Karabelas et al. [1997]. If the deposit thermal conductivity and density are constant the following equation is said to give the time evolution of the fouling thermal resistance:

$$R_f(t) = R_f^*(1 - e^{-t/t_c}) \quad (2.20)$$

The constant t_c was taken as the duration of the experiment which was 800 hours and the asymptotic fouling resistance R_f^* was determined by minimizing the quadratic error between the measured and calculated fouling thermal resistance. At a fluid velocity of 0.16 m/s (0.52 ft/s) the asymptotic fouling resistance for the 30^0 and 60^0 chevron plates was found to be 0.00057 m^2K/W (0.0032 hr-ft^2-^{0}F/Btu) and 0.001 m^2K/W (0.00058 hr-ft^2-^{0}F/Btu). The corrugation angle is the angle of inclination of the grooves or corrugations measured from the direction of the flow (90 – β), present on the heat transfer surface to increase the turbulence of the fluid thereby aiding the heat transfer. The relationship between asymptotic fouling resistance and fluid velocity was found to be:

30^0 of corrugation angle: $Rf^* = (1.481 \times 10^{-5} / u_m^2)$ (2.21)

60^0 of corrugation angle: $Rf^* = (2.626 \times 10^{-6} / u_m^2)$ (2.22)

Where,

U_m – fluid velocity (m/s); $0.02 < U_m < 1.4$

Kim et al [2001] used an experimental method to visualize the process of scale formation on a min-channel heat exchanger system using a copper plate as the heat transfer surface. The water used for the tests was artificially hardened by mixing sodium bicarbonate and calcium

chloride solutions to have equivalent hardness of750 ppm of calcium carbonate. Duration of the fouling tests was between 6 and 11 hours, the hot water used to heat the copper plate had constant inlet and exit temperature of 94^0C and 90^0C respectively. The effect of inlet temperature and velocity of the cooling water on scale formation were analyzed. Tests were conducted at water velocities of 1.2 and 3.5 m/s and cooling water inlet temperature varying from 30 – 55 ^{0}C. It was found that initially in the first half hour small crystals of sizes about 90 μm were already present and begin to grow rapidly up 160 μm and covered the entire surface at 2 hours. It is suggested that the crystal present initially were due to roughness or imperfections on the heat transfer surface. It was found that at half hour the number of crystals present at a cooling water inlet temperature of 55^0C was 2.5 times more than what was present at 30^0C. It was found that the induction period of scale formation was greater when the velocity was higher but decreased with an increase in cooling water inlet temperature, the fouling resistance to follows the same trend.

Andritsos and Karabelas [2003] investigated scale formation in a plate heat exchanger in the presence of various types of added particles along with the effects of flow velocity, particle concentration and direction of flow inside the heat exchanger. A plate heat exchanger with 8 plates each had a flow area of 186 cm^2 and a chevron angle of 60^0. Tap water was used for all tests and sodium hydroxide was added to it to modify the PH. Scale formation was examined in the presence of 3 different kinds of particles, large calcite particles having a size of 15 μm, smaller aragonite particles having a size of 5.3 μm, both are forms of calcium carbonate and lastly extremely small anatase TiO_2 particles of 0.8 μm size are used. Tests were conducted at two different water temperatures of 25^0C and 40^0C. An increase in the concentration of aragonite particles tends to increase the scale formation and cause a greater pressure drop across the heat exchanger compared to the smaller calcite and Tio_2 particles. Flow direction seemed to have no effect on the scale formation though it would seem that particle detachment was more likely to occur when the flow is in the downward direction. The deposit enhancement was found to be larger at low velocities due to an increased detachment rate at higher flow velocities.

Bansal et al. [2000, 2007] investigated performances of plate heat exchangers during calcium sulfate fouling. The calcium sulfate solution used as the fouling fluid was prepared by calcium nitrate tetrahydrate and sodium sulfate solutions as it was not possible to prepare a solution by simply dissolving calcium sulfate reagent in water due to its low solubility, which led

to undissolved calcium sulfate particles being present in the fouling fluid which would lead to particulate fouling. Supersaturated calcium sulfate solutions with concentrations ranging between 2.8 to 3.2 kg/m^3 at room temperature, were used to foul the heat exchanger. The saturation concentration at the operating temperatures of the heat exchanger was found to vary between 1.8 and 2.2 kg/m^3. The deposition of calcium sulfate was found to be a second order reaction and the deposition rate (m_d) is given by:

$$m_d = K_R(c_b - c_s)^2 = \left(A_0 e^{-\frac{E}{Rt}}\right)(c_b - c_s)^2 \quad (2.23)$$

Where,

K_r is the reaction rate constant	[m^3/kg.s]
C_b is the bulk solution concentration	[kg/m^3]
C_s is the saturation solution concentration	[kg/m^3]
E is the activation energy	[J/mol]
A_0 is the Arrhenius constant	[m^3/kg.s]
R is the gas constant	[J/mol.K]
T is the temperature at which crystals occur (wall temperature)	[K]

During the tests a 1μm filter was installed before the heat exchanger to minimize the particulate fouling. It was found that initially the fouling resistance fluctuated between 0 and a negative value for some time after which it picked up, this period was said to be the roughness delay time. The fouling curve was found to increase with a falling rate, this is due to the lower deposit rates caused due to the lowering of the temperature of the deposit/solution interface with time. If the filter was removed the fouling resistance was found to increase significantly which is due to increase in particulate fouling. When the plates were removed and examined after each test most of the deposit was found to occur in the corner where the hot fluid entered, i.e. the hottest part of the plate which is in accordance with previous works reviewed. The pressure drop across the heat exchanger was found to be significantly larger when the solution concentration was increased since deposits formed near the exit ports of the heat exchanger and the deposition being a second order reaction the fouling resistance was found to be proportional to the square of the difference between the bulk and saturation concentrations.

The effect fluid velocity, water hardness, and alkalinity, solution and wall temperatures on the fouling process was experimentally analyzed by Zhenhua et al. [2008]. A coaxial heat exchanger was used for these tests with the hot fluid flowing in the inner tube and cooling water

in the outer tube, hence fouling occurs on the outer surface of the inner tube. The cooling liquid used for this experiment was obtained by mixing sodium bicarbonate and calcium chloride in pure water. The hot water used had a constant inlet temperature of 70^0C and the average wall temperature was between 51^0C and 60^0C and was found to increase slightly with fouling. In this experiment it was found that fouling crystals formed not only on the heat transfer surface but also inside the fluid solution, and the particles present in the solution took part in the fouling process on the heat transfer surface, hence particulate and precipitations fouling were to occur simultaneously. The fouling tests were conducted for a time of 32 hours or till the fouling resistance curve was found to be asymptotic, in almost all cases the asymptotic fouling curve was obtained within a time of 15 hours. The asymptotic fouling resistance was found to increase with increasing harness, alkalinity, solution temperature and heat transfer surface temperature; however an increase in the fluid velocity resulted in a decrease in the value of asymptotic fouling resistance.

The previously reviewed literature deals with fouling in heat exchangers in which a phase change does not occur. The effect of water side fouling inside smooth and augmented copper alloy condenser tubes was studied by Chamra [2006]. The effect of tube geometry on the fouling resistance at a water velocity of 2 ft/s (0.6 m/s) was investigated. Nine different tubes each 10 feet long with the same outside fin geometry and diameter but different inside fin geometry (helix angle, fin height and number of starts) connected in parallel were used to condense R134a entering with a saturation temperature around 105 ^{0}F (40.6 ^{0}C) inside a shell. Initially for a period of two days clean water was run through the tubes and the heat transfer characteristics of the tubes were determined. The fouling tests were conducted using simulated water determined to have a low fouling potential, the chemical properties of the simulated water are listed in Table 2-1. The duration of the fouling tests was conducted was 58 days, it was found that the plain tube (without fins on the inside) fouled the least while the tubes with larger helix angle and number of starts fouled the most. The tubes with 45 starts and helix angles of 35^0 and 48^0 had reached an asymptotic fouling resistance close to 0.000001 hr-ft^2-^{0}F/Btu (1.76E^{-7} ^{0}C- m^2/W).

Table 2-1. Water properties, Chamra [2006]

Total Hardness	Calcium	Magnesium	"M" Alkalinity	Chloride	Silica	Sulfate	Specific Conductance
240	180	59	96	<200	5.7	72	TBD
pH	Total Iron	Copper	TDS	TSS	P-Type Alkalinity	Phosphate	Ortho-Phosphate
7.8	0.15	0.03	1140	8	0	0	0

Webb and Li [1999a] conducted long term fouling tests for cooling water flowing inside enhanced tubes used to condense refrigerant R-11 in a 235 ton (880 KW) centrifugal refrigeration unit. Eight tubes of equal length but different geometries connected in parallel were used; the geometries vary the number of starts, helix angle and fin height. The tests were conducted for a period of 2400 hours (100 days) using water having approximately 800 ppm total calcium hardness, 1600-1800 μΩ electrical resistance and 8.5 PH and the water velocity was kept constant at 3.5 ft/s (1.07 m/s). Tubes with greater number of starts and larger helix angles were found foul significantly more than those with lesser number of starts and smaller helix angles. The tube containing 45 starts and having a helix angle of 45^0 was found to have an asymptotic fouling resistance of 0.000144 m^2K/W (0.000817 hr-ft^2-^{0}F/Btu) while a tube with 18 starts and 25^0 helix angle had an asymptotic fouling resistance of 0.000035 m^2K/W (0.0001987 hr-ft^2-^{0}F/Btu). The analysis of the deposits on the tube was done at the end of the experiment (Webb and Li [1999b]), the deposit was found to contain 57% calcium carbonate, 2% calcium phosphate, 14% non-carbonate and 26% particulates, it was concluded that the 59% calcium deposits were due to precipitation fouling and the remaining 40% are due to particulate fouling and fouling process occurring is a combination of particulate and precipitation fouling.

Haider et al. [1992] conducted tests to study the tube- side fouling resistance in water-chiller-flooded evaporators. It was found that the fouling resistance was evenly distributed and was about zero irrespective of the water quality or flow velocities. Hence it can be concluded that fouling occurs only when the water is used for cooling purposes.

The extent of the fouling (scaling) problem depends upon the water quality, operating conditions, monitoring system, and maintenance practice. Guidance to the industry has been provided by AHRI standard 450 [2007] and from recommendations by the Tubular Exchanger Manufacturers' Association (TEMA). A large part of this work was to identify the current

methodologies used to measure the fouling performance in condensers. An extensive review of the most recent work on fouling measurement techniques was conducted and, to date, it was found that there is not a consistent and standardized method. The range of the refrigerant and water operating conditions that must be maintained during the laboratory tests are often not well defined. Water quality and its fouling potential were also found to be somehow linked to local water sources and most of past experiments were conducted using from local wells, rivers, or created in ad-hoc laboratory. In this work, a general methodology to obtain cooling tower water with specified fouling potential is given and details of this methodology can be found in a complementary thesis in the School of Mechanical and Aerospace Engineering at Oklahoma State University [Lim 2010]. In order to better understand the characteristics of the test apparatus used in this thesis, a summary of the previous techniques for measuring the fouling resistance is given next.

2.4 Review of test facilities used to study fouling

Figure 2-3 shows the schematic of the test facility used by Bansal et al. [2000] to determine the fouling of a plate heat exchanger subject to precipitation fouling. The test plate heat exchanger is connected to a fouling water loop and a hot water loop. The fouling water ($CaSO_4$ solution) is circulated between the solution tank (50 liters capacity) and test plate heat exchanger through a filter which removes particles above a size of 1μm to minimize particulate fouling and an orifice meter which is used to measure the flow rate. The fouling water is heated in the test plate heat exchanger using hot water that is preheated in another heat exchanger using steam as shown in Figure 2-3, the fouling water that is heated in the plate heat exchanger is cooled back to its initial temperature in the solution tank by passing cooling water through a pipe immersed in it.

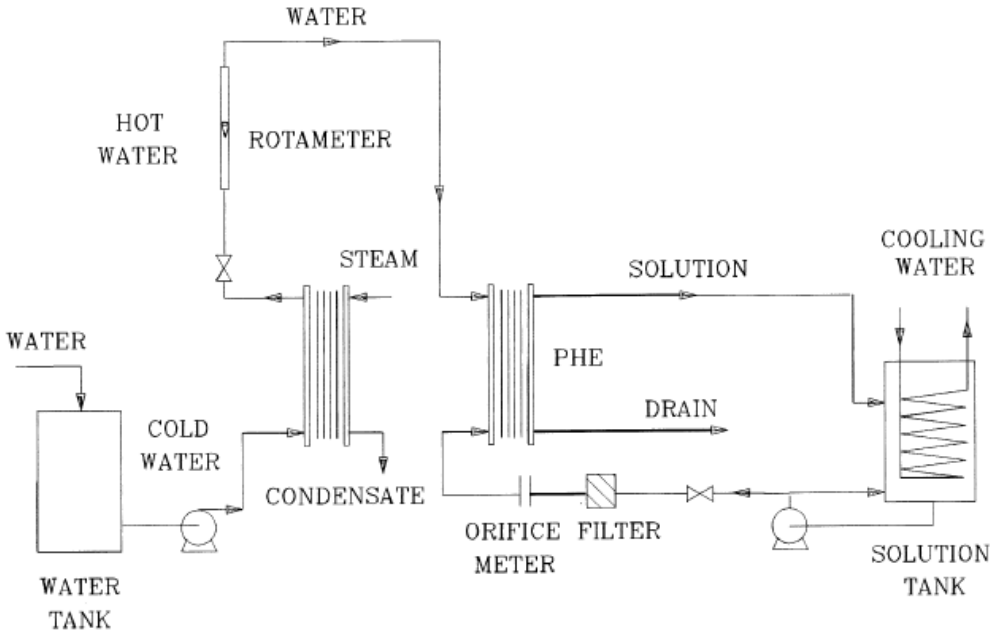

Figure 2-3. Test facility used by Bansal et al. [2000]

An experimental facility used by Grandgeorge et al. [1998] to measure the particulate fouling of heat exchangers is shown in Figure 2-4. There are two independent flow networks connected to the test plate heat exchanger termed as the foulant circuit and coolant circuit. The foulant is a mixture of anatase TiO_2 particles in deionized water is circulated between a 500 liters tank and the test plate heat exchanger. The tank is provided with a 9 kW heater capable of reaching foulant temperatures of 50 ^{0}C (122 ^{0}F) and a stirrer which is used to homogenize the solution. The foulant is cooled in the test heat exchanger using cooling water, it should be noted that in this case the fouling fluid is being cooled and hence precipitation fouling is not likely to occur and the fouling is 100% particulate. Temperature, pressure and flow measurement devices are installed in the set up as shown in Figure 2-4.

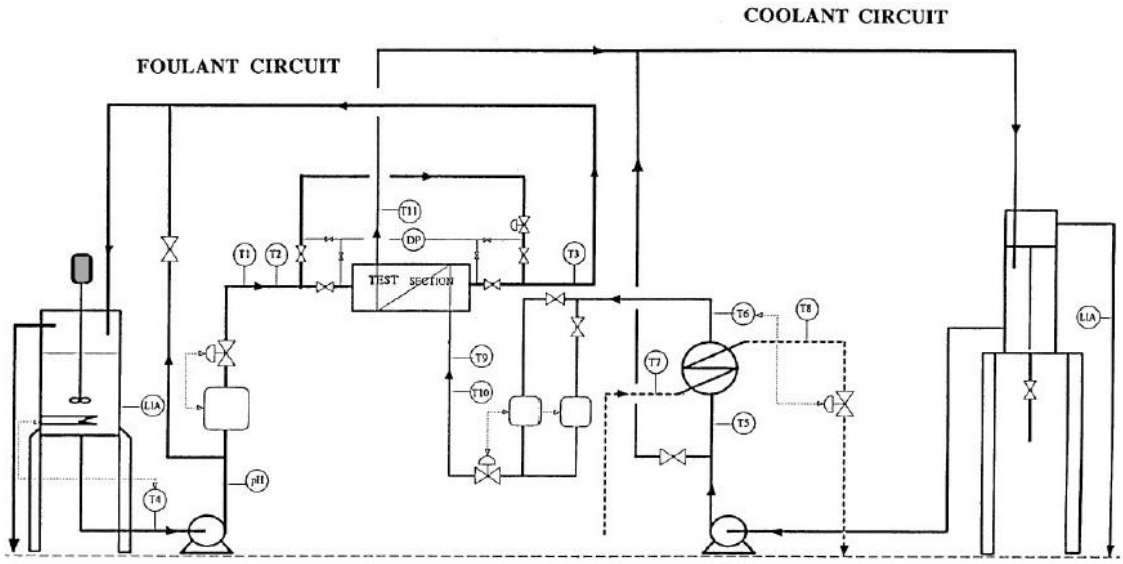

Figure 2-4. Test facility used by Grandgeorge et al. [1998]

The experimental facility used by Chamra [2006] to study the effect of water side fouling inside smooth and augmented copper alloy condenser tubes is shown in figure 2-5. There are two independent loops, the water loop and the refrigerant loop; the water loop consists of a mixing tank and water cooling heat exchangers (not seen in Figure 2-5), the mixing tank contains the cooling tower water and the water cooling heat exchangers using city water to cool the cooling tower water after it is heated by the refrigerant in the test section. The test section is basically a shell and tube heat exchanger with refrigerant flowing through the shell and water flowing through the tubes. The refrigerant loop consists of refrigerant tanks containing R134a at boiling conditions; all the tanks had rupture disks which are supposed to burst if the pressure exceeds 200 psi. All the refrigerant tanks were provided with two ring heaters each with a capacity of 2.25 kW and a tape heater is wrapped around the pipe of the refrigerant before it enters the test section to superheat the refrigerant which is at a saturation temperature of 105 ^{0}F (~ 40.5 ^{0}C), a chilled water heat exchanger using chilled water at a temperature of 45-50 ^{0}F (~ 7-10 ^{0}C) is used to cool the refrigerant after it exits the test section. It is to be noted that the refrigerant loop did not incorporate any refrigerant pumps; the flow of refrigerant (vapor) into the test section was by means of buoyance and the return to the tank (liquid) was die to gravity.

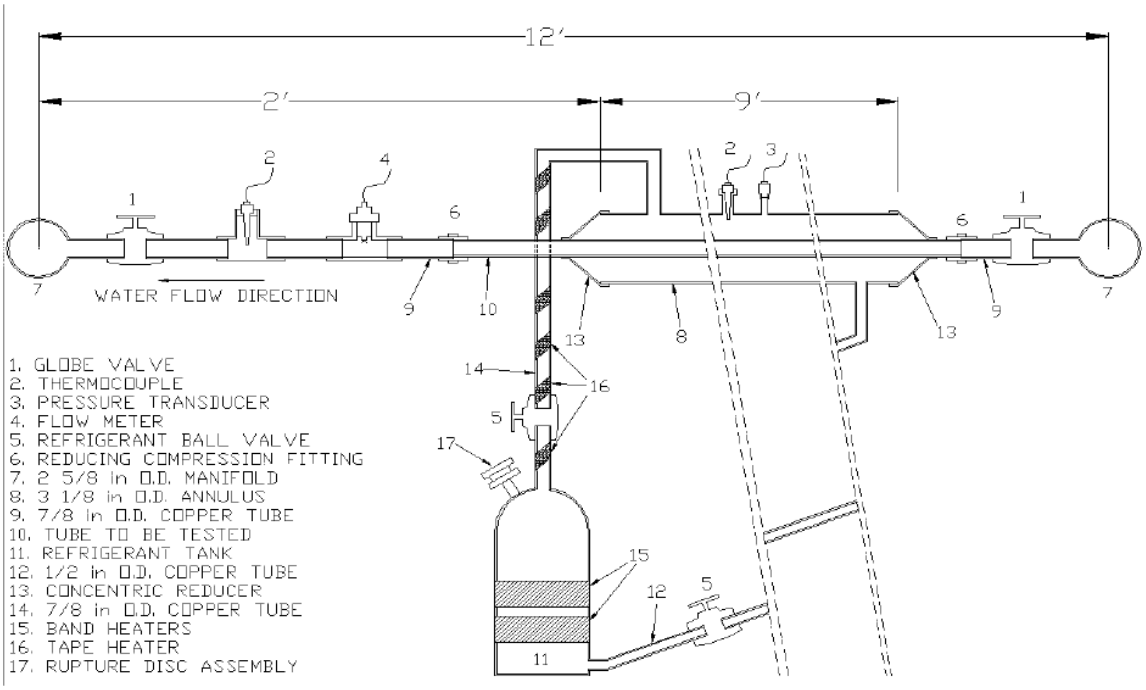

Figure 2-5. Test facility to determine water side fouling in condenser tubes (Chamra [2000])

All though the test facility used by Chamra [2000] involves using of refrigerant to heat the cooling tower water, it does not have the capabilities to accurately control parameters such as the degree of superheat, saturation temperature and flow rate of the refrigerant entering the test section. The refrigerant loop of the test facility constructed by Longo [2008] is shown in Figure 2-6 is capable of achieving better control of the previously mentioned parameters. A variable speed refrigerant pump is used to achieve better control of refrigerant flow rate. The refrigerant is first pumped into a heat exchanger which serves as an evaporator; using hot water the refrigerant is evaporated and eventually super-heated before it enters the condenser. The refrigerant exiting the condenser is then passed through a post condenser and a sub-cooler where it is sub-cooled before it enters the pump inlet thereby eliminating the chance of vapor bubbles. The pressure of the refrigerant is controlled using a bladder accumulator connected to a nitrogen bottle.

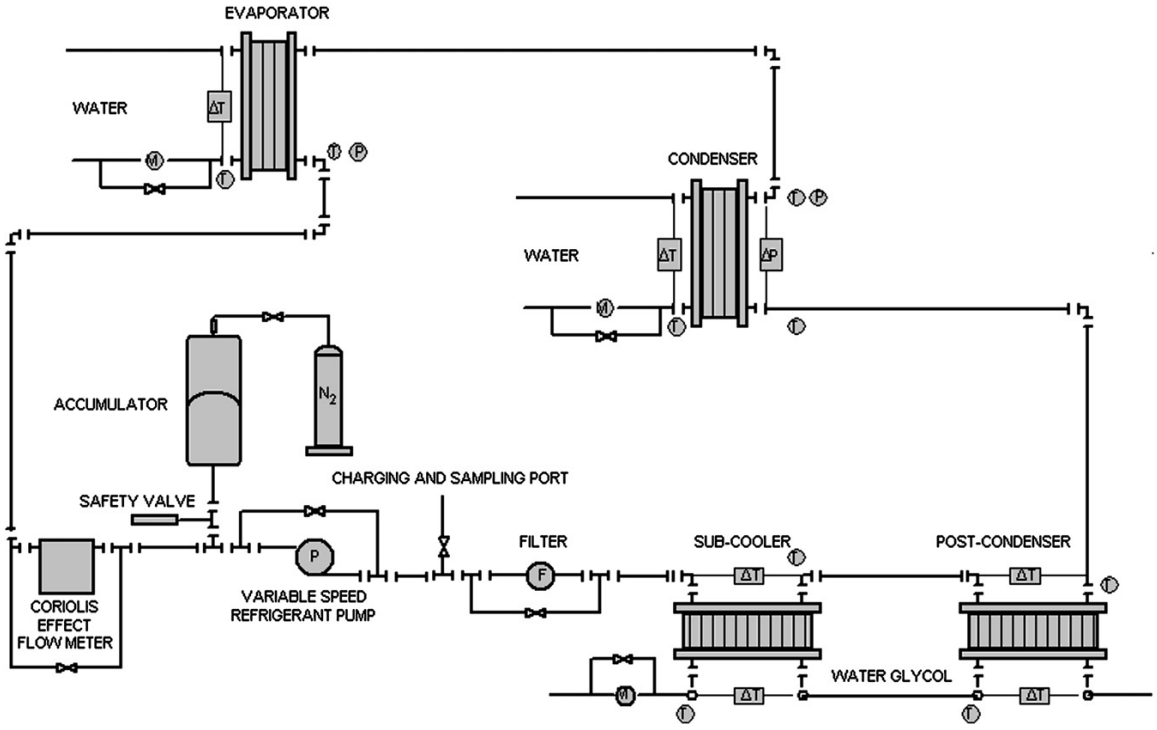

Figure 2-6. Test facility used by Longo [2008]

2.5 Conclusion from the literature review

Even though some work on fouling of plate heat exchangers is available in the literature, no data are available on fouling of plate heat exchangers operating as condensers. In the previous work the fouling water is used from specific water sources and though its chemical properties might be maintained throughout, the previous tests did not involve the use of an actual cooling tower. Hence whether the water was saturated in minerals or not was difficult to say. The effect of water degree of supersaturation on the fouling resistance of PHE was not studied systematically and the fouling tests were generally not repeatable due to the variation of multiple operating conditions. It is concluded that there is a need for a better understanding of the precipitation and particulate fouling mechanisms in PHEs and for developing an experimental methodology that is able to measure the fouling resistance and pressure drop in these types of exchangers. The methodology should be accurate, repeatable, and independent from the geographic location of the water source. This thesis summarizes such test methodology and focuses on the propensity for fouling in PHEs used in cooling tower applications. Since fouling is a very slow process accelerated-type tests are developed in laboratory. The accelerated tests progressively concentrate the water while running the water through the PHE and through a

small cooling tower at the same time. The water is maintained saturated in minerals and becomes supersaturated within the PHEs, thus promoting mineral precipitation and deposition in the vicinities of the test PHE. A complete and thorough uncertainty analysis of the experimental methodology is presented. The uncertainty analysis aimed to identify the main sources of inaccuracy for heat transfer and pressure drop and how to operate the experimental facilities in a way that the inaccuracy are kept to the minimum. This thesis also reports the fouling performances of the first two brazed plate heat exchanger geometries tested in the facility. Two PHEs have same chevron angle and different aspect ratio while the third brazed PHE consists of same aspect ratio of one of the first three plate exchangers but with a different chevron pattern that yields a low pressure drop. The preliminary results from this thesis allow quantifying the impact of plate geometry and water velocity on the fouling performance of brazed plate heat exchangers. It should be emphasized that the work in this thesis deals with mineral fouling only, sometimes referred as scaling. The effects from biological fouling and corrosion were reduced by treating the cooling tower water with a sufficient amount of bleach and azole, which is a chemical additive that prevents corrosion.

CHAPTER III

DESIGN AND CONSTUCTION OF TEST FACILITY

The basic layout of the facility along with all the components used is described in this chapter. The original design of the facility was modified and upgraded several times based on lessons learnt during calibration and preliminary tests. The final version of the water fouling test facility is shown in Figure 3-1.

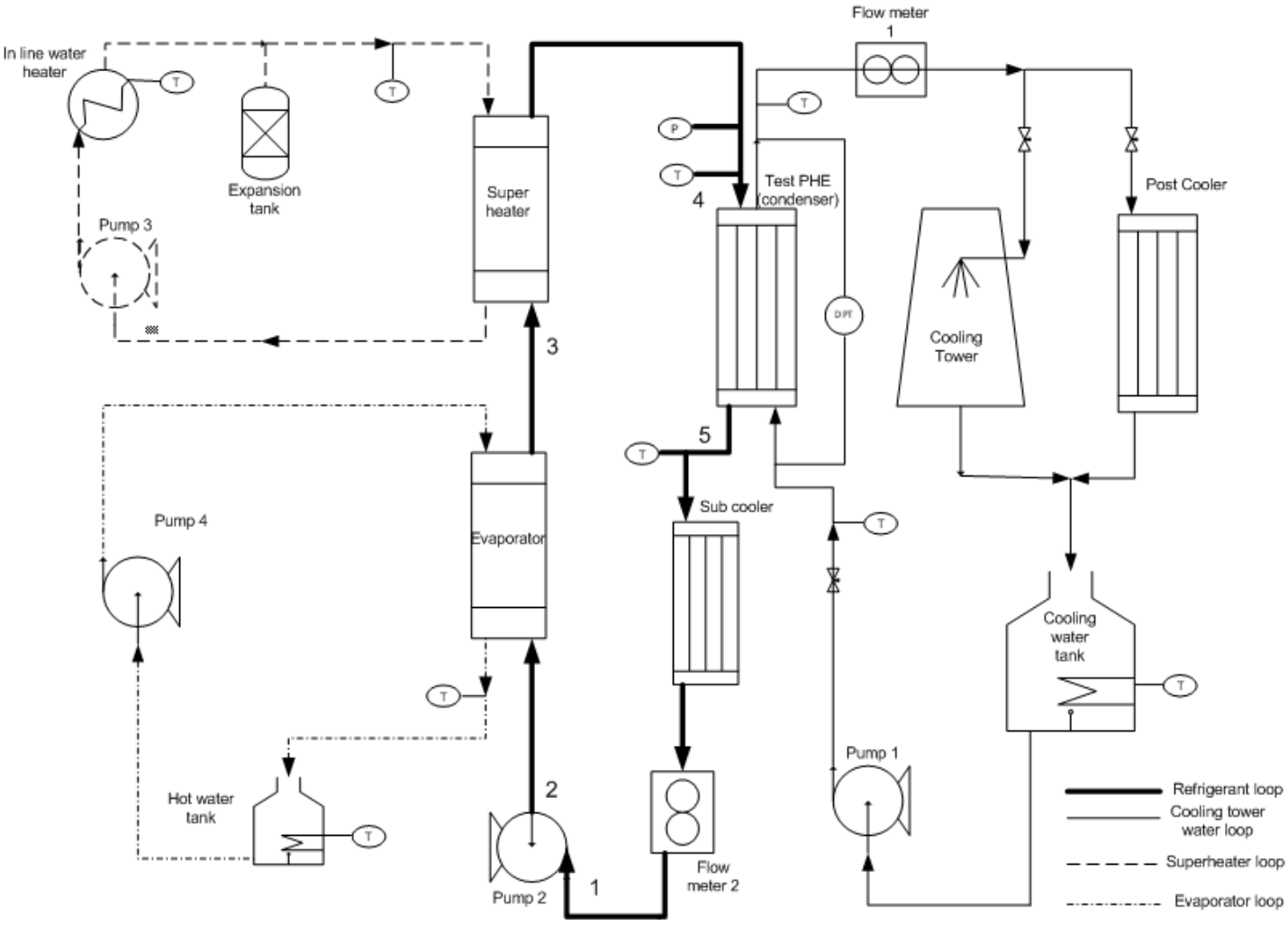

Figure 3-1. Schematic of test facility for the fouling experiments

There are 5 different loops or main piping layouts termed as the cooling tower water loop, refrigerant loop, evaporator loop, superheater loop and the chilled water loop. Typical thermodynamic state points of the refrigerant in the loop are shown in the p-h diagram of Figure 3-2 and in the T-s diagram of Figure 3-3.

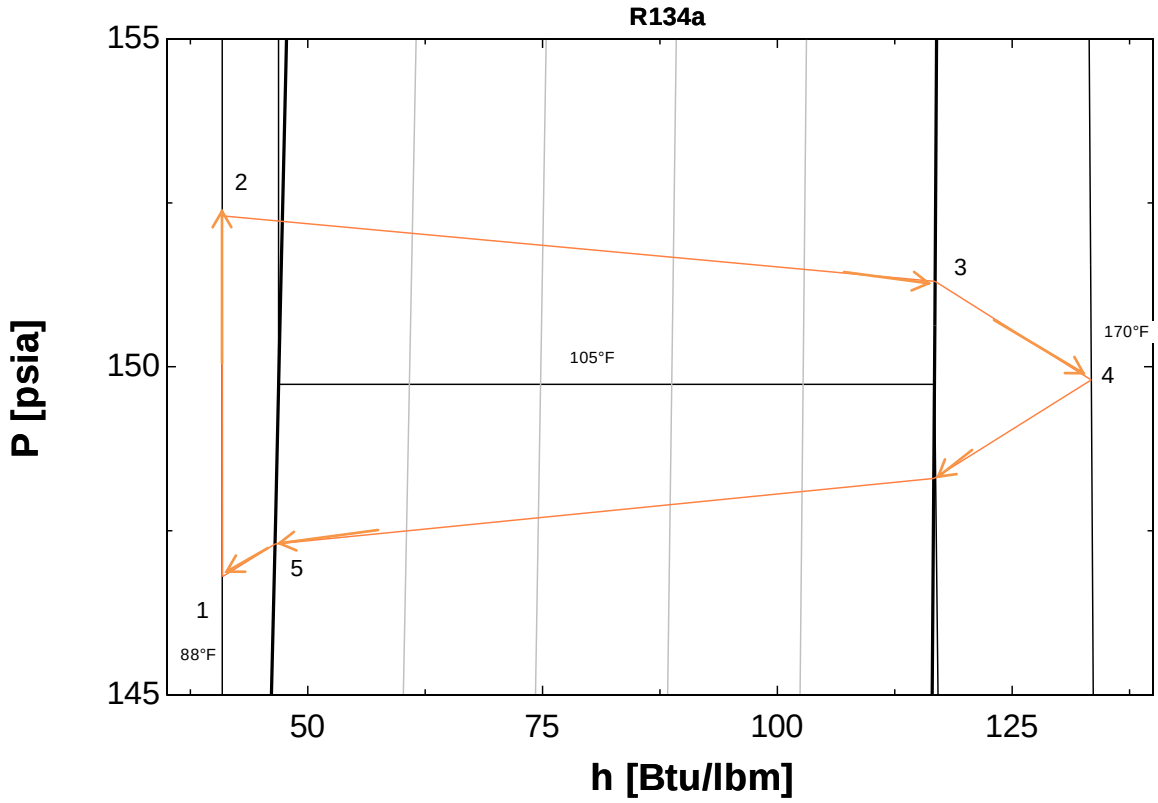

Figure 3-2. R134a P-H Diagram

Subcooled liquid refrigerant enters a pump at about 145 psi. It is pushed at higher pressure toward the evaporator. Referring to the p-h and T-s diagrams of figures 3-2 and 3-3, the refrigerant is at state 1 and 2 before and after the pump, respectively. The pump operates entirely in the subcooled region. The refrigerant then passes through the evaporator from state 2 and exits at state 3 where it is completely dry or slightly superheated. Then it flows through the superheater, process 3-5 where the vapor is superheated to a temperature of 170 ^{0}F before entering the condenser at state 4. The refrigerant exits the condenser at state 5 where is close to the liquid region; in practice the refrigerant may be slightly subcooled or still within the 2 phase region depending on the heat transfer characteristics of the condenser. Finally the refrigerant is passed through a subcooler where it is subcooled about 10 – 15 ^{0}F (process 5-1) before it enters

the pump. It should be noted that in the T-s diagram points 1 and 2 are almost is identical since there is no temperature rise across the pump and the difference in entropy is extremely small.

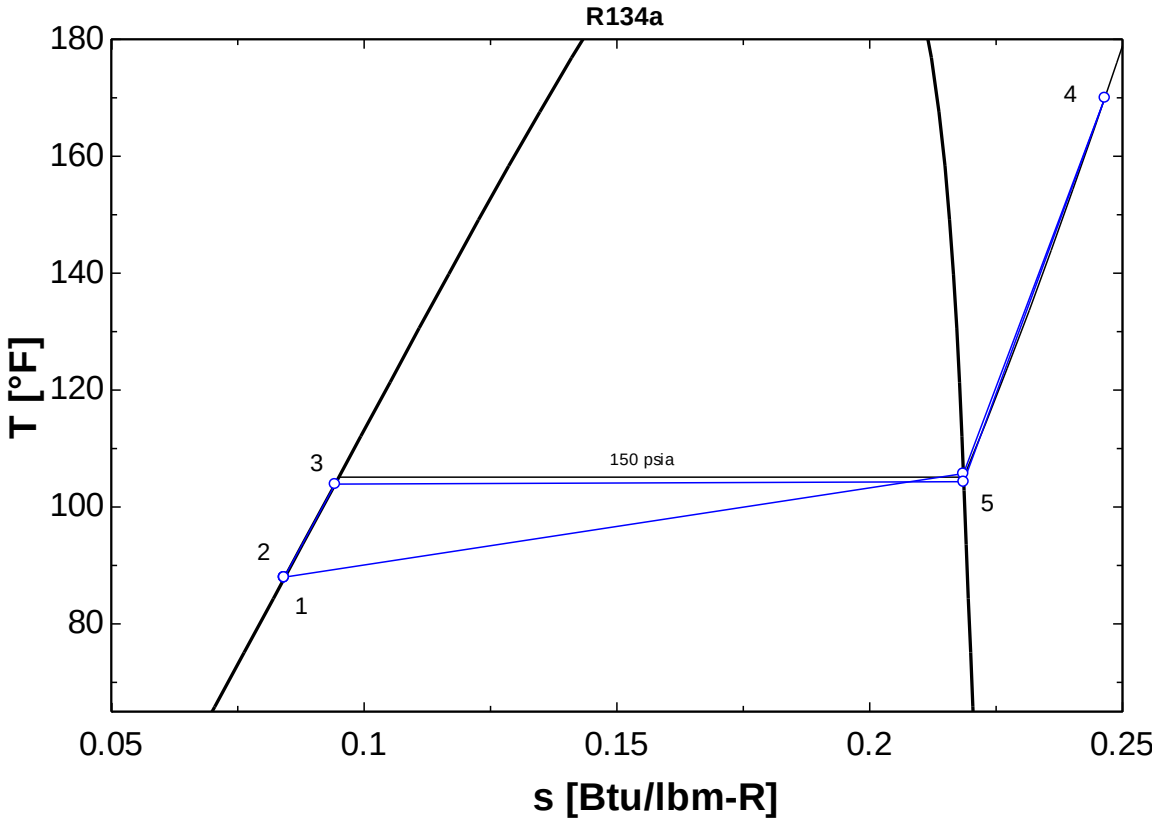

Figure 3-3. R134a T-s Diagram

The first four loops can be seen in figure 3.1 while the chilled water loop is shown separately in Figure 3-8. All the heat exchangers used are of the brazed plate type and are termed as condenser, evaporator, super heater, etc, based on their functioning; details on the heat exchangers are available in Tables 3-1 and 3-2. The entire setup is constructed on a steel stand of about 10 feet length , 3.5 feet wide and 10 feet tall shown in Figure 3-4(a), large amounts of piping, heat exchangers, tanks and pumps were mounted in this stand quickly congesting the available as shown in Figure 3-4(b).

Figure 3-4. Test facility

3.1 Evaporator Loop

Unlike the test facility used by Longo [2008] seen in Figure 2-6, this facility does not have a bladder accumulator connected to a nitrogen tank to control the pressure of refrigerant in the system. The pressure of the refrigerant is controlled by the saturation temperature of condensation and evaporation and by the refrigerant charge.

According to the ideal gas equation:

$PV = mRT$

The pressure of the vapor refrigerant in the system depends on the following three factors:

1. Mass of vapor refrigerant in the system (m)
2. Average Temperature of system (T)
3. Volume of system available for the refrigerant vapor (V)

The following parameters affect the average temperature of the system:

1. Temperature of hot water entering the super heater.
2. Temperature of cooling tower water entering the condenser.
3. Temperature of cooling water entering the refrigerant sub-cooler.

The temperature of hot water entering the super heater is used to control the degree of super heat of the refrigerant while the temperature of cooling tower water entering the condenser is set constant at 85 ^{0}F (29.4 ^{0}C) and the temperature of cooling water entering the sub-cooler depends on the lab chilled water supply and it was in the range of 56 to 62°F.

Figure 3-5 zooms the schematic of the evaporator loop isolated from rest of the facility.

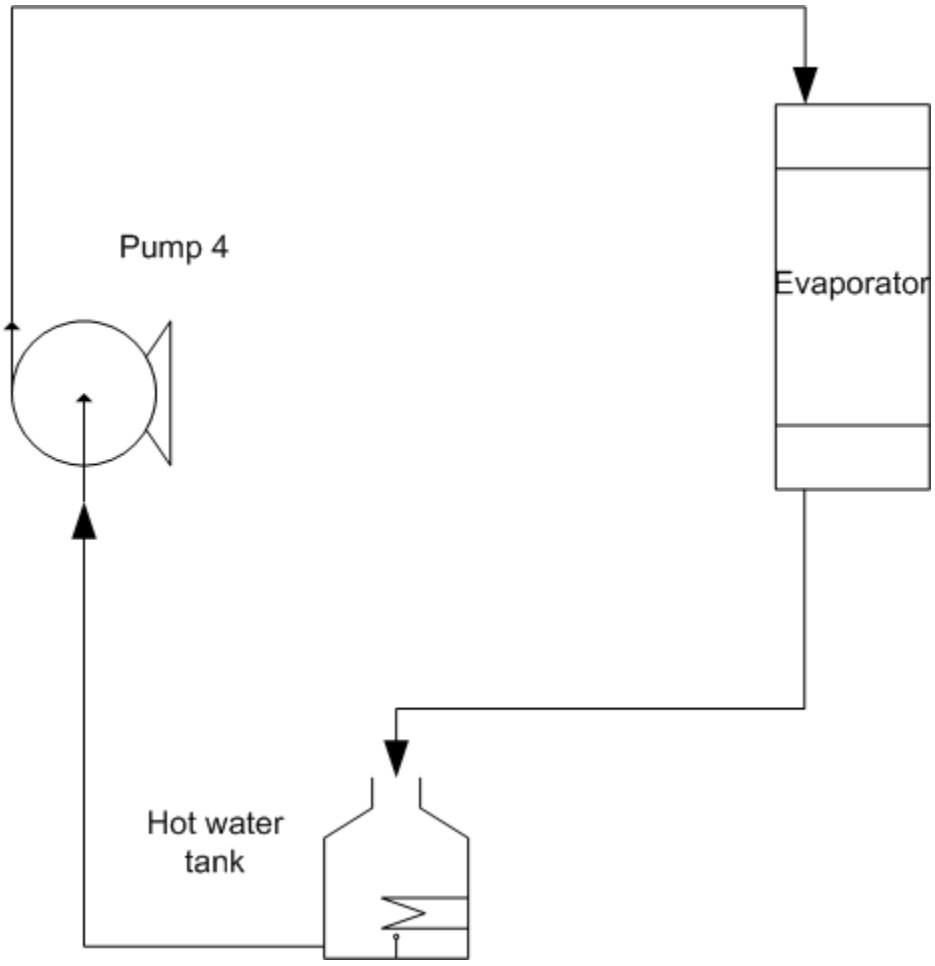

Figure 3-5. Schematic of evaporator loop

Water circulates from the pump, tank, immersion heater and a plate heat exchanger used to evaporate the refrigerant. The pump used is a model 6K582A manufactured by Dayton operating on 115 V single phase at 60 Hz frequency and at 3450 rpm. Since this pump is obsolete the pump curve is not available, based on the temperature differences and heat transfer it is estimated that the flow rate lies between 1 to 2 gpm. The heater used is a model KTLS-33A-036 manufactured by Chromalox which required 480 V, 3 phase power supply and has a 3 kW capacity and was controlled using a Chromalox Minimax SCR proportional controller.

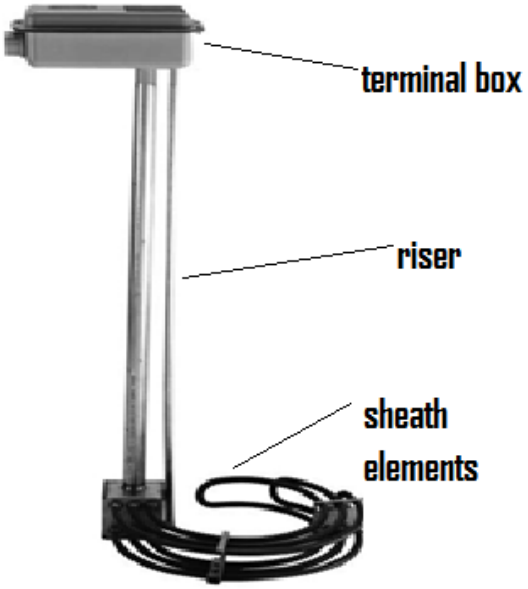

Figure 3-6. Heater

The heater as seen in Figure 3-6 has three stainless steel sheath elements capable of generating 40 W/in^2 heating, a riser which is also made of stainless steel and a moisture resistant thermal enclosure; it can be used for mildly corrosive fluids. Figure 3-7 shows the different components of the evaporator loop as installed in the setup. The piping for this loop is entirely of 1" copper tubing.

Figure 3-7. Components of evaporator Loop

The plate heat exchanger functioning as the evaporator is a model GB400H-44 manufactured by GEA more details of which are available in Table 3-1. A large heat exchanger

is used here because the refrigerant undergoes a phase change in the heat exchanger and a large amount of heating capacity is required due to the latent heat of vaporization. Lastly the tank used has a capacity of 35 gallons and can handle water temperatures up to 120 ^{0}F.

Passing the refrigerant through an additional heat exchanger (evaporator) where it is heated by warm water the temperature of which can be accurately controlled is necessary to have a good control of the refrigerant pressure in the system. Also when there are small leaks in the system the mass of the refrigerant decreases causing a decrease in refrigerant pressure, this can be compensated by increasing the temperature of warm water entering the evaporator which leads to an increase in the average temperature of the system thereby increasing the pressure of refrigerant.

3.2 Superheater Loop

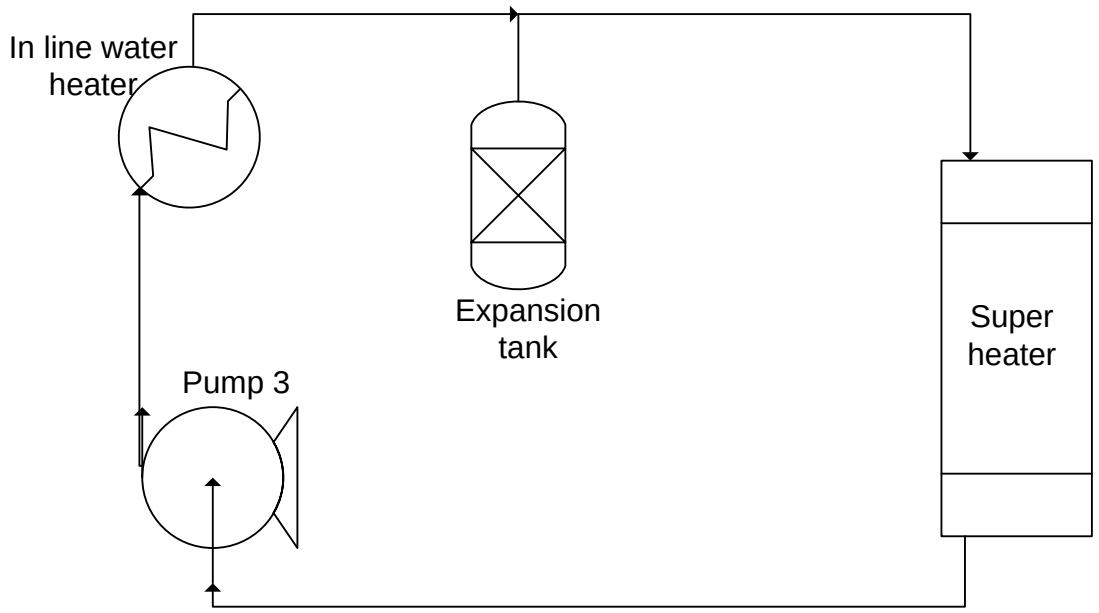

Figure 3-8. Schematic of superheater loop

The function of the super-heater is to accurately control the degree of superheat of the refrigerant entering the condenser. Figure 3-8 shows the schematic of the superheater loop isolated from the rest of the system. The super heater loop consists of a pump, inline heater, expansion tank and plate heat exchanger. This is a closed system and there is no open tank. The higher water temperatures close to the boiling point generate quite a lot of steam in an open tank and the superheated steam might melt the plastic walls of the water tank. While steel tanks can

overcome the latter issue, large amount of steam is not advisable in a laboratory for safety and humidity conditions. Steams will condensate on the cold surfaces providing a humid, wet, and dangerous environment to work in. For these reason a close loop was chosen for the superheater loop. A 1/6 Hp Grundfos – UP – 26 – 99F inline pump is used and it is powered by 115 V single phase. The plate heat exchanger used is a model GB400L-14 manufactured by GEA more details of which are available in Table 3-1. The heater used is a circulation heater manufactured by Chromalox and is a model NWHSRG 06-024P -E1 VersaTherm with a heating capacity of 24 KW, the ports on the heater are provided with 1" female NPT connections and the net weight is 45 lbs. This being a closed loop requires an expansion tank; a Bell and Gosset HFT- 15 expansion tank is used, it has a total volume of 3 gallons and an acceptance volume of 1 gallon, the shell and diaphragm are made up of carbon steel and heavy duty butyl rubber respectively. It is pre charged to 12 psi and can handle pressures up to 100 psi and temperatures up to 240 ^{0}F and has an approximate weight of 5 lbs. The different components of the superheater loop are shown in Figure 3-9.

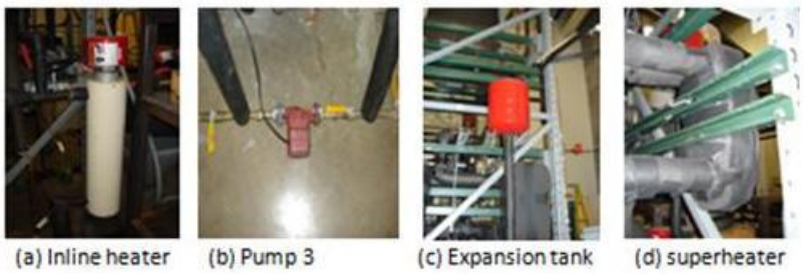

Figure 3-9. Components of superheater loop

3.3 Chilled water loop

The chilled water loop is a close system consisting of 3 plate heat exchangers, a pump, expansion tank and metering valves. A schematic of the chilled water loop is shown in Fig 3-10, the three plate heat exchangers are termed as subcooler, post cooler and chiller. The subcooler is used to cool the liquid refrigerant from the brazed plate condenser below its saturated temperature before entering the refrigeant pump. The degree of subcooling is maintained to 10 to 20°F. This would reduce vapor refrigerant being circulated through the pump. The post cooler is used to cool the cooling tower water exiting the other side of the brazed plate condenser before water is circulated back to the batch tank, which is used as constant temperature water reservoir.

The chiller is connected to the campus chilled water supply, with chilled water entering at 50 ^{0}F and it is used to provide the cooling to the subcooler and the post cooler.

The subcooler and post cooler might be directly connected to the campus chilled water supply eliminating the need for an additional pump and expansion tank; however this is avoided because any leak on the piping will result in a loss of campus chilled water and damage to the building hydronic system. The expansion tank used is a Bell and Gosset HFT-15 similar to the expansion tank used in the super-heater loop. Metering valves are used to control the flow of cooling water into the subcooler and the post cooler. The large number of metering valves in the circuit helps in keeping precise control and making fine adjustments of the cooling water supplied to the post cooler and sub cooler. The pump used is a Dayton 6K818A with a ¾ HP rating operating at 3450 rpm; since this pump is obsolete the pump curves are not available, but based on temperature differences and heat transfer calculations it is estimated the flow rate is between 1.5 to 3 gpm. Figure 3-11 shows the different components of the chilled water loop.

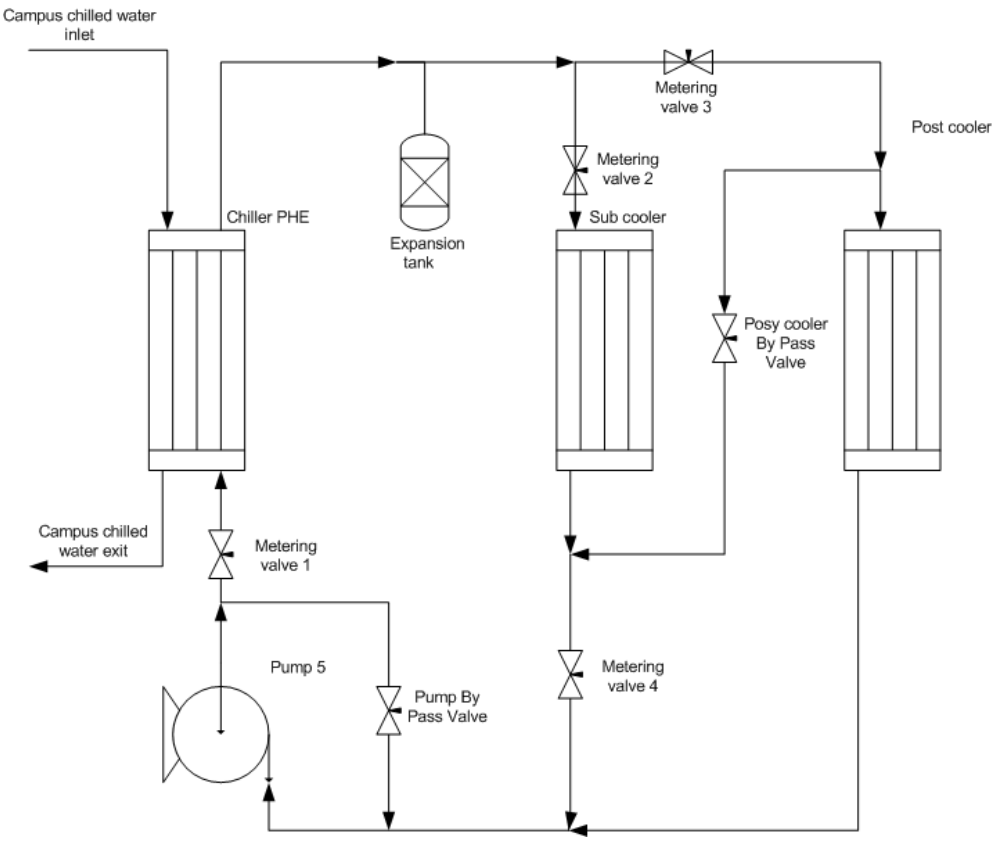

Figure 3-10. Schematic of chilled water loop

Figure 3-11. Components of chilled water loop

3.4 Refrigerant loop

The refrigerant loop consists of a pump, flow meter and four plate heat exchangers as seen in Figure 3-12. While centrifugal pumps are used in the water loops, a gear pump is used for the refrigerant loop. The pump is a model GC-M32-JV5E manufactured by micropump and it is coupled with a Baldor VS1SP variable frequency drive (VFD), more details of the VFD drive are provided in the next chapter. The subcooler is a model GB200H-10 more details about it are provided in Table 3-1. The plate heat exchanger which is to be tested for fouling is used as the condenser; a description of the different test plate heat exchangers is given section 3.6. A model DS025 micromotion coriolis flow meter manufactured by Emerson process management is used to measure the refrigerant flow rate, the flow meter should always be placed close to the exit of the subcooler since it has to have only liquid flowing through it.

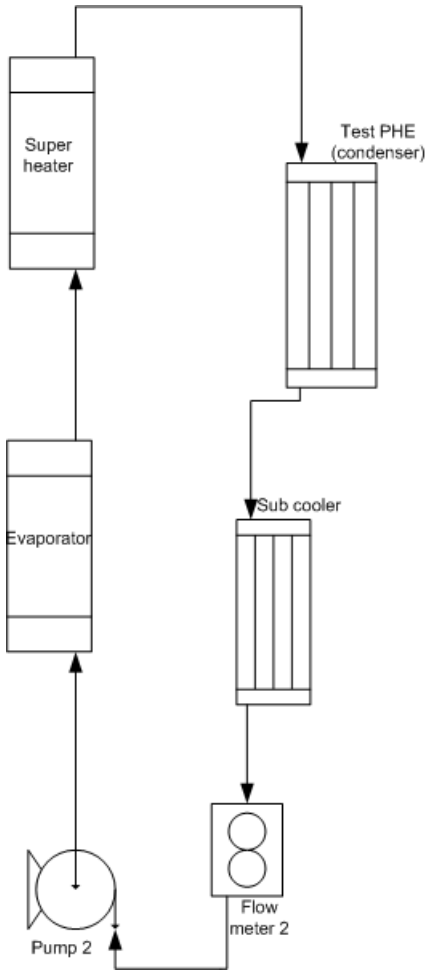

Figure 3-12. Schematic of refrigerant loop

A side glass was installed on the suction line of the refrigerant pump (pump 2) shown in Figure 3-13, to observe the flow of refrigerant and the appearance of vapor bubbles in the flow. If two phase refrigerant is formed by any flashing process due to the pressure drop of the flow meter for example, vapor bubbles can be viewed through the side glass. Excess bubbles will cause cavitation of the pump and they can be avoided by increasing the degree of subcooling in the liquid refrigerant.

Figure 3-13. Refrigerant Pump

3.4.1 Selection of a suitable pump for the refrigerant loop

A centrifugal pump consists of an impeller rotating inside the pump casing, liquid is directed into the center and picked up by the rotating vanes and accelerated to a high velocity. A gear pump consists of two or more rotating gears that mesh together. One of the gears is connected to the power source and it drives the other gears. . During the rotation the volume between the gear teeth diminished and fluid is pumped from the inlet to the exit.

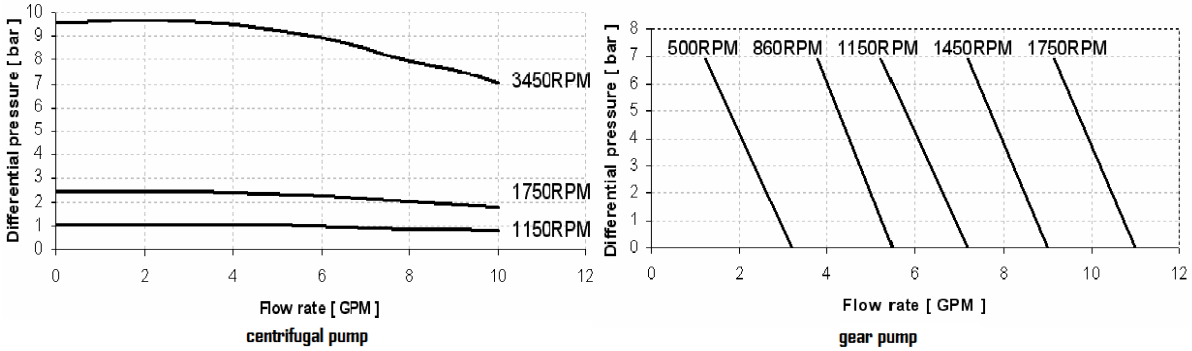

Figure 3-14. Comparison of pump curves

Gear pumps are more suited to systems with high pressure drops operating with fluids having greater viscosity. Figure 3-14 shows the pump curves for both centrifugal and gear pumps. It can be seen that with an increase in pressure the gear pump offers much more stable flow than the

centrifugal pump, this is essential to maintain a constant flow rate as slight changes in refrigerant pressure are likely to occur throughout the running of the facility.

Another feature associated with the selected pump is the magnetic coupling of the pump head to the motor shaft. Most pumps use a dynamic (mechanical) seal on the pump shafts which rely on fine clearances to minimize pump leakage; however these types of seal require cooling and lubrication since they convert friction to heat which can lead to cavitation within the pump resulting in need for over sizing of motor and shorter life. In magnetic coupling there are two magnets, a drive magnet that is attached to the motor shaft and a driven magnet that is completely sealed within the pump head and is connected to the driving gear, the two magnets couple automatically such that the drive magnet turns the driven magnet and gears without physical contact. Also when the load on the pump exceeds the coupling torque decoupling occurs between the two magnets, which acts as a safety feature.

3.5 Cooling tower water loop

Figure 3-15 shows the schematic of the fouling water loop. The main components are the water tank, heater, pumps, test heat exchanger, cooling tower and post cooler and flow meter.

Due to the presence of a large number of heat exchangers in this loop, a relatively high pressure drop is found to occur at low flow rates and hence it is decided to use two pumps connected in series. A single pump would not be able to provide the required head at the desired flow rate and if a single pump, which could provide the required head was used it would provide a much greater flow rate than set point. Two identical high capacity circulating pumps shown in Figure 3-16, model 1400 – 50 –A operating at 3450 rpm manufactured by TACO are connected in series.

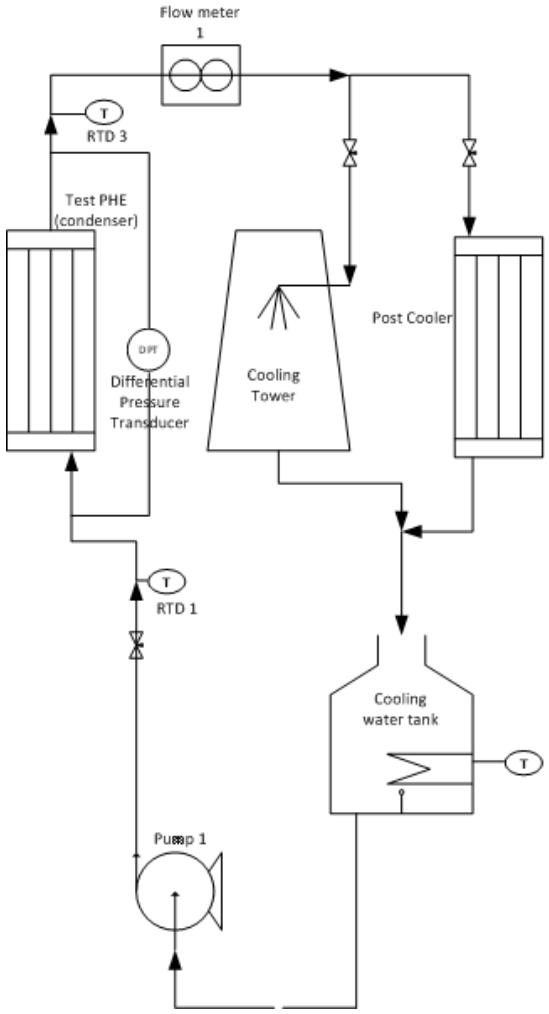

Figure 3-15. Schematic of cooling tower water loop

Figure 3-16. Taco pumps in series

Figure 3-17 shows the pump curves for a single pump and that for two pumps connected in series.

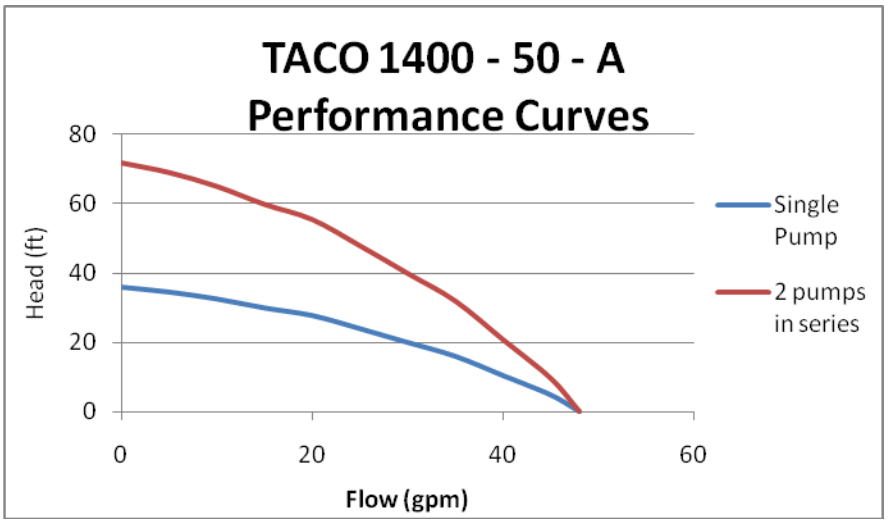

Figure 3-17. Performance Curves

The water post cooler is connected in parallel with a small scale cooling tower. The cooling load is shared between the cooling tower and post cooler and the cooling tower concentrates the minerals in the water through direct air-to-water droplets evaporative process.

This concentration method was key to be able to provide cooling tower water with desired fouling potential, that is, specified amount of minerals saturated and supersaturated in the water. Two metering valves were used to control the flow to the cooling tower and to the post-cooler.

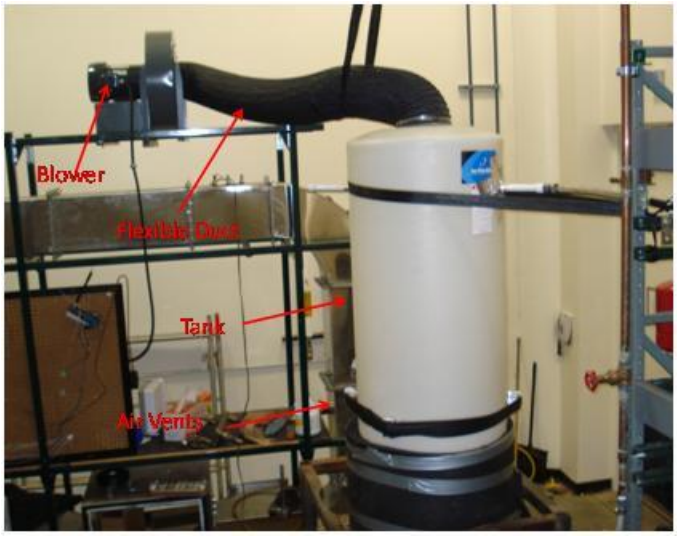

Figure 3-18. Small scale Cooling Tower for laboratory accelerated tests of fouling

The cooling tower as seen in Figure 3-18 consists of a 105 gallon tank, 5 feet tall with a 12” opening at the top. Holes are drilled near the top of the tank to provide for entry of the piping, the end of the pipe are two nozzles which create a fine spray, holes are also drilled along the circumference of the tank 2 feet from the base to provide for entry of air. The opening of the tank is connected to the suction of a 3 HP model 9KX03 Dayton blower operating at 3505 rpm using a flexible Duct.

Figure 3-19. Water batch tank with customized heater

The batch water tank, which is shown in Figure 3-19, acts as constant temperature and constant species concentration water solution reservoir for the fouling experiments. It has a capacity of 150 gallon and it has a KTLS 360A 036 immersion heater manufactured by Chromalox. This heater is identical to the heater used in the evaporator loop except that the sheath elements are larger and it has maximum capacity of 9 kW. The heater is controlled by a PID SCR (silicon controlled rectifier) module, which modulate the heating capacity based on the water temperature entering the test plate heat exchanger.

3.6 Plate Heat Exchangers used in the test facility

The test plate heat exchanger is to be used as a condenser; Refrigerant R134a is to be condensed using cooling tower water. Four different heat exchangers are to be tested one at a time to measure the variation in fouling resistance and pressure drop with time. Figure 3-20 shows the 4 different heat exchangers that are to be tested. All the plate heat exchangers are manufactured by GEA, Table 3-1 lists the specifications of the all the plate heat exchangers used in the test facility excluding the condensers which is listed in Table 3-2 in greater detail.

Table 3-1. Heat exchanger specifications

	Model	No of plates	Heat transfer area [Nominal Surface] (ft^2)	Minimum heat transfer capacity (Btu/hr)
Postcooler	GB400H	20	6.9	21000
Subcooler	GB200H	10	1.5	1100
Superheater	GB400L	14	4.6	6500
Evaporator	GB400H	44	16.1	15750
Campus Chiller water loop	FP5x12	14	4.6	22100

Figure 3-20. Test plate heat exchangers - Condenser-type brazed plate heat exchanger

Table 3-2. Test heat exchanger (condenser) specifications

	PHE A	PHE B	PHE C	PHE C
Length (a) [in]	13.29	13.29	21.02	20.3
Width (b) [in]	5.08	5.08	5.08	9.8
Protracted Length (Lp) [in]	11.06	11.06	18.82	17
Number of plates	14	14	8	6
Heat Transfer Ares [ft^2]	4.6	4.6	3.9	5.3
Volume Side A [ft^3]	0.018	0.018	0.015	0.017
Volume Side B [ft^3]	0.021	0.021	0.016	0.026
Chevron Angle (degrees from flow direction)	30	63	63	63
Corrugation Depth [in]	0.079	0.079	0.079	0.079
Corrugation Pitch transverse to ribs [in]	0.236	0.236	0.236	0.25
Max operating pressure [psi]	300	450	450	450
Max operating temperature [F]	350	350	350	350

3.7 Problems encountered with design and construction of test facility and lessons learnt

The initial design of the system was almost completely different from the final version of the system because several practical issues occurred during preliminary calibration and testing of the experimental set up. They are briefly mentioned here to justify some of the choices that were made for the final version of the facility.

3.7.1 Leaks on the refrigerant loop

Probably the most difficult and time consuming problem encountered during the construction of this facility were leaks on the refrigerant loop. Unlike the water loop which runs at relatively low pressures, the refrigerant loop has to operate at pressures up to 200 psi and even an extremely small leak would cause the refrigerant pressure to decay with time. In order to ensure that the loop was leak free, compressed nitrogen was pumped into it, the presence of a

large number of threaded joints and unions was responsible for most leaks. Large leaks could be identified by a hissing sound emanating from the point of the leak; smaller leaks are identified by applying a fluorescent leak detector solution on the joints and fittings, presence of bubbles indicates a leak. Once these leaks are eliminated the system would be left pressurized at around 220 psi overnight. If any extremely small leaks were present the pressure would drop, the system would then have to be charged to pressures around 300- 350 psi so that the leak can be identified by the leak detector solution.

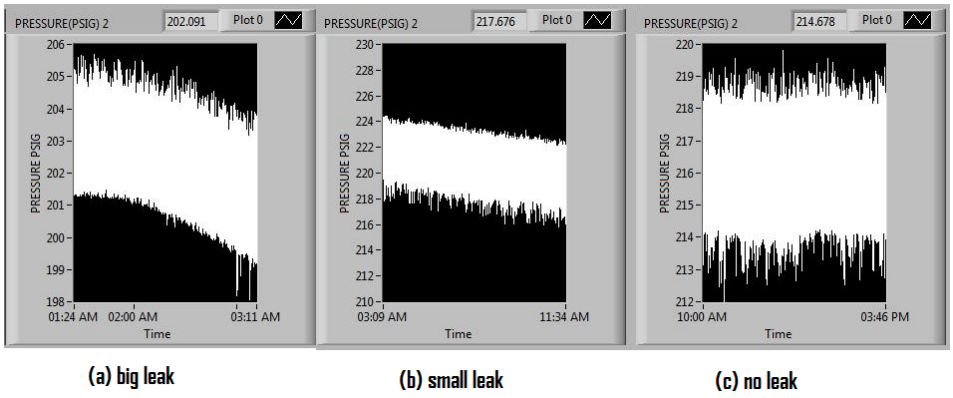

Figure 3-21. Leak Check

Figure 3-21 shows plots of pressure versus time when the system has a large, small and no leak. A large leak is represented by a curve, while a small leak is represented by a line with a declining slope and an almost straight line represents no leak. Small fluctuations are present due to changes in pressure corresponding to changes in ambient conditions and due to noise in the data acquisition system.

3.7.2 Cavitation of refrigerant pump

Cavitation is a condition that occurs within a pump when the fluid being pumped experiences a pressure drop and is converted to the vapor stage, i.e the fluid is in the vapor phase at the pump inlet. In the initial design of the setup the refrigerant pump was placed close to the subcooler but above it. In theory the pump should not cavitate as the refrigerant loop is a closed system and the location of the pump should not be a problem. However when the refrigerant is charged it is in two phase, the liquid tends to settle at the bottom and the vapor at the top. The pump being placed above the subcooler had vapor being present in the pump inlet leading to cavitation. This was overcome by placing the pump below the subcooler at the lowest point of the loop so only liquid was present at the inlet of the pump.

3.7.3 Melting of water tank of superheated loop

In the initial design of the superheater loop a water tank made of composite material capable of withstanding temperatures up to 212 ^{0}F was used with a 9 KW immersion heater in it and a lid on top, similar to the setup of the evaporator loop. To reach the desired level of superheat on the refrigerant side it was determined that the water in the tank had to be heated to 185 ^{0}F. The process of heating the water to 180 ^{0}F resulted in the formation of steam at temperatures higher than what the tank could handle, this resulted in a portion of the tank being melted. To fix this problem, the tank and immersion heater were replaced with a circulation heater forming a closed system, hence any steam formed will remain within the system. Figure 3-22 shows the schematic of the original and upgraded designs.

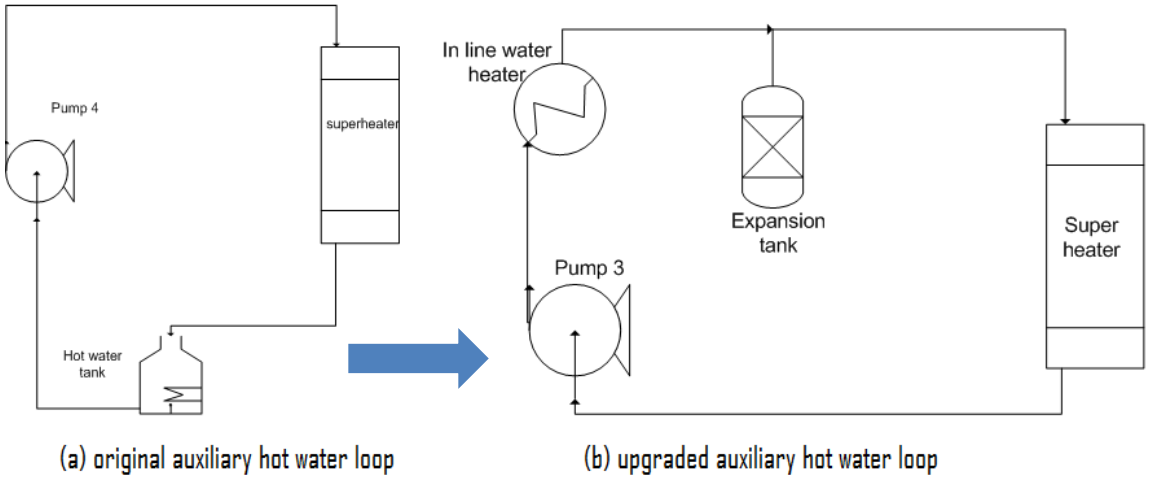

Figure 3-22. Schematic of original hot water auxiliary loop and upgraded loop designs

3.7.4 Testing two heat exchangers simultaneously

Because the fouling experiments are very time consuming tests, the original plan was to test two heat exchangers simultaneously by connecting them in parallel. However, after preliminary tests it was concluded that running two or multiple plate heat exchangers in parallel is not feasible due to the following reasons:

1. It is not possible to achieve the same refrigerant flow rate, inlet temperature and pressure at the inlet of both heat exchangers and is unadvisable since the fouling resistance is found to depend largely on the refrigerant pressure.
2. The cooling capacity available on the campus chilled water does not provide sufficient cooling to the fouling water and subcooling to the refrigerant when two heat exchangers are being tested simultaneously.
3. Under fouling conditions the pressure drop across on the water side of the heat exchangers increases and the pumps are not able to provide the additional head required which results in a decrease in the water flow rate.

CHAPTER IV
CALIBRATION AND CONTROL OF FACILITY

This chapter contains a brief description of the data acquisition systems, the different measurement and control devices used including the calibration and detailed uncertainty analysis on the fouling resistance.

4.1 Measurement and Control Devices

1. Flow meters

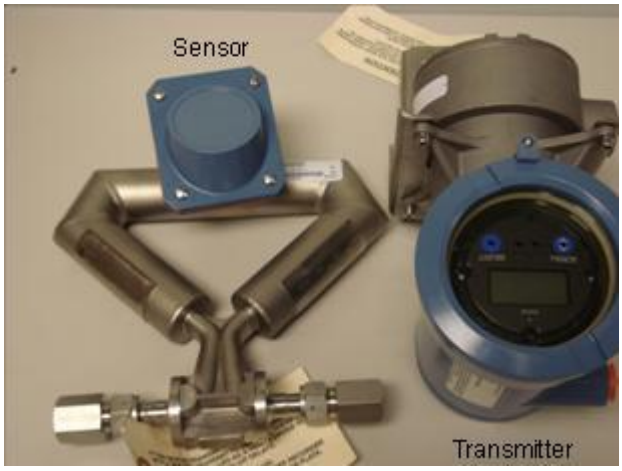

Figure 4-1. Flow meter

There are two flow meters used in the facility to measure the water and refrigerant flow rates. The flow meter consists of two components a sensor and a transmitter as shown in Figure 4-1. It measure fluid flow based on the coriolis force, which arises when a fluid is moving within a rotating frame of reference. The rotation produces an angular outward acceleration together with a linear velocity to define the coriolis force which is proportional to the flow rate of the fluid. The sensor contains oscillating flow tubes and the transmitter controls the oscillations and analyzes the results.

The flow meter used to measure refrigerant flow rate consists of a model DS025S119SU sensor and a model RFT9739E1SUJ transmitter, capable of measuring flow rates up to 11.33

kg/min, the standard uncertainty on the flow meter is ± 0.03 %. Figure 4-2 shows the error associated with the flow meter at different flow rates.

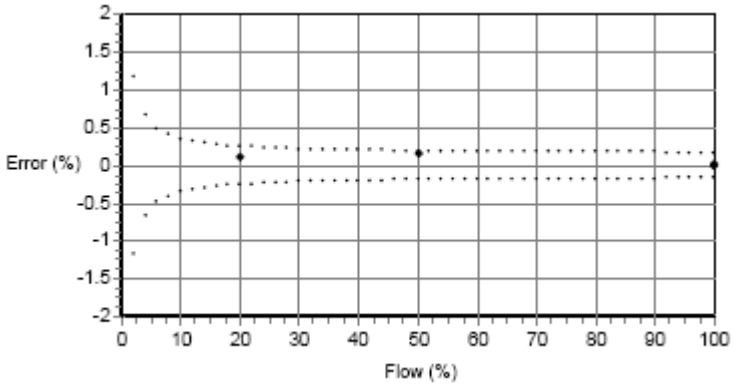

Figure 4-2. Flow meter Calibration

The flow meter used to measure the water flow rate has a model CMF025M319 sensor and a model 2700C12 transmitter, it can measure flow rates up to 18.14 kg/min and has a standard uncertainty of ± 0.03 % similar to the refrigerant flow meter. The transmitter outputs a current, ranging between 4 and 20 mA, 4 mA being no flow and 20 mA being the maximum flow capacity of the flow meter. The flow rate varies linearly between the limits and by using a linear equation fit the flow rate is computed in the data acquisition program.

2. Pressure Transducer

Figure 4-3. Pressure Transducer

The pressure transducer is used to measure the pressure of the refrigerant entering the test heat exchanger (condenser), the saturation temperature of the refrigerant is computed from the measured pressure. A model 207 setra pressure transducer shown in Fig 4-3 is used; it can measure pressures up to 250 psi with an accuracy of ± 0.13 %. The pressure transducer requires a power excitation between 12-24 VDC and the output is a voltage varying between 0.1 (minimum value) and 5.1 (maximum value) volts. The pressure follows a linear relationship with the voltage and is computed using a simple linear equation fit in the data acquisition program. Even though the pressure transducer virtually accepts a range of power excitation DC voltage, it was found that the actual value of the power excitation slightly affects the output signal of the pressure transducer. While the fluctuation of pressure might not be significant they are large enough to impact the measurement of the fouling resistance in brazed plate heat exchangers. For this reason, a dedicated power supply with adjustable voltage and current controls was used to power the pressure transducers. The power excitation was set to 13 VDC at all time and the current to the transducer was less than 0.75 amp.

3. Differential Pressure Transducer

A differential pressure transducer is used in the setup to measure the pressure drop across the water side of the test heat exchanger (condenser). A validyne model P855 differential pressure transducer shown in Figure 4-4 is used; it has an accuracy of 0.1% of full scale. The pressure transducer requires an excitation of 7-55 VDC and it outputs a current ranging between 4-20 mA.

Figure 4-4. Differential Pressure Transducer

4. Variable Frequency Drive

A variable frequency drive (VFD) is used to control the speed of the refrigerant pump in order to maintain a constant flow rate. For incompressible fluids like water the flow rate can be controlled using metering valves, for refrigerant when a certain flow rate and pressure is required, use of a metering valve to control flow rate will cause a drop in pressure, or using a metering valve to control the pressure will cause a change in the flow rate, hence to achieve a certain flow rate and pressure, a metering valve is used to achieve the pressure and a VFD drive is used to achieve the flow rate.

Figure 4-5. Baldor VFD Drive

A Baldor VS1SP21-1B drive shown in Figure 4-5 with a 2 HP rating requiring 240V input is used. An input voltage ranging between 0 - 10 V is supplied to the drive by the Lab View system used for data acquisition and control, the speed varies linearly with the voltage, 10 V corresponding to the maximum speed of 3450 rpm.

5. Heater Controls

Each heater in this facility is controlled by a Minimax 2, three phase, 2 leg SCR power pack controller, which is shown in Figure 4-6. The controller receives an input voltage from the LabView program. The input voltage ranges between 0 and 10 V with 0 being no power supplied to the heater and 10 V enables the heater to operate at its maximum capacity. A PID control

determines the input voltage to the controller based on the temperature difference between the actual temperature and the set point temperature. Each heater has specific PID factors, the default values provided by the Lab View software were used, the proportional gain of the controller was set to 1, the integral time 0.01 minutes and the derivative time to 0 minutes.

Figure 4-6. SCR power pack

6. Temperature Measurement

The facility has 5 RTDs and 4 thermocouples, of these only two of the RTD's are used to determine the fouling resistance, the rest are used to control the heaters. Three of the four thermocouples are of the T-type and the other is a J-Type. Calibration of the two RTD's was done twice over the course of the project. During the first calibration the exact range of operating temperatures was not known and to be safe the RTD's were calibrated within 26 – 45 ^{0}C (~ 78 – 113 ^{0}F). Figure 4-7 shows the error for both RTDs in the calibrated range. RTD 1 used to measure the temperature of water entering the test plate heat exchanger had a maximum error of 0.0287 ^{0}C (~0.052 ^{0}F) and RTD 3 that measures the temperature of water exiting the test plate heat exchanger had a maximum error of 0.06 ^{0}C (~0.11 ^{0}F).

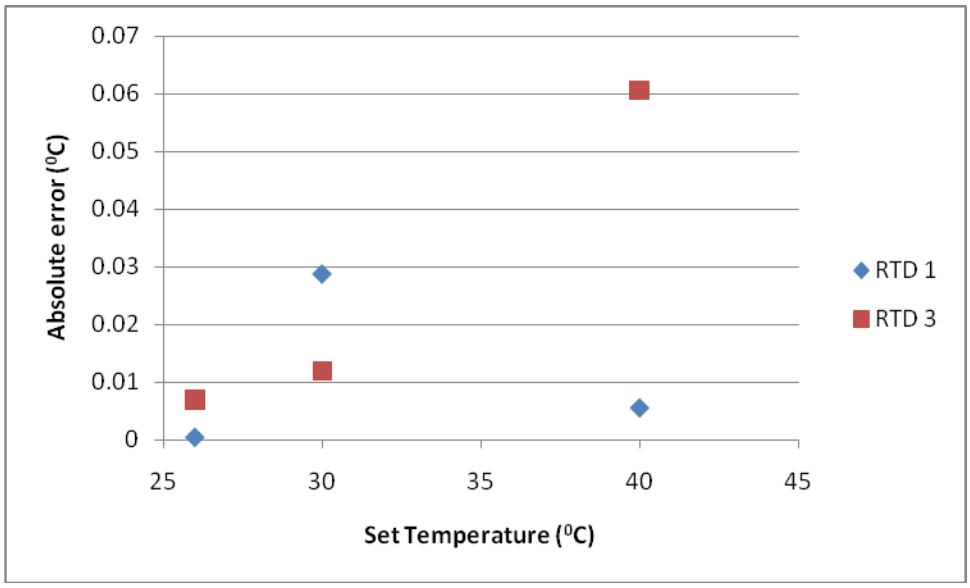

Figure 4-7. Calibration 1

The second calibration was done after the completion of two tests, at this point a better idea of the operating temperatures was known and the RTDs were calibrated within a closer range of their expected operating temperature. This technique allowed to improve the accuracy of the RTDs. RTD 1 was calibrated between 28.3 – 30.6 ^{0}C (~ 82.9 – 87 ^{0}F) and had a maximum error of 0.01 ^{0}C (~0.019 ^{0}F) while RTD 3 was calibrated within 31.1 – 35.6 ^{0}C (~ 88 – 96 ^{0}F) and had a maximum error of 0.011 ^{0}C (~0.02 ^{0}F), figure 4-8 shows the error during calibration for both RTDs.

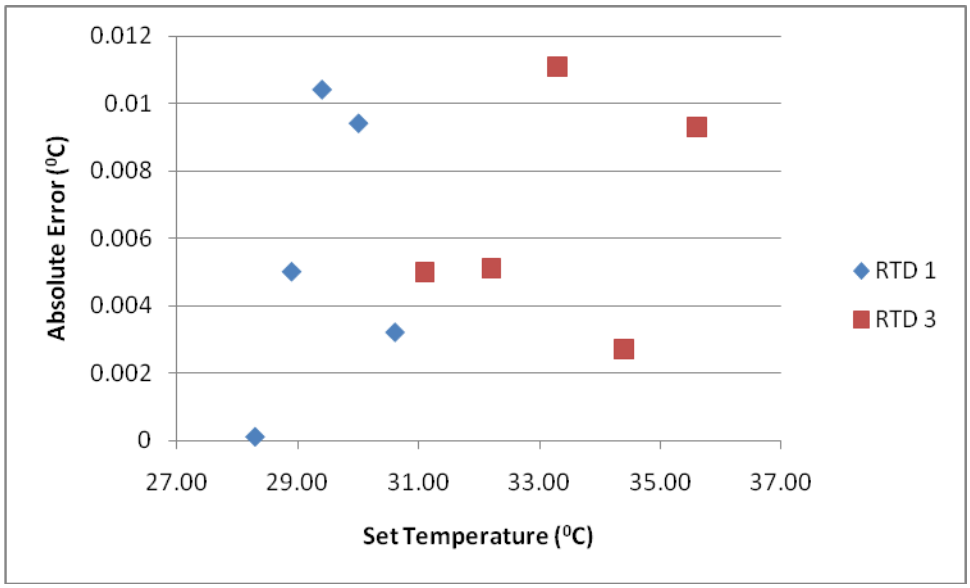

Figure 4-8. Calibration 2

4.2 Data acquisition and Control systems

The data acquisition and control systems for the facility consist mainly of 3 parts, a SCXI module and, a PXI computer from National Instruments and LabView software.

1. SCXI

SCXI stands for Signal Conditioning and Extension for Instrumentation; it is a high performance signal conditioning and switching platform for measurement and automation systems. It consists of multichannel signal conditioning modules installed in a rugged chassis; the modules are capable of taking measurements from a wide variety of sensor and signal types like temperature, sound, strain, etc. Figure 4-9 shows the model 1000 SCXI manufactured by National Instruments that is used in this setup.

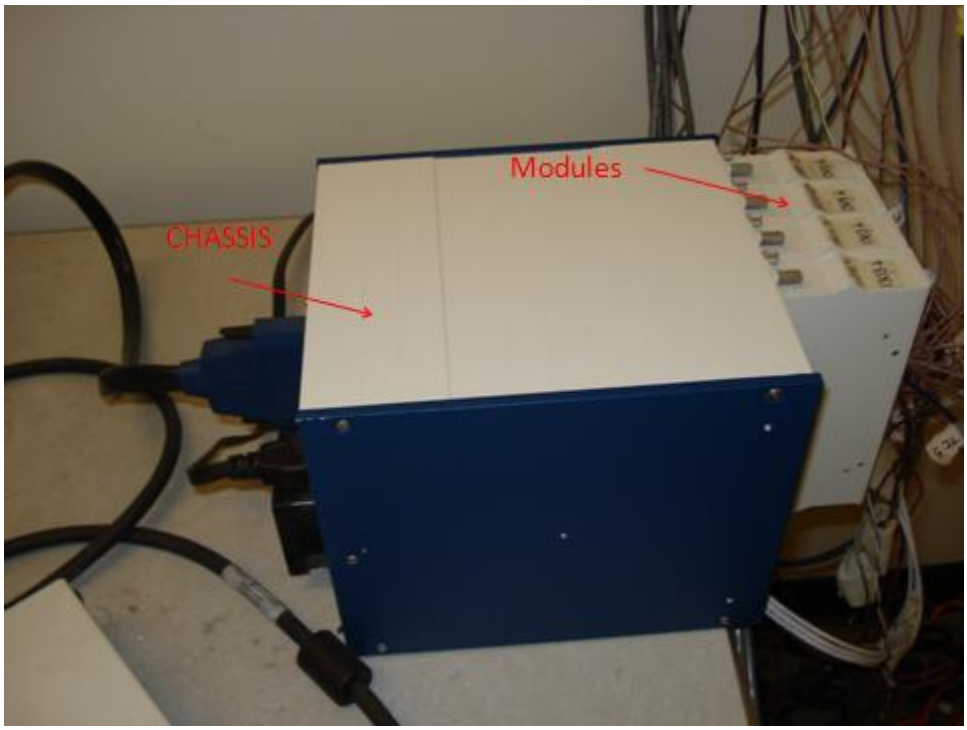

Figure 4-9. SCXI

2. PXI

A PXI is basically a PCI extension for instrumentation that offers a high performance low cost solution for measurement and automation systems. A PCI (Peripheral Component Interconnect) is a computer bus for attaching hardware devices in a computer. A compactPCI system is a Eurocard based industrial computer where all boards are connected via a PCI backplane. PXI combines the PCI electrical bus with rugged, modular Eurocard packaging for

CompactPCI and adds specialized synchronizing buses and software packages. A PXI is composed of three parts, a chassis, system controller and peripheral modules. The PXI used in this project is manufactured by National Instruments and the model NI PXI-1031 (shown in Figure 4-10).

Figure 4-10. PXI

3. Lab View Program

Lab View is a graphical programming environment used to develop sophisticated measurement, test and control systems using graphical icons and wires resembling a flowchart. The Lab View program consists of two windows, a front panel and a block diagram as shown in Figure 4-11. The front panel contains controls and indicators which enable the operator to input or extract data from the program. The block diagram contains the code for all the controls and indicators located on the front panel, the code is usually graphical, front panel indicators and controls appear as terminals on the block diagrams.

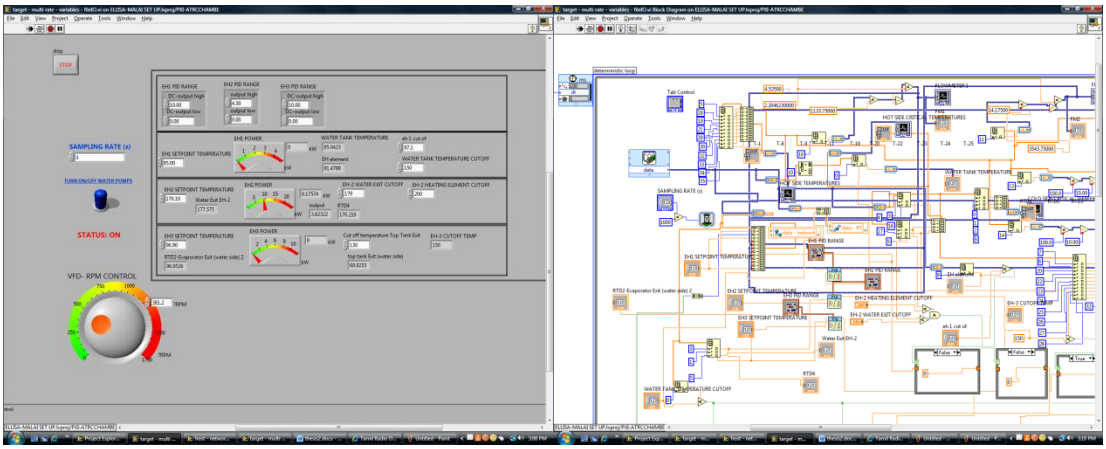

(a) **(b)**

Figure 4-11. Labview program Front Panel (a) and Block Diagram (b)

LabView was selected for the data acquisition system because its robustness during operation, high sample rate, easiness to program and maintain the code, flexibility for modifications and expansion, and user-friendly graphic interfaces. Real Time, an additional module of the LabView platform, was used for the controls system because of the high sample rate, robustness of the program during operation, and easiness of integration with PXI and SCXI systems.

4.3 Monitoring and Control of test facility

All the controls and indicators required for running of the facility are found in the front panel of the LabView program. The refrigerant flow rate is viewed in a wave form chart and controlled manually by adjusting the speed of the pump using the VFD control shown in Figure 4-12.

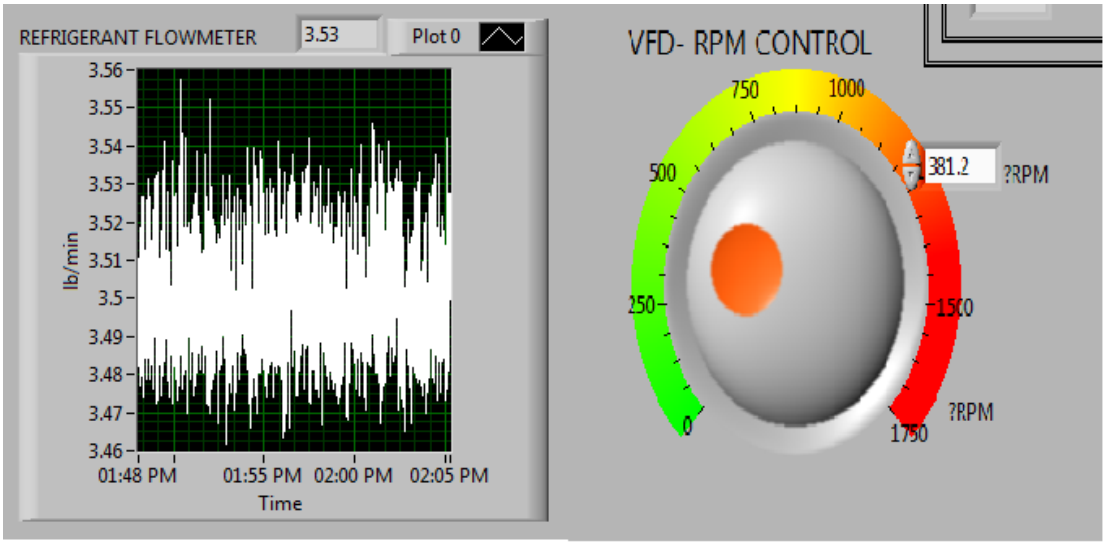

Figure 4-12. Refrigerant Flow control

The fouling water flow rate is controlled by adjusting a number of metering valves provided on the water loop; the total flow rate is measured by the flow meter and is displayed on a wave form chart shown in Figure 4-13. However the flow being sent to the cooling tower needs to be measured manually using a stop watch and monitoring the level in the cooling tower, around 25% of the total flow, that is roughly 1gpm, needs to be sent to the cooling tower for water evaporation and concentration. The TACO pumps used in the cooling tower water loop are connected to a solid state switch as a safety measure and can be turned on and off using the LabView program.

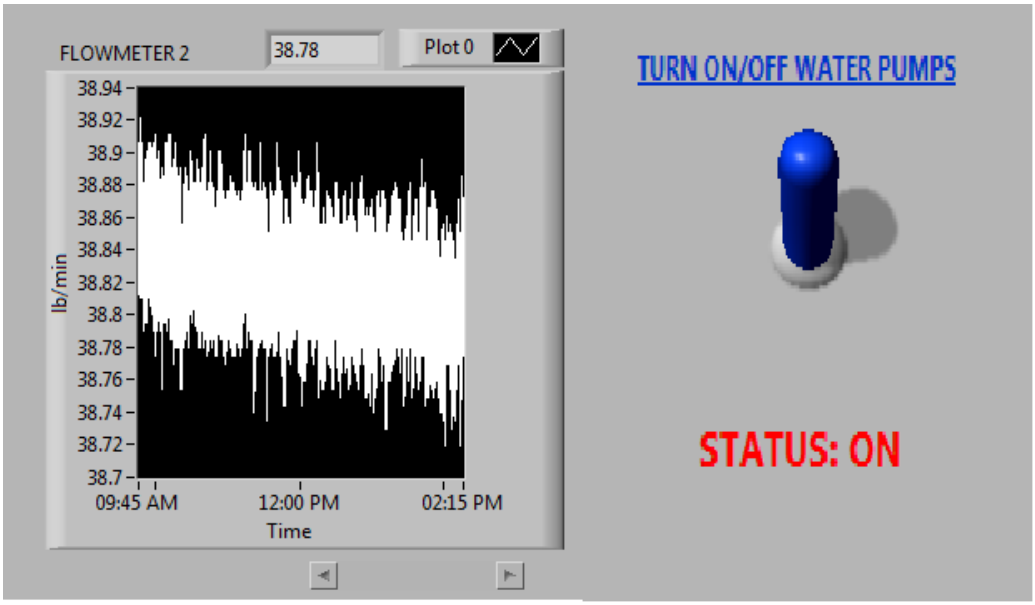

Figure 4-13. Water flow control

The temperature of cooling tower water entering the test heat exchanger (condenser) is kept constant using a PID control built in the LabView program to control the 6 kW heater located in the batch tank. The temperature and pressure of refrigerant entering the test heat exchanger are controlled using PID controls on the 24 kW inline water heater located in the super heater loop and the 3 kW heater in the evaporator loop. Manual adjustments of set point temperature, element cut off temperature and maximum power supplied to the heaters need to be made as shown in Figure 4-14 for effective control of process variables.

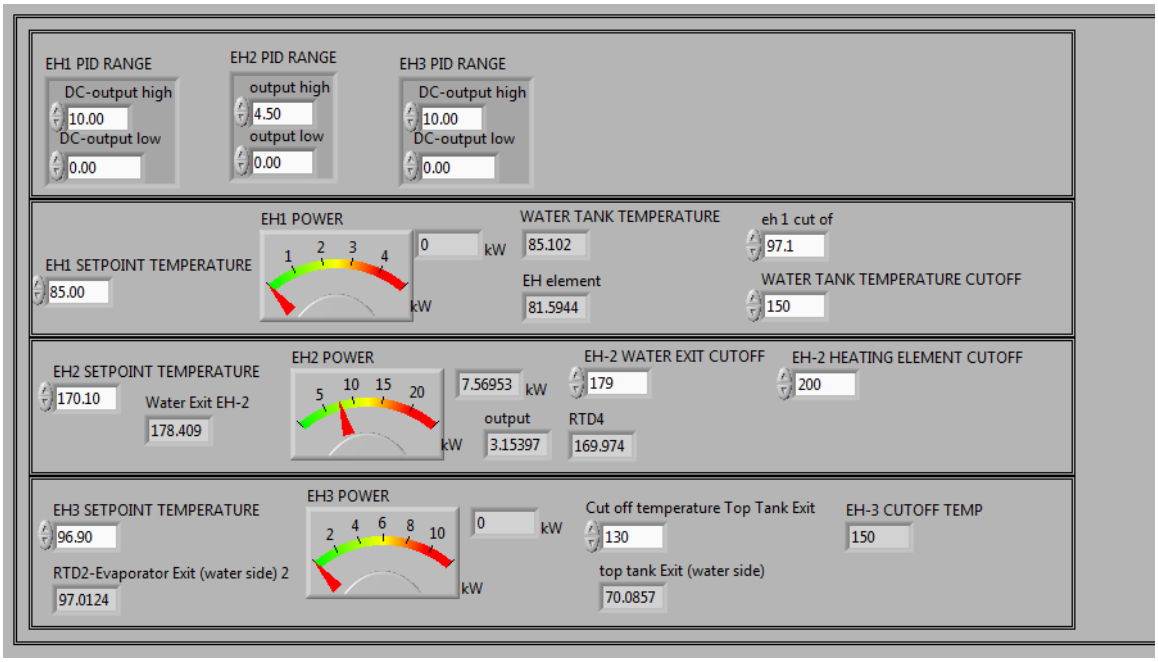

Figure 4-14. Heater controls

The cooling supplied to the post cooler and sub cooler is controlled by adjusting the metering valves provided in the chilled water loop. About 10 - 20 ^{0}F of subcooling are needed on the refrigerant side to prevent cavitation of the pump, excessive subcooling will result in a drop in the system pressure which needs to be compensated by increasing the heating capacity in the evaporator.

4.4 Data reduction of Fouling Resistance in Brazed-type plate Condensers

The data reduction for fouling resistance in brazed plate heat exchangers was carried out similarly to the steps of Table 4-1. The logarithmic mean temperature difference is based on refrigerant saturation temperature in agreement with AHRI standard 450 [2007]. The heat

transfer surface area of the heat exchanger (A) is obtained from the manufacturer and the saturation temperature ($Tsat_{)}$ is calculated from the saturation pressure (P_{sat}.)

Table 4-1. Measuring Fouling Resistance

Step 1:	At initial time t=0 measure m_c, $\Delta T_{w,c}$, P_{sat}
Step 2:	Calculate UA_c as follows: $Q_c = m_c \times C_p \times \Delta T_{w,c}$ $LMTD_c = \frac{\Delta T_{w,c}}{\ln[\frac{T_{sat} - T_{w,c,o} + \Delta T_{w,c}}{T_{sat} - T_{w,c,o}}]}$ $UA_c = Q_c / LMTD_c$
Step 3:	At initial time t=t measure m_f, $\Delta T_{w,f}$, P_{sat}
Step 4:	Calculate UA_f as follows: $Q_f = m_f \times C_p \times \Delta T_{w,f}$ $LMTD_f = \frac{\Delta T_{w,f}}{\ln[\frac{T_{sat} - T_{w,f,o} + \Delta T_{w,f}}{T_{sat} - T_{w,f,o}}]}$ $UA_f = Q_f / LMTD_f$
Step 5:	Compute the fouling resistance R_f as follows: $R_f = A\,(\left(\frac{1}{UA_f}\right) - \left(\frac{1}{UA_c}\right))$

4.5 Uncertainty Analysis

The uncertainty analysis was performed using Engineering Equation solver (EES) [2006]. Initially a model of the condenser was created in EES with water flow rates, water temperatures, refrigerant flow rates and pressures under clean and fouled conditions as inputs. The model outputs are the UA factor, the LMTD and the fouling resistance of the plate heat exchanger. The water inlet temperatures under clean and fouled conditions was taken as 85 ^{0}F (29.4 ^{0}C), the water exit temperature under clean conditions was assumed to be 95 ^{0}F (35 ^{0}C) resulting in a water temperature rise (ΔT) of 10 ^{0}F (5.6 ^{0}C) across the heat exchanger and the refrigerant saturation temperature was taken as 105 ^{0}F (40.6 ^{0}C). The water and refrigerant temperatures correspond to a standard rating condition 2 listed in AHRI standard 450 [2007]. The water flow

rate to achieve the required temperatures was computed from software provided by the heat exchanger manufacturer, it was found to be 38.8 lbm/min (17.63 kg/min), and in volumetric terms around 4.7 gpm. The fouling resistance was computed with water exit temperatures ranging from 95 – 90 ^{0}F (35 – 32.2 ^{0}C) assuming that the temperature difference due to fouling (ΔT_f) varies between 0 – 5 ^{0}F (0 – 2.8 ^{0}C). Figure 4-15 shows a plot of the predicted fouling resistance in EES versus exiting water temperature difference between clean and fouled conditions.

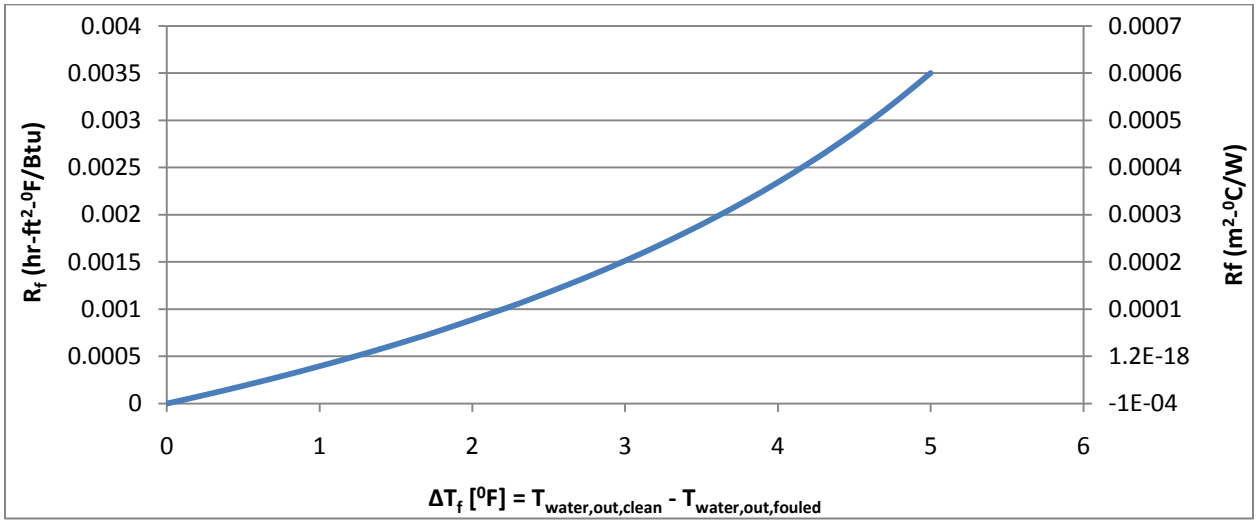

Figure 4-15. Fouling Resistance Vs Exiting water temperature difference between clean and fouled conditions

The accuracy of the measurement devices used in the fouling experiments is listed in Table 4-2.

Table 4-2. Accuracy of measurement devices

	RANGE	Accuracy		Uncertainty type
Flow rate	4.5 - 4.8 gpm	0.05	%	Relative
Pressure	145 to 155 psi	0.33	psi	Absolute
Temperature	85 - 95°F			
(RDTs)		0.11	F	Absolute

The overall uncertainty in the fouling resistance was calculated in EES and using Taylor's Series uncertainty propagation. The method defines the uncertainty as follows: Assume that a dependent variable Y is a function of several variables X_i:

$$Y = f(X_1, X_2, \ldots, X_n) \tag{3.1}$$

Each X_i has an associated uncertainty U_{xi}, that is, $X_i \pm U_{xi.}$ Then, according to the Taylor expansion method, the uncertainty of the variable Y can be calculated according to the following equation:

$$U_Y = \sqrt{\sum_i \left(\frac{\partial Y}{\partial x_i}\right)^2 U_{X_i}^2} \geq 0 \tag{3.2}$$

Where

U_Y, represents the uncertainty of the variable Y, that is, $Y \pm U_Y$

The fouling resistance is calculated using the following equation:

$$R_f = A * \left(\frac{1}{UA_c} - \frac{1}{UA_f}\right) \tag{3.3}$$

In the case of the fouling resistance, the uncertainty U_{Rf} is calculated according to the following equation:

$$e_{R_f} = \pm \sqrt{\left(\frac{\partial R_f}{\partial T_{ExWT}} e_{T_{ExWT}}\right)^2 + \left(\frac{\partial R_f}{\partial T_{EWT}} e_{T_{EWT}}\right)^2 + \left(\frac{\partial R_f}{\partial \dot{m}_{water}} e_{m_{water}}\right)^2 + \left(\frac{\partial R_f}{\partial P_{sat}} e_{P_{sat}}\right)^2} \tag{3.4}$$

Where: $\frac{\partial R_f}{\partial T_{ExWT}}$ = sensitivity coefficient due to exiting water temperature

$\frac{\partial R_f}{\partial T_{EWT}}$ = sensitivity coefficient due to entering water temperature

$\frac{\partial R_f}{\partial \dot{m}_{water}}$ = sensitivity coefficient due to water mass flow rate

$\frac{\partial R_f}{\partial P_{sat}}$ = sensitivity coefficient due to refrigerant saturation pressure

$e_{T_{ExWT}}$, $e_{T_{EWT}}$ = accuracy of RTD for existing and entering water, respectively (°F) or (°C)

$e_{m_{water}}$ = accuracy of a mass flow meter (lb/min) or (kg/s)

$e_{P_{sat}}$ = accuracy of a pressure transducer (psi) or (kPa)

The values in table 4-4 are fed into the EEs program which returns the uncertainty on the computed values of fouling resistance (R_f), the uncertainty propagation is shown in Figure 4-16.

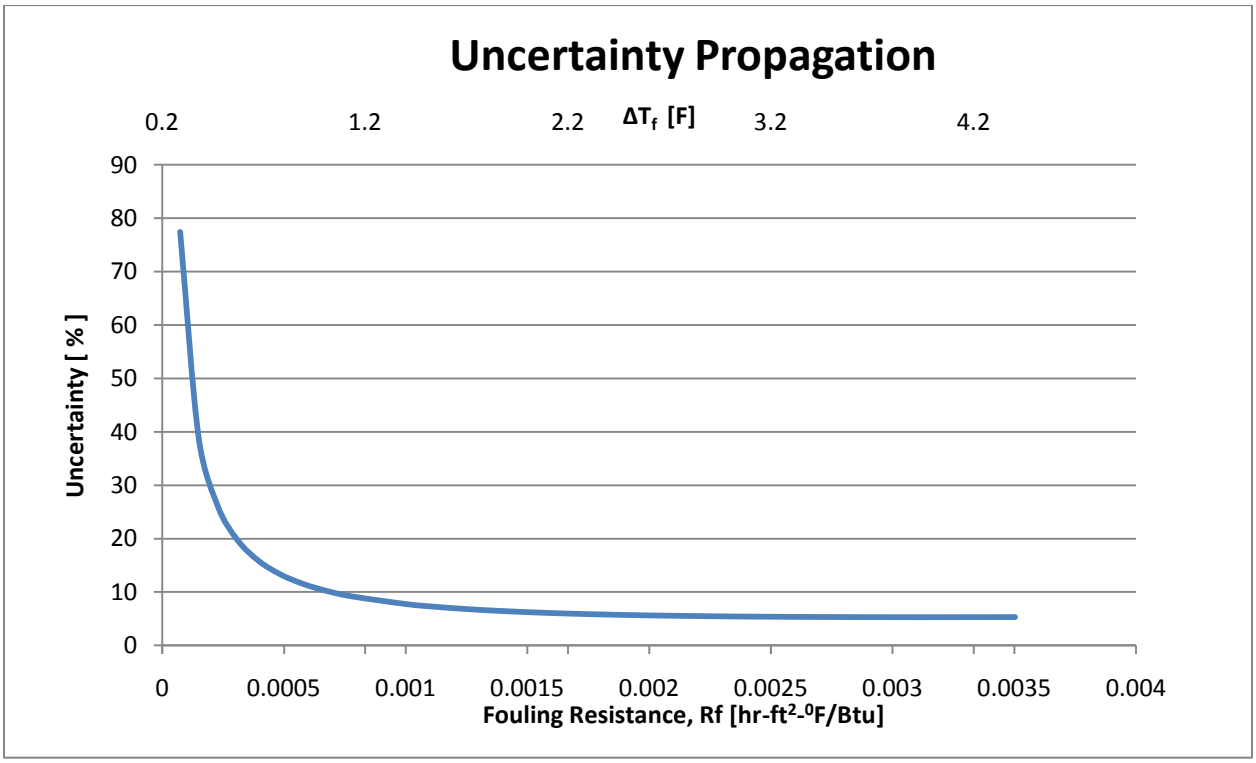

Figure 4-16. Overall uncertainty of the fouling resistance, (U_{RF} in percentage) versus estimated fouling resistance R_f and expected water temperature difference ΔT_f

In Figure 4-16 the uncertainty is plotted against the fouling resistance (R_f) and the corresponding temperature difference between the exiting temperature of water under clean and fouled conditions (ΔT_f). It can be seen that for a ΔT_f of 0.2 ^{0}F the theoretical uncertainty on R_f is about 77 % and it reduces to 10 % as ΔT_f increases to about 1.4 ^{0}F.

To analyze the contribution of each measurement device to the uncertainty associated with the fouling resistance of ΔT_f of 0.3 ^{0}F was selected. The region of ΔT_f between 0.2 ^{0}F and 0.8 ^{0} F is the expected operating area for the fouling experiments. From the literature review,

typical fouling resistances for plate heat exchangers are generally less than 1×10^{-3} hr-ft2-°F/Btu and in my tests the fouling resistance was less than 5×10^{-4} hr-ft2-°F/Btu. . Table 4-3 shows the output of the EES model during the uncertainty analysis. The fouling resistance and uncertainty associated with a ΔT_f of 0.3 ^{0}F was 0.000111 ± 0.000057 hr-ft^2-^{0}F/Btu or 52%. The uncertainty on the overall heat transfer coefficient under clean and fouled conditions were approximately 2.1% and similar to each other.

Table 4-3. Contributions of the variables to the uncertainty (U_{RF}) in percentage

Variable±Uncertainty	Partial derivative	% of uncertainty
R_f = 0.000111±0.00005746 [hr-ft^2-F/Btu]		
$\dot{m}_w$ = 2328±1.164 [lbm/hr]	$\partial R_f / \partial \dot{m}_w$ = -4.753E-08	0.00 %
P_{sat} = 149.8±0.33 [psi]	$\partial R_f / \partial P_{sat}$ = 0.000002216	0.02 %
$T_{w,i}$ = 85±0.11 [F]	$\partial R_f / \partial T_{w,i}$ = 0.00001633	0.10 %
$T_{w,o,c}$ = 95±0.11 [F]	$\partial R_f / \partial T_{w,o,c}$ = 0.0003584	47.07 %
$T_{w,o,f}$ = 94.7±0.11 [F]	$\partial R_f / \partial T_{w,o,f}$ = -0.0003796	52.82 %
UA_c = 1609±33.32 [btu/hr-f]		
$\dot{m}_w$ = 2328±1.164 [lbm/hr]	$\partial UA_c / \partial \dot{m}_w$ = 0.6911	0.06 %
P_{sat} = 149.8±0.33 [psi]	$\partial UA_c / \partial P_{sat}$ = -52.08	26.61 %
$T_{w,i}$ = 85±0.11 [F]	$\partial UA_c / \partial T_{w,i}$ = -116.1	14.70 %
$T_{w,o,c}$ = 95±0.11 [F]	$\partial UA_c / \partial T_{w,o,c}$ = 231.9	58.63 %
$T_{w,o,f}$ = 94.7±0.11 [F]	$\partial UA_c / \partial T_{w,o,f}$ = 0	0.00 %
UA_f = 1540±32.24 [btu/hr-f]		
$\dot{m}_w$ = 2328±1.164 [lbm/hr]	$\partial UA_f / \partial \dot{m}_w$ = 0.6616	0.06 %
P_{sat} = 149.8±0.33 [psi]	$\partial UA_f / \partial P_{sat}$ = -49.05	25.21 %
$T_{w,i}$ = 85±0.11 [F]	$\partial UA_f / \partial T_{w,i}$ = -116.1	15.70 %
$T_{w,o,c}$ = 95±0.11 [F]	$\partial UA_f / \partial T_{w,o,c}$ = 0	0.00 %
$T_{w,o,f}$ = 94.7±0.11 [F]	$\partial UA_f / \partial T_{w,o,f}$ = 225.2	59.03 %

From Table 4-3 it can be observed that that 99.9% of the uncertainty associated with the fouling resistance is due to the temperatures of water exiting the heat exchanger under clean and fouled conditions $T_{w,o,c}$ and $T_{w,o,f}$, or the term ΔT_f which is equal to the difference between the two temperatures, $\Delta T_f = T_{w,o,c} - T_{w,o,f}$. Hence it can be concluded that an increase in the accuracy of the temperature measurement devices would result in a significant decrease on the uncertainty associated with the fouling resistance. Figure 4-17 shows the theoretical uncertainty versus ΔT_f under various accuracies of RTDs ranging from 0.05 ^{0}F to 0.15 ^{0}F. It is evident that a careful in-

situ calibration of the RDTs is beneficial for improving the accuracy of the fouling resistance measurements. Thus, the calibration of the RTDs was performed at the beginning of the preliminary tests and checked in between the tests. It was also found that cleaning of the RDT probes is necessary after each fouling test. Since the RDTs probes are installed in line to the pipelines and directly immersed in the flow of the cooling tower water, several minerals accumulate on the metal rods of the sensors. Cleaning and checking the calibration of the RDT probes increased the accuracy and repeatability of the temperature measurements.

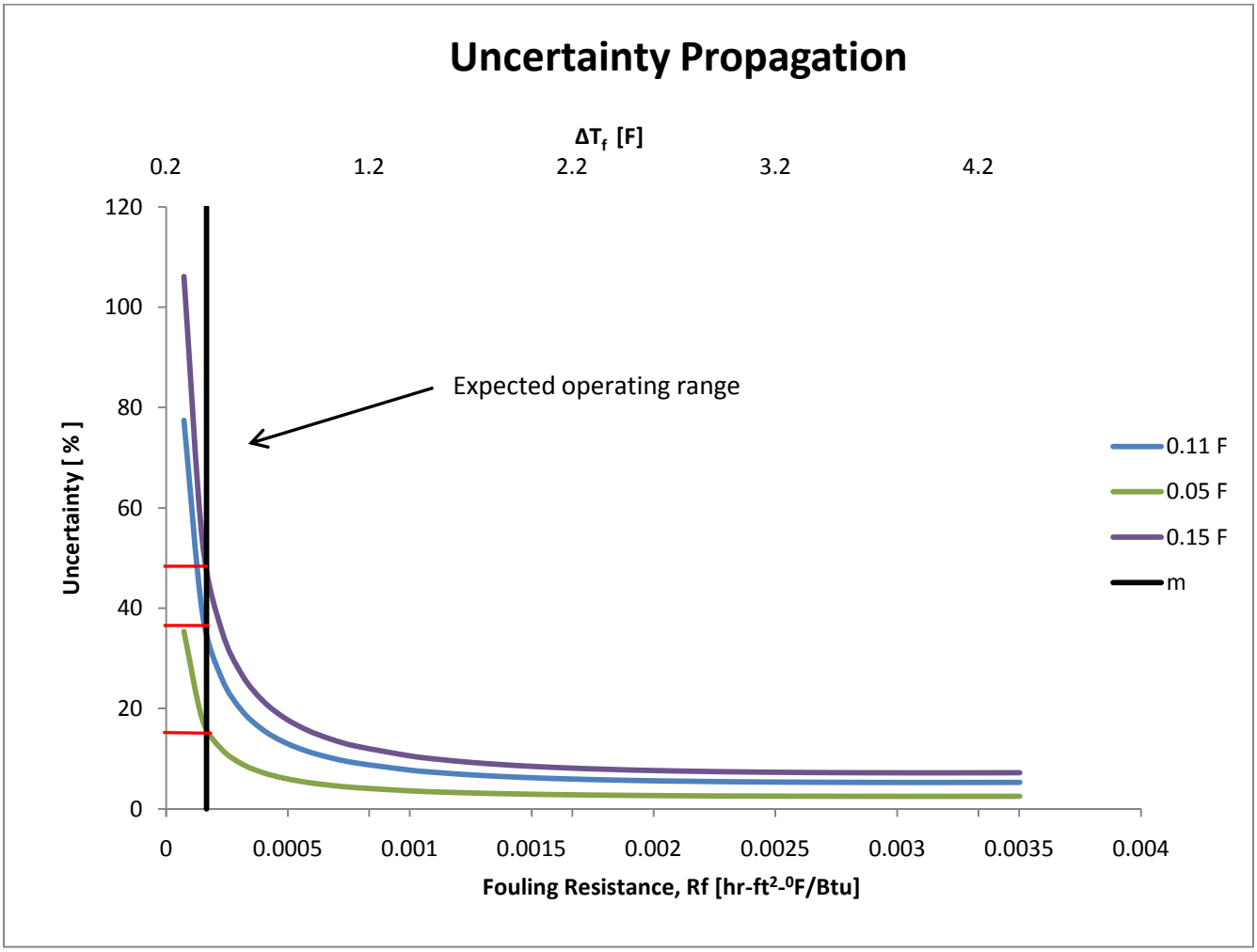

Figure 4-17. Effect of accuracy of water temperature measurements on the overall uncertainty (U_{RF} in percentage) versus estimated fouling resistance R_f

CHAPTER V

METHODOLOGY AND FINDINGS

The overall aim of this research is to conduct accelerated-type fouling experiments on PHEs under controlled operating conditions and with water quality that are close to the ones of actual cooling tower applications. Each PHE was tested for a period between 30 and 60 days until either an asymptotic fouling resistance was identified or it was not possible to maintain the test operating conditions due to excessive flow blockage in the components of the cooling tower water loop. The following parameters were maintained nearly constant during the tests:

1. Saturation temperature, degree of superheat and flow rate of the refrigerant entering the test PHE.
2. Inlet temperature and flow rate of cooling tower water entering the test PHE.
3. Evaporation rate of the water in the cooling tower loop since it greatly influence the water quality.

The water and refrigerant inlet conditions were selected based on standard ratings listed in AHRI Standard 450 [2007]. The flow rates during the tests were calculated using software from the PHEs manufacturer, which compute the nominal flow rate for given heat transfer capacity and temperature difference. The flow rate of water was selected such that a measurable temperature difference across the heat exchanger on the water side is obtained as recommended by the AHRI Standard 450 [2007]. Table 5-1 lists the selected operating conditions at the inlet of the PHE:

Table 5-1. Nominal operating conditions during the fouling tests

Refrigerant Flow rate	3.50 lbm/min (1.59 kg/min)
Water flow rate	38.8 lbm/min (17.6 kg/min) or 4.7 gpm
Refrigerant saturation temperature	105.0 ^{0}F (40.6 ^{0}C)
Refrigerant Degree of superheat	65.0 ^{0}F (36.1 ^{0}C)
Water temperature	85.0 ^{0}F (29.4 ^{0}C)

The water and refrigerant exit temperatures depend on the heat transfer characteristics of the PHEs at the initial stage with clean plates and over time on the extent of fouling on the heat exchanger plates.

5.1 Water quality and cooling tower cycle

The cooling tower water used in the tests is created by mixing chemicals with reverse osmosis water. The chemicals added are calcium chloride, calcium hydroxide and magnesium sulfate. Small quantities of bleach and azole are added to the water to minimize biological fouling and corrosion fouling. The chemicals are added in fixed ratios to obtain the quality of water listed in table 5-2. It should be noticed that the water chemistry can be replicated quite well in any laboratory and it is independent from the geographical location of the water source. More details on the preparation of the cooling tower water are available in a complimentary M.S thesis at Oklahoma State University (Lim [2010]).

Table 5-2. Water properties

Total Hardness		207.00
Calcium	(ppm)	47
Magnesium	(ppm)	22
Alkalinity	(as CaCO3)	55
Chloride	(ppm)	141.7
Sulfate	(ppm)	88.7
pH		8.9
Iron	(ppm)	0
Copper	(ppm)	0
TDS	(ppm)	523.38
LSI		0.64

The cooling tower water is circulated from the batch tank, through the test heat exchanger and part of flow is sent to the post cooler while the remaining is directed to the cooling tower before it returns to the batch tank. Around 20-25 % of the total water flow rate, that is, approximately 1

gpm is sent to the cooling tower. Around 10% of the water entering the cooling tower is transferred to the air stream during the direct exchange evaporative cooling process. The total water lost in the loop resulted in approximately 25 gallons per day. In real application 100 % of the water flow rate is sent to the cooling tower but this would require a large cooling tower, larger water tank and a more powerful fan and pumps.. Also around 100 gallons of water would be evaporated each day which would result in large quantities of make-up water required and also create a large latent load on the building HVAC system and finally a large flow rate through the spray nozzles in the cooling tower would require greater pumping power. Considering the available power and space in the laboratory and in order to have feasible operating conditions in laboratory, the cooling tower was scaled down and only a fraction of the water was directed to it.

The cooling tower provides both cooling for the water and acts as concentrator for the minerals in the water since the various salts dissolved into the water do not evaporate. The initial concentrations of minerals in the cooling tower water are listed in Table 5-2. Then the concentrations of these salts increases by evaporating pure water in the cooling tower and by adding make up water, that is, a water solution with the same initial concentration of Table 5-2, to the system. Hence the cooling tower gradually decreases the volume of the pure water in the system and increases the concentration of the minerals. This mechanism leads to an increase in the LSI of the water during the actual fouling tests. The LSI represents the degree of supersaturation of the water and controls the precipitation of the minerals. Recall that if the temperature of the water increases its solubility decreases. The water temperature rises from 85 to about 95°F in the test PHEs and thus the water solubility decreases near the plates of the heat exchangers. Since the water is always maintained saturated with minerals, even a slight decrease in the local solubility causes minerals precipitation, or fouling. This phenomenon is promoted in vicinity of the plates within the tests PHEs while in other sections of the water system the water solubility is maintained high enough to avoid any precipitation. In practice, as more water is evaporated and make-up water added, the concentration of salts in the system along with the LSI continue to increase and reach values that cause visible scaling and particulate fouling not only in the test PHEs but in all sections of the water loop. However, the main scaling is always enhanced in the test PHEs, where the water is warmest.

The control parameter of the fouling process is the LSI, which is computed using the water evaporation rate, PH, conductivity and alkalinity. The evaporation rate is measured on a

daily basis while a sample of the simulated cooling tower water is sent every two to three weeks to the Soil, Water and Forage Analytical Laboratory at Oklahoma State University to obtain its conductivity and alkalinity. More details on the computation of the LSI of the system are available in a complimentary M.S thesis at Oklahoma State University (Lim [2010]). The PH of the simulated cooling tower water in the batch tank is adjusted by adding Potassium hydroxide at regular intervals to maintain it between 9 -9.5.

5.2 Calibration of overall heat transfer coefficient (UA)

The fouling resistance of the heat exchanger is computed as the difference between the overall heat transfer coefficients under clean and fouled conditions as described in Table 4.1. The overall heat transfer coefficient depends on the refrigerant and water conditions at the inlet of the heat exchanger listed in Table 5-1. In practice the operating conditions cannot be maintained at the nominal values throughout the entire duration of test and even small fluctuations within the limits specified by the standards might cause a systematic error in measuring the fouling resistance. A trial run of the set up was conducted to assess the sensitivity of the UA to the different operating parameters listed in Table 5-1. It was found that the UA was most sensitive to the saturation temperature of the refrigerant which is obtained from the pressure of the refrigerant. A saturation temperature of 105 ^{0}F (40.6 ^{0}C) corresponds to a saturation pressure of 149.8 psi (1032.8 KPA). During the tests the refrigerant condensation pressure might fluctuate from the nominal value by ± 1.5 psi. The UA of the heat exchanger was sensitive to this fluctuation: for example a 0.9 psi variation in the average pressure with respect to the nominal value resulted in a 40 btu/hr-^{0}F change in the UA. Even though this accounts for only about 2 % of the total UA, the effect it has on the fouling resistance is significant because the fouling resistance is typically very small and it is computed based on the difference between the UAs. In normal circumstances the difference between the UA under clean and fouled conditions is between 0-150 btu/hr-^{0}F. The UA was found to vary linearly with respect to pressure and can be computed based on the pressure using equation 5-1 as follows.

$$UA = C_1 + (C_2 \times Pressure) \quad (5.1)$$

Where C_1 and C_2 are empirical constants determined for each PHE at the initial clean conditions and operating at constant flow rates and constant inlet temperatures of the water and the refrigerant. Table 5-3 contains values of the coefficients C1 and C_2 for PHEs A,B and C. Each set is obtained by varying the condensation pressure within ± 2 psi from the nominal value of 149.8 psi while keeping all other inlet parameters close to their nominal values as listed in Table 5-1.

Table 5-3. Calibration Constants

	C_1	C_2
PHE A	-10.8	2564
PHE B	-40.5	7270
PHE C	25.6	-2585

In addition to the refrigerant saturation pressure the flow rate of the cooling tower water was found to have a significant impact on the overall heat transfer coefficient. Hence a calibration test was conducted on each heat exchanger under clean conditions first keeping all conditions listed in Table 5-1 constant but varying the refrigerant pressure, then keeping the pressure constant and varying the water flow rate. Figures 5-1, 5-2 and 5-3 show the results of the calibration tests conducted on plate heat exchangers A, B and C as listed in Table 3-1.

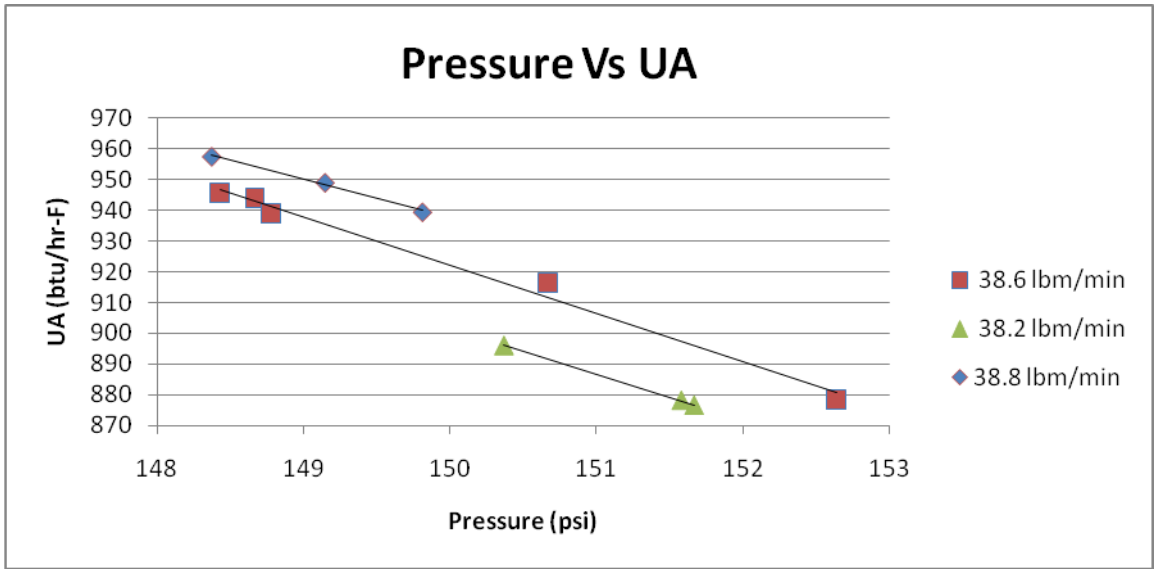

Figure 5-1. Determination of the coefficients C_1 and $C_2$for the PHE A

Figure 5-1 shows the calibration results for PHE A which is a low pressure drop chevron design. It can be seen that the overall heat transfer coefficient increase almost linearly with the refrigerant pressure and also increases with the water flow rate.

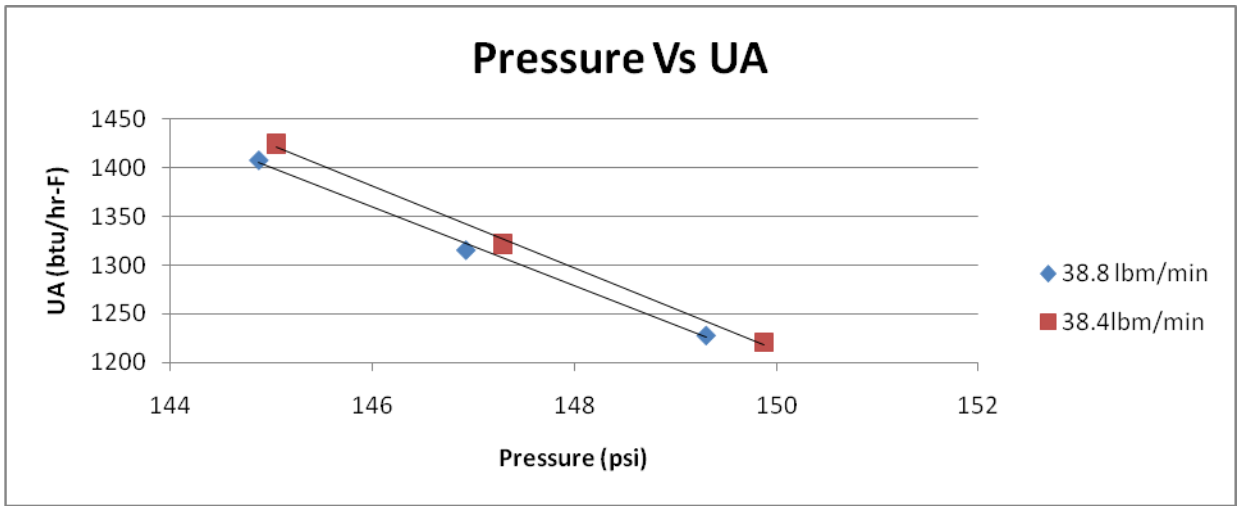

Figure 5-2. Determination of the coefficients C_1 and C_2 for the PHE B.

Figures 5-2 and 5-3 show the calibration results for PHE's B and C which are high pressure drop chevron designs, it can be seen that the overall heat transfer coefficient increase linearly with refrigerant pressure but unlike PHE A it tends to decrease with increasing water flow rate.

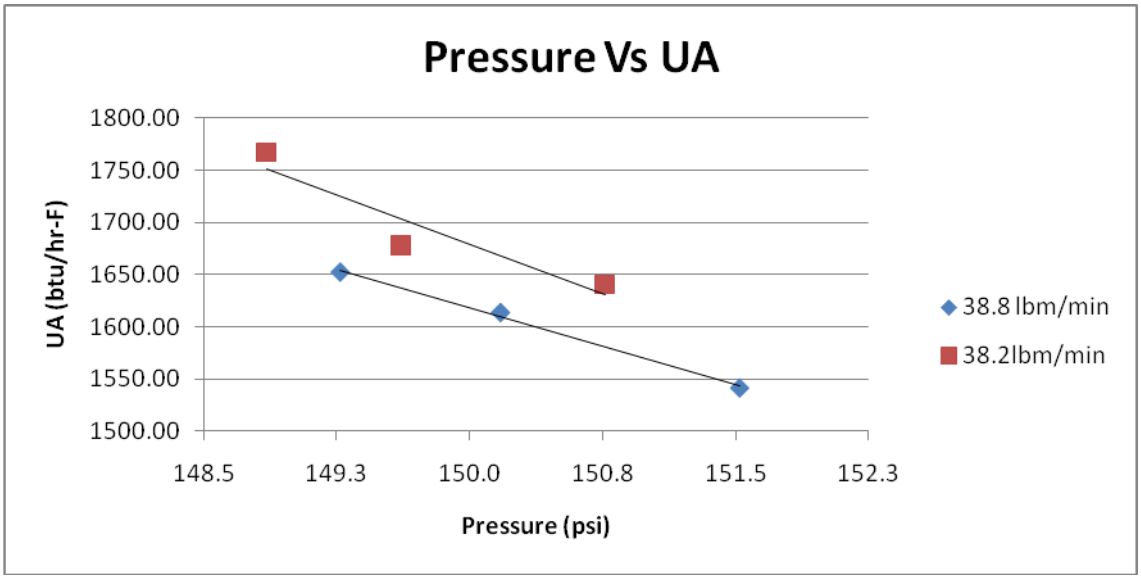

Figure 5-3. Determination of the coefficients C_1 and C_2 for the PHE C.

It can be seen that the overall heat transfer coefficient is around 950 btu/hr-^{0}F for PHE A which is considerably less than that of PHE B which is 1300 btu/hr-^{0}F. The two PHE's are identical except for their chevron pattern; PHE B has a higher chevron pattern which leads to a better flow distribution increasing the heat transfer. The pressure drop across the heat exchanger was found to be higher. PHE C has the highest overall heat transfer coefficient of the three PHEs. PHE C has the same chevron design as PHE B but a smaller heat transfer area which causes an increase in the velocity of the fluids in between the plates. This creates more turbulence thereby enhancing the heat transfer. The pressure drop across PHE C was found to be significantly higher than that of PHE A and B.

This calibration procedure is extremely important in order to avoid a systematic error during the measurements of the actual fouling resistance. For example consider PHE B, if we did not perform this calibration we would compute a clean UA value at the start of the experiment, assuming the refrigerant pressure was 149.8 psi and all other parameters the same as that mentioned in Table 5-1, and we would obtain a UA clean around 1205 Btu/hr-^{0}F. Now assume that after 5 days when the UA was next estimated, the average pressure is 150.4 psi and a UA is measured around 1192 Btu/hr-^{0}F. We see a decrease in the UA and the first attempt would be to conclude that fouling has occurred. Now if we take a closer look at the calibration data and compute the clean UA based on the pressure we would find that at 150.4 psi the clean UA is 1192 Btu/hr-^{0}F. This is the same value we obtained after 5 days. Thus, the different UA at day 5 was recorded not because fouling occurred but because the average condensation pressure was slightly higher than the original nominal value. During the data analysis the effects resulting from small variations in the average refrigerant pressure and small variations in the average water flow rate were taken into consideration by using the above mentioned correction procedure. After the UA clean was corrected for the actual operating conditions of the PHE, the difference between the UA and UA clean and corrected is due to only the fouling developed on the plates. Thus, with this new data reduction procedure the effect due to fouling is properly isolated and the fouling resistance is quantified more accurately.

5.3 Complete data reduction procedure of Fouling Resistance in Brazed-type plate Condensers

As mentioned in section 5.2 the overall heat transfer coefficient (UA) of the heat exchanger is extremely sensitive to the refrigerant saturation pressure and computation of fouling resistance using the method described in Section 4.4 will lead to generation of a systematic error in the actual fouling resistance. Hence a new data reduction method must be used and the key steps are summarized in Table 5-4.

Table 5-4. Complete data reduction procedure to determine actual fouling resistance

Step 1:	At initial time t=0 start the facility keeping all parameters except the refrigerant pressure constant and identical to the nominal values listed in Table 5-1. The water loop is charged with water as specified in Table 5.2. This chemistry yields to very low fouling potential. The cooling tower is off line and the water stream by-passes the cooling tower. The entire water stream is directed to the post-cooler. In these conditions no water evaporation occurs, the LSI remains below 0.7 and there is not any mineral scaling forming on the surfaces of the PHE under testing.
Step 2	Perform a first test with refrigerant conditions as close as possible to their nominal values of Table 5-1. When reaching steady state operating conditions record the data for at least 3 hours and estimate the average heat transfer rates on both water side and refrigerant side. Calculate the heat balance as follows

	HB [%]= (Heat Transfer$_{\text{Water Side}}$ – Heat Transfer $_{\text{Refrigerant Side}}$) / Heat Transfer$_{\text{Water Side}}$ × 100 Insulate well the PHE until the heat balance is within 3 to 5%. Then estimate the maximum fluctuations on the refrigerant flow rate and on water flow rate from their nominal values. These are the limits that must be preserved during the fouling test. Calculate the average values, for example: Refrigerant flow rate = 3.5 ± 0.1 lbm/min Water flow rate = 38.6 ± 0.3 lbm/min This step is needed to define the acceptable range of variability in the flow rates during the actual fouling experiments. In particular variations of the refrigerant flow rate outside the boundary range determined in this step might affect the capacity of the PHE and thus alter the temperature difference of the water across the PHE. This effect on the water temperature might be attributed to fouling but instead it is due to excessive variation of the refrigerant flow rate.
Step 3:	Perform a calibration of the overall heat transfer (UA) coefficient by computing the UA at 3 to 4 different pressures slightly above and below but close to the nominal value listed in Table 5-1. The UA at each pressure is computed using the following procedure. $Q_{psat} = m_c \times C_p \times \Delta T_{w,c}$ $LMTD_{psat} = \frac{\Delta T_{w,c}}{\ln[\frac{T_{sat} - T_{w,c,o} + \Delta T_{w,c}}{T_{sat} - T_{w,c,o}}]}$

	$UA_{psat} = Q_{psat} / LMTD_{psat}$ Where p_{sat} is the refrigerant pressure. For example, perform step 3 at refrigerant p_{sat} of about 148,149,150 and 151 psi.
Step 4:	Plot the different values of UA against their corresponding pressures and obtain the curve fit using the procedure mentioned in Section 5.2 in the form to determine the constants C_1 and C_2: $UA = C_1 + (C_2 \times Pressure)$
Step 5	Turn on the cooling tower fan and send about 25% of the water flow rate to the cooling tower. This can be done by adjusting metering valves on the water pipelines. In this step the concentration phase begins as water starts evaporating in the cooling tower. The mineral concentrations and the LSI begin to increase.
Step 5:	At any time t during the experiment, measure m_f, $\Delta T_{w,f}$, P_{sat}
Step 6:	Calculate UA_f as follows: $Q_f = m_f \times C_p \times \Delta T_{w,f}$ $LMTD_f = \frac{\Delta T_{w,f}}{\ln[\frac{T_{sat} - T_{w,f,o} + \Delta T_{w,f}}{T_{sat} - T_{w,f,o}}]}$ $UA_f = Q_f / LMTD_f$
Step 7:	Calculate the clean overall heat transfer coefficient (UA_c)at the corresponding pressure (P_{sat}) as follows: $UA_c = A + (B \times P_{sat})$

Step 8:	Compute the fouling resistance R_f at time t as follows: $R_f = A\left(\left(\frac{1}{UA_f}\right) - \left(\frac{1}{UA_c}\right)\right)$
Step 9:	Calculate pressure drop penalty factor (P) as follows: $P = \frac{\Delta P_f}{\Delta P_c}$ Where ΔP_f and ΔP_c are the pressure drops across the heat exchanger measured under clean and fouled conditions respectively.

5.4 Uncertainty Analysis of the complete data reduction procedure

Since a revised method is used to determine the fouling resistance in the brazed plate condensers the procedure listed in Section 4.5 is updated to perform a more accurate uncertainty analysis. Initially a model of the condenser was created in EES with water flow rates, water temperatures, refrigerant flow rates and pressures under fouled conditions as inputs along with the coefficients determined during the calibration of the overall heat transfer coefficient. The model outputs are the UA factor, the LMTD and the fouling resistance of the plate heat exchanger using the procedure listed in Table 5-4. The accuracy of measurement devices is obtained from Table 4-2 and input into the EES program. The only difference is that in this case the overall heat transfer coefficient under clean condition is computed using the curve fit and not from recorded data. Hence it is treated as an independent variable. From Table 4-3 it was found that the uncertainty on the overall heat transfer coefficient (UA_c) was within 2.3 % irrespective the operating conditions and hence the uncertainty on the UA_c is taken as 2.3 % for this calculation.

5.5 Accelerated-type fouling test on PHE A

The first plate heat exchanger tested was PHE A, the specifications of this heat exchanger are listed in Table 3-2, and its main characteristic is the low chevron angle which results in lower heat transfer rates and pressure drop. The operating conditions were kept almost constant to the nominal values listed in Table 5-1. However since each heat exchanger was to be tested between 1-2 months it was decided to record the data 2 times a day for 3 hour periods at a sampling rate of 2 seconds. The data collected over each 3 hour period (~ 5500 - 6000 points) are averaged to a single value resulting in two points per day. Table 5-5 lists the average values of the operating conditions and the standard deviations during the entire duration of tests which lasted for 34 days. The operating conditions are very close to the nominal values listed in Table 5-1.

Table 5-5. PHE A: Operating conditions

	Average	Standard Deviation
Water inlet temperature (^{0}F)	85.04	0.11
Water flow rate (lbm/min)	38.78	0.28
Refrigerant flow rate (lbm/min)	3.50	0.01
Refrigerant pressure (psi)	149.97	0.68
Refrigerant saturation temperature (^{0}F)	105.09	0.31
Refrigerant inlet temperature (^{0}F)	170.06	0.55

The test consists of four phases, first once the facility is turned on and running at the required operating condition the calibration of the overall heat transfer coefficient is done as described in Section 5.2 which is used later to compute the UA_c at different pressures during the course of the test, at this time the cooling tower is not in operation and the entire flow circulates through the post cooler in order to avoid any fouling during the calibration process; this phase is termed as the calibration phase. The calibration phase is followed by the concentration phase.

During this phase the cooling tower is turned on and around 25 % of the total flow is passed through it. During this phase the evaporation of water in the spray nozzles leads to a concentration of minerals in the water remaining in the system. Over time as more water is evaporated the fouling potential increases from 0.7 up to 2. The concentration phase usually lasts for around 2 days. This is followed by the testing phase, which is Day 0 in Fig 5-4, where the actual recording of data of the fouling resistance takes place.

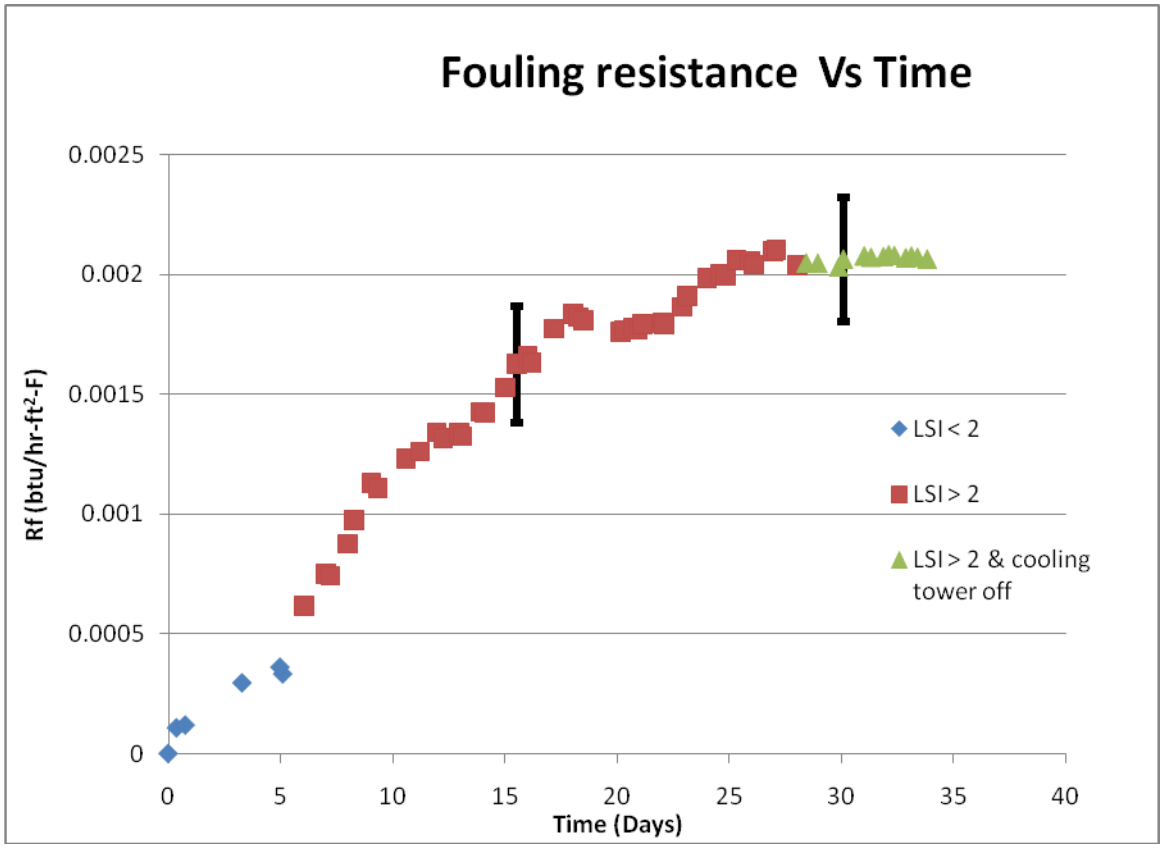

Figure 5-4. PHE A: Fouling Resistance vs. Time

During the testing phase the fouling potential of the water which is indicated by the Langalier Stability Index (LSI) defined in Chapter 2 continues to increase due to the increase in concentration of minerals in the system. The pH of the simulated cooling tower water was found to have a significant effect on the LSI. Because of natural evaporation of water in the batch tank, the pH tends to drop over time. Potassium hydroxide was added in regular intervals to keep the pH constant between 9 – 9.5. Figure 5-5 shows the increase of LSI with time and it can be observed that after the LSI reaches a value of 2 around Day 5, the fouling resistance in Figure 5-

4 begins to increase faster right after this time. This is evident from the change in the slope of the fouling resistance in Figure 5-4 around day 5.

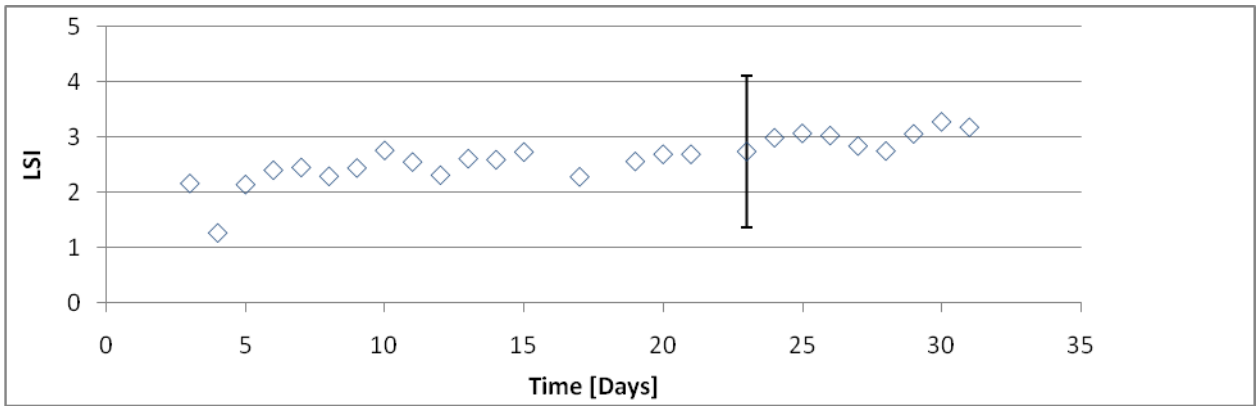

Figure 5-5. PHE A: LSI vs Time

During the course of this testing phase the pressure drop across the heat exchanger continued to increse as shown in Fig 5-6. Also the pressure losses in the water system continued to increase due to particulates adhering to control valves, flow spray nozzles and even the post cooler. After day 28 the pumps could not not produce the requried flow rate due to the increased pressure losses and the cooling tower was turned off. The test was forced to be concluded but sufficeint data were collected to identify the trend of the fouling resistance and calculate its asymptotic value. A large part of the pressure drop was due to the flow spray nozzles which were clogged in the cooling tower. The final phase of this test was conducted (i) to determine the effect of the cooling tower on the fouling resistance and (ii) to verify the assumpotion that with no continuous concentration of the water the fouling phenomena ceases. The facility was run with the cooling tower off for a period of 5 days. In these 5 days, which consititue the final phase of the test, the fouling resistance was fairly constant as seen in Figure 5-4. This confirmed that fouling occurred only if water is maitained saturated in the water loop and supersaturated within the test PHE and to achieve these conditions the cooling tower must be on line. .

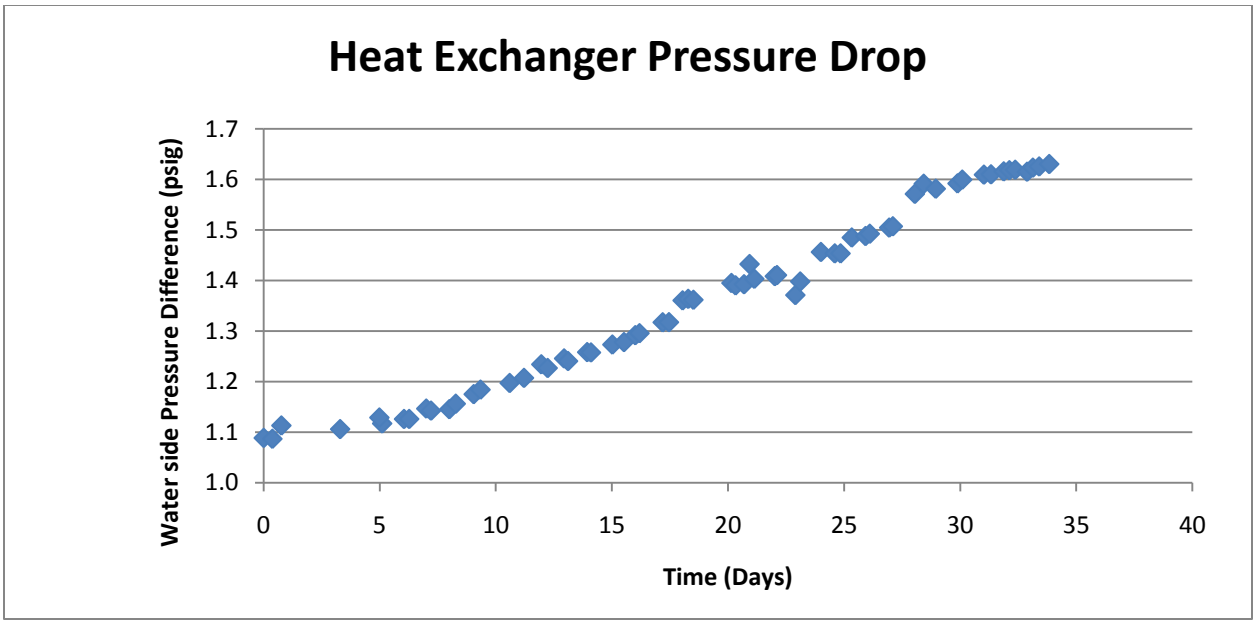

Figure 5-6. PHE A: Pressure Drop

Following the procedure mentioned in section 5.4 an uncertainty analysis was conducted for the fouling resistance at two points during the test, first at Day 15 when the fouling resistance was 0.0016 hr-ft^2-^{0}F/Btu the uncertainty was around 15% and on Day 30 when the fouling resistance is 0.002 hr-ft^2-^{0}F/Btu it was around 12.5 % and is shown in Fig 5-4.

5.6 Accelerated - type fouling test on PHE B

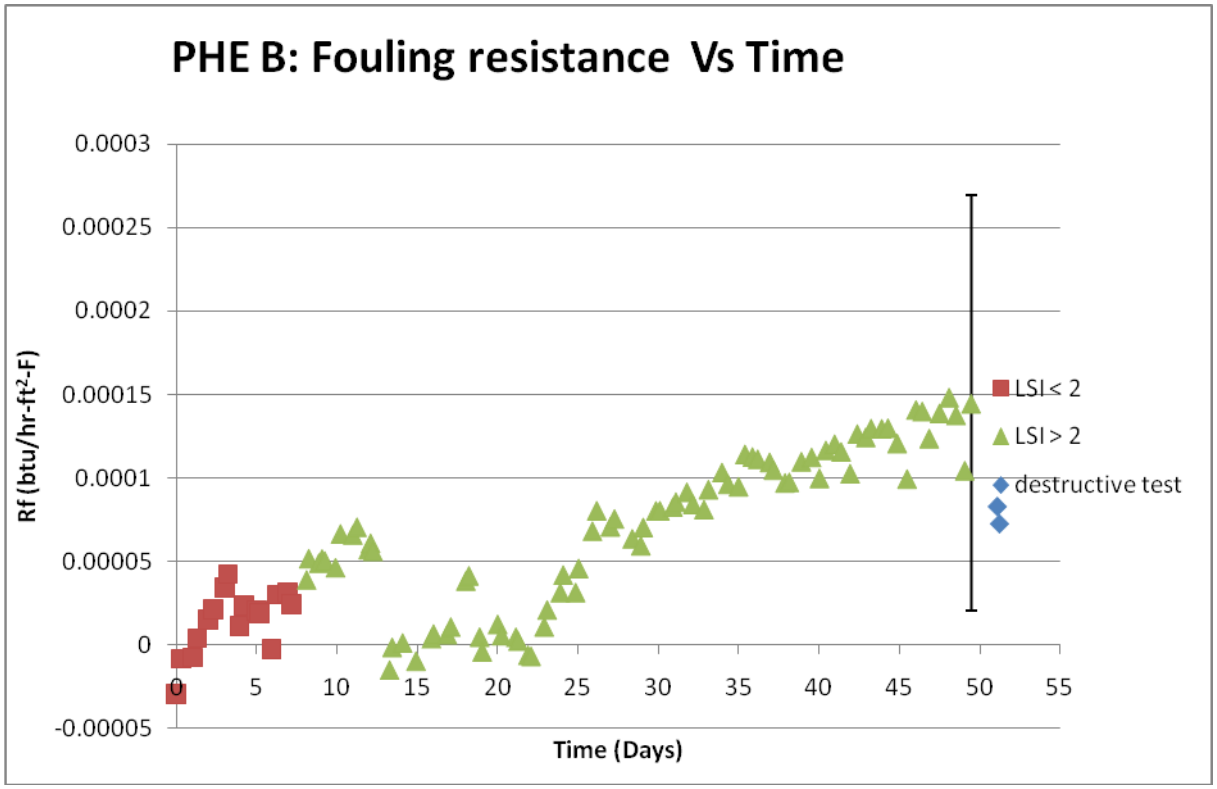

Figure 5-7. PHE B: Fouling Resistance

PHE B is identical to PHE A except for the chevron angle which is larger resulting in an increased heat transfer and greater pressure drop across the heat exchanger, the specifications of PHE B are available in table 3-2. The testing procedure is identical to that used for PHE A, first the calibration and concentration phases were carried out followed by the testing phase. The fouling resistance beings to increase gradually until day 12, the LSI of the system is greater than 2 after day 7 as seen in Fig 5-8.

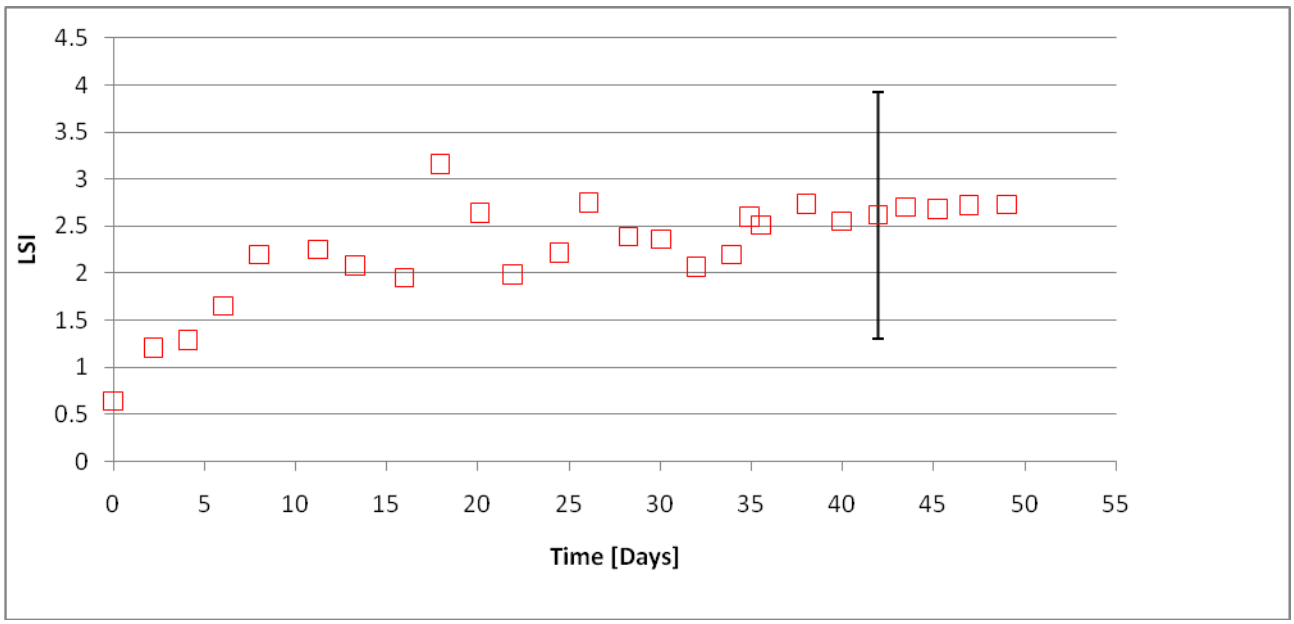

Figure 5-8. PHE B: LSI vs Time

The operating conditions were maintained almost constant during the entire duration of the test as can be seen in Table 5-6. It can be seen that the standard deviation is significantly less than that in Table 5-5 for PHE A largely due to the experience gained with the control of the system from the previous test.

However at Day 12 the refrigerant loop of system was stopped briefly to charge more refrigerant while the simulated cooling tower water loop continued to run. A sudden decrease in the fouling resistance to its initial value was observed immediately following the brief stoppage of the refrigerant loop. The exact reason for this is not known, but one theory is that when the refrigerant loop was turned off, the temperature of the heat transfer surface decreased causing the cooling tower water to shift from being supersaturated to unsaturated and resulting on absorbing the deposit from the heat transfer surface. These reverse phenomena might have caused the fouling resistance to decrease. The pressure drop across the heat exchanger was also found to decrease during this time period as seen in Fig 5-9.

Table 5-6. PHE B: Operating Conditions

	Average	Standard Deviation
Water inlet temperature (^{0}F)	85.04	0.03
Water flow rate (lbm/min)	38.82	0.05
Refrigerant flow rate (lbm/min)	3.50	0.01
Refrigerant pressure (psi)	149.7	0.32
Refrigerant saturation temperature (^{0}F)	104.97	0.14
Refrigerant inlet temperature (^{0}F)	170.03	0.08

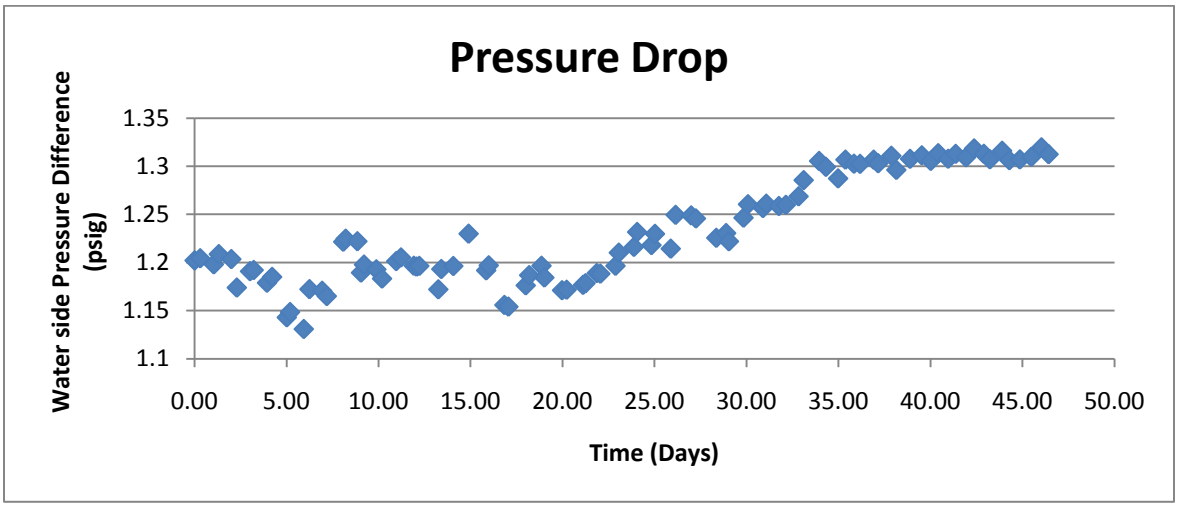

Figure 5-9. PHE B: Pressure Drop

After day 20 the fouling resistance and pressure drop continue to increase and at Day 49 the test was concluded. The testing phase for this test lasted significantly longer than that for PHE A since the fouling resistance measured for PHE B was almost one order of magnitude less than the one of PHE A. At the end of the testing phase it was decided to conduct a "destructive test" by turning off the refrigerant loop for a period of 2 days and continuing to run the cooling

tower water loop. This was done to try to replicate the reverse process observed right after Day 12 and observe if the similar drop in fouling resistance and pressure drop would occur. However, no decrease in pressure drop across the heat exchanger was observed, even though the fouling resistance appears to have dropped during this "destructive test" as seen in Fig 5-7, it cannot be termed as a conclusive test.

An uncertainty analysis was done using the procedure mentioned in section 5.4 at two points, on Day 10 when the fouling resistance was 0.000068 hr-ft^2-^{0}F/Btu the uncertainty was found to be 178%, is not shown in in Fig 5-7 and on Day 50 when the fouling resistance was 0.000145 hr-ft^2-^{0}F/Btu it was around 86% as shown in Fig 5-7, the values of uncertainty are much higher than that of PHE A due to the low values of fouling resistance.

5.7 Accelerated type fouling test on PHE C

Table 5-7. PHE C: Operating Conditions

	Average	Standard Deviation
Water inlet temperature (^{0}F)	85.01	0.04
Water flow rate (lbm/min)	38.84	0.04
Refrigerant flow rate (lbm/min)	3.50	0.01
Refrigerant pressure (psi)	149.72	0.19
Refrigerant saturation temperature (^{0}F)	104.98	0.09
Refrigerant inlet temperature (^{0}F)	169.99	0.11

PHE C has the same chevron pattern as PHE B but different aspect ratio and lesser heat transfer area. This results in a higher flow velocity through the heat exchanger since the flow rates are constant irrespective of the heat exchanger size thereby producing a greater pressure drop across it. Its specifications are listed in Table 3-2. The testing procedure was carried out similar to the two previous tests, first the calibration phase followed by concentration and testing phases. However during the calibration phase and the first 2 days of the testing phase the

refrigerant loop was undercharged and large fluctuation in refrigerant flow rate were observed. The heat balance on the water and refrigerant loops showed a difference of 16-20 % during this period while during all other times it was between 3-8 %. Hence the data collected during this period including the calibration for the overall heat transfer coefficient cannot be used to compute the fouling resistance in clean conditions because the variation of the refrigerant flow rate was excessive. However, during this test the fluctuation of the refrigerant condensation pressure and flow rates were so small that their effect can be reasonable neglected. It was decided to compute the overall heat transfer coefficient (UA) at Day 3 and use it as the clean UA and proceed to compute the fouling resistance using the method described in Table 4-1 with the controls of Table 5-3. The operating conditions during the course of this test are listed in Table 5-7.

5-10, 5-11 and 5-12 show the fouling resistance, LSI and pressure drop across the heat exchanger PHE C.

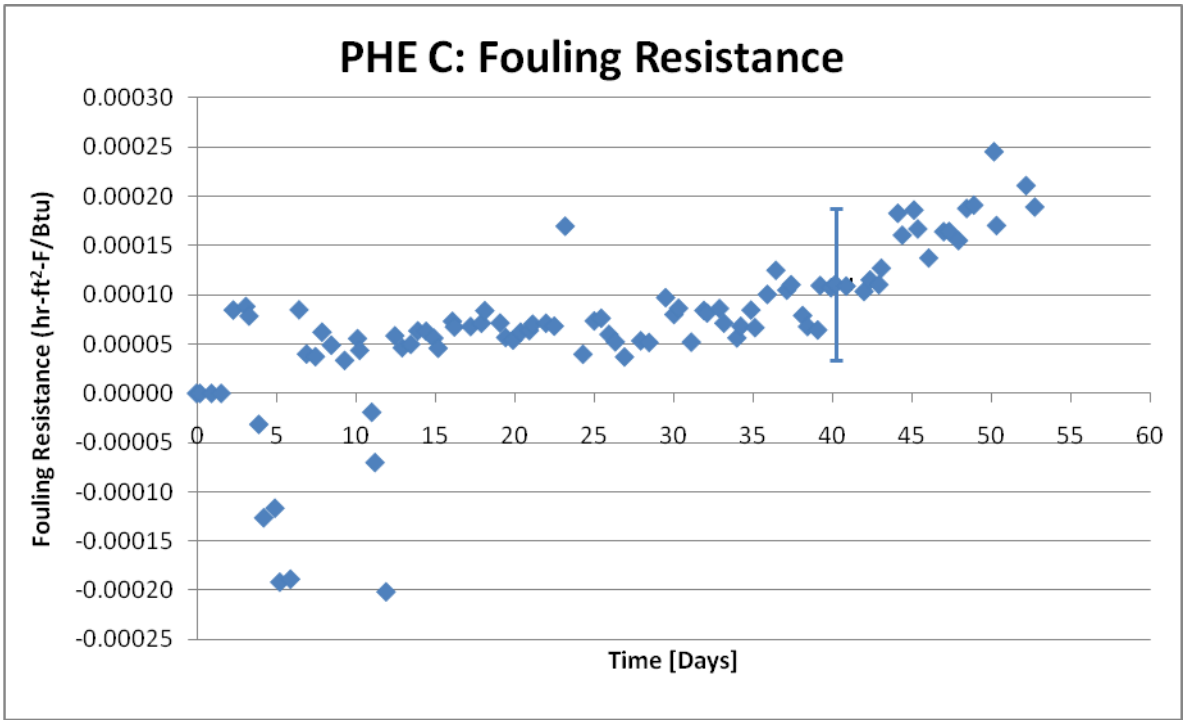

Figure 5-10. PHE C: Fouling Resistance

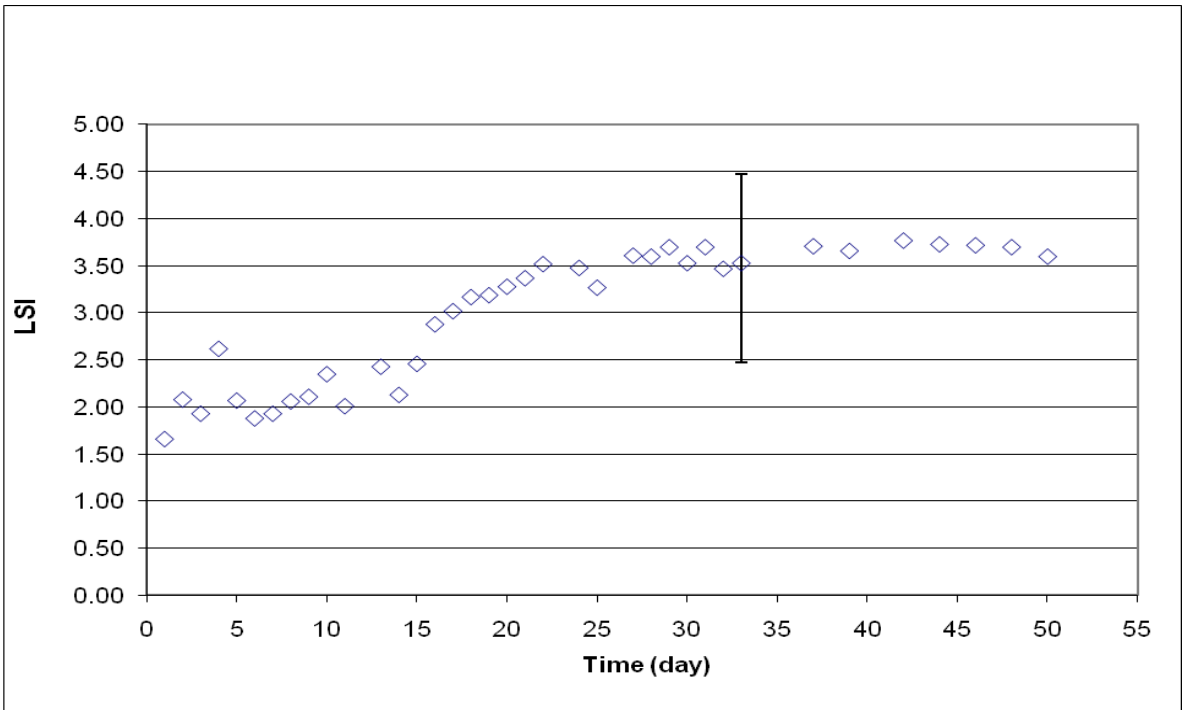

Figure 5-11. PHE C: LSI vs Time

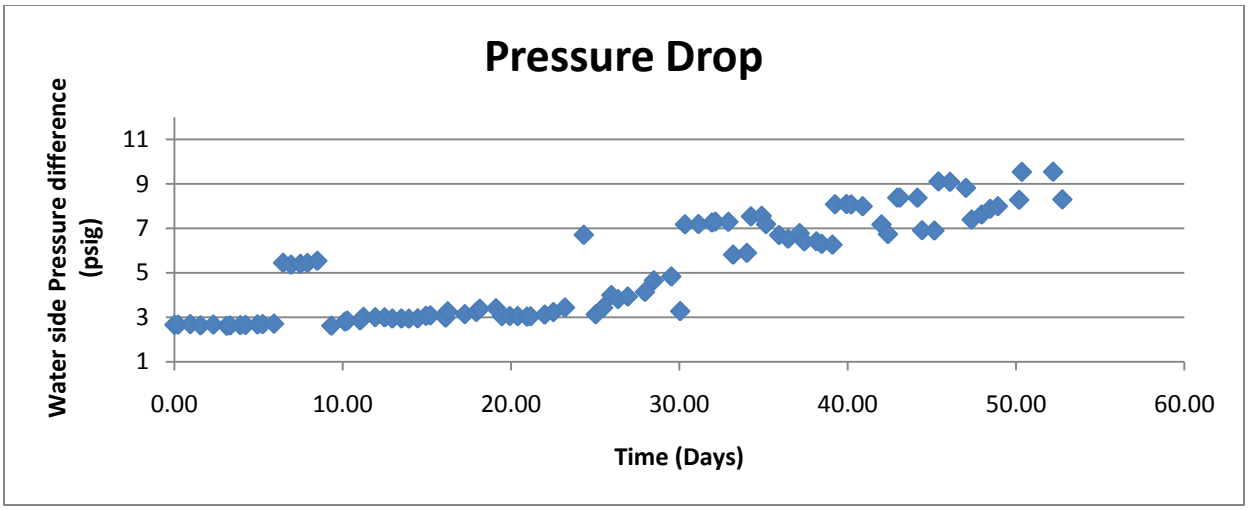

Figure 5-12. PHE C: Pressure Drop

An uncertainty analysis was performed on the fouling resistance similar to the previous two heat exchangers. From in-situ calibration of the RTDs, the accuracy of the RTDs was measured to be within 0.011 ^{0}F for a very narrow range around the nominal temperature of the water inlet and outlet. The UA under clean conditions was taken as the UA calculated during day 2 and, as in the previous case; a 2.3% uncertainty was taken on the clean UA. On Day 10 the fouling resistance was found to be 0.000066 hr-ft^{2}-^{0}F/Btu, the uncertainty associated with it is 143 % and on Day 40 for a fouling resistance of 0.00011 hr-ft^{2}-^{0}F/Btu the uncertainty was 70%. It should be observed that due to the improved accuracy of the RTDs the uncertainty reduces from 86 % as calculated for PHE B to 70 % under similar operating conditions. Thus, cleaning and in-situ calibration of the RTDs is recommended before commencing each experiment. This guarantees that the temperature measurements of the water inlet and outlet to the test PHE remain accurate enough to provide reasonable value for the experimental uncertainty.

A summary of the experimental data in both clean and fouled conditions for the three PHEs is given in table 5-8 below. It should be noticed that the refrigerant and water flow rate were fairly constant throughout the tests while the water temperature difference across the PHE decrease by 1.6 ^{0}F for PHE A, 0.2 ^{0}F for PHE B and 0.2 ^{0}F for PHE C with respect to the initial clean conditions. This degradation was the net effect of the fouling (scaling) on the PHEs.

Table 5-8. Overall operating conditions

	PHE A		PHE B		PHE C	
	Clean	Fouled	Clean	Fouled	Clean	Fouled
Water inlet temperature [^{0}F]	85.3	85.1	85.1	85.0	85.0	85.0
Water exit temperature [^{0}F]	91.9	90.0	92.2	92.9	93.0	92.8
Water side temperature difference [^{0}F]	6.5	4.9	8.1	7.9	8.0	7.8
Water flow rate [lbm/min]	38.8	38.8	38.8	38.8	38.8	38.8
Heat transfer rate (Q) [Btu/hr]	15200	11382	18842	18283	18586	18146
Refrigerant saturation temperature [^{0}F]	105.0	104.8	105.1	105.0	105.0	105.0
Refrigerant flow rate [lbm/min]	3.50	3.50	3.50	3.50	3.50	3.50
LMTD [^{0}F]	16.2	17.1	15.66	15.69	15.6	15.7
Overall heat transfer coefficient [Btu/hr-^{0}F]	939.5	665.3	1203.1	1165	1189.5	1145.5
Fouling resistance [hr-ft^2-F/Btu]	0	0.002	0	0.00012	0	0.00018

Water side pressure drop [psig]	1.1	1.6	1.2	1.3	2.6	9.5

5.8 Estimates of asymptotic fouling resistance

The asymptotic fouling resistance is calculated using the following expression, which was originally proposed by Grandgeorge et al. [1998]:

$$R_f(t) = R_f^*(1 - e^{-\frac{t}{t_c}}) \quad (5.2)$$

Where,

$R_f(t)$ – fouling resistance at time t (hr-ft^2-^{0}F/Btu)

R_f^* - asymptotic fouling resistance (hr-ft^2-^{0}F/Btu)

T_c – time constant (duration of test) (hours)

The instantaneous fouling resistance is calculated and is used in the equation 5.1 along with the corresponding time 't' and the value of R_f^* is computed by minimizing the quadratic error taking all data points into consideration. Table 5-9 lists the asymptotic fouling resistance values for all three heat exchangers tested along with the time constants.

Table 5-9. Asymptotic fouling resistance at 85°F entering water temperature, 105°F Refrigerant T_{sat}, and 65°F refrigerant superheat degree, Water LSI ~ 3 (severe fouling potential).

	Asymptotic fouling resistance [hr-ft^2-^{0}F/Btu](m^2-^{0}C/ W)	Time constant [hours](Days)
PHE A (chevron angle, 90 - β = 30^0 Aspect ratio, (L/W) = 2.6 Flow velocity = 0.63 ft/s)	0.0035 (0.000616)	694 (29)
PHE B (chevron angle, 90 - β = 63^0 Aspect ratio, (L/W) = 2.6 Flow velocity = 0.63 ft/s)	0.00024 (0.000042)	1187 (49.5)
PHE C (chevron angle, 90 - β = 63^0 Aspect ratio, (L/W) = 4.1 Flow velocity = 1.09 ft/s)	0.00019(0.000033)	995 (41.5)
Tube and tube heat exchanger from Li and Webb [2001] (enhanced tube with: helix angle = 35^0, no of starts = 25, flow velocity 3.5 ft/s)	0.00048(0.000086)	2500 (104)

Using the values listed in Table 5-8 the fouling resistance curve is plotted and forecasted for a period of 60 days, Figures 5-13, 5-14 and 5-15 show the comparison of the fouling resistance obtained from the curve fit and the experimental data. Figure 5-16 shows a comparison asymptotic fouling curves for the different plate heat exchangers plotted in a logarithmic scale. A comparison with typical values of fouling in tubular heat exchanger is also given in table 5-8. The asymptotic fouling resistance and the time constant for the tube and tube heat exchanger are obtained from Webb and Li [2001]. Webb and Li [2001] conducted long term fouling tests on enhanced condenser tubes using cooling tower water, tubes with different helix angles and number of starts were used. Tube 6 in Webb and Li [2001] is selected for comparison since the asymptotic fouling resistance of this tube was closest to the average of all the tubes tested. It had a helix angle of 35^0 and 25 starts. The water used had a calcium hardness of 800 ppm, conductivity around 1700 μΩ and a pH around 8.5 which corresponds to an LSI around 2.1 and the water velocity was 3.5 ft/s. The water velocity in my plate heat exchangers ranged from 0.6 to 1.1 ft/s. The water used by Li and Webb [2001] remained constant throughout instead of increasing with time since there is no cooling tower to provide the concentration of the minerals. The fouling resistance in plate heat exchanger with the low chevron angle of 30^0 is around 7 times larger that of the tube and tube heat exchanger, while the tube and tube heat exchanger has a fouling resistance around 2.5 times larger than the plate heat exchangers with a chevron angle of 63^0. The comparison of the 63^0 chevron angle PHEs with the tube and tube heat exchanger is more realistic since in applications which involve fluids with high potential for fouling low chevron angle PHEs are less likely to be used. Based on the literature review an lower value of LSI and higher flow velocities will lead to a lower value of fouling resistance, the tube and tube heat exchanger has a flow velocity around 3-5 times higher than the PHEs with the 63^0 chevron angle and a lower LSI but still has a higher fouling resistance which indicates the tube and tube is likely have much greater fouling under similar operating conditions.

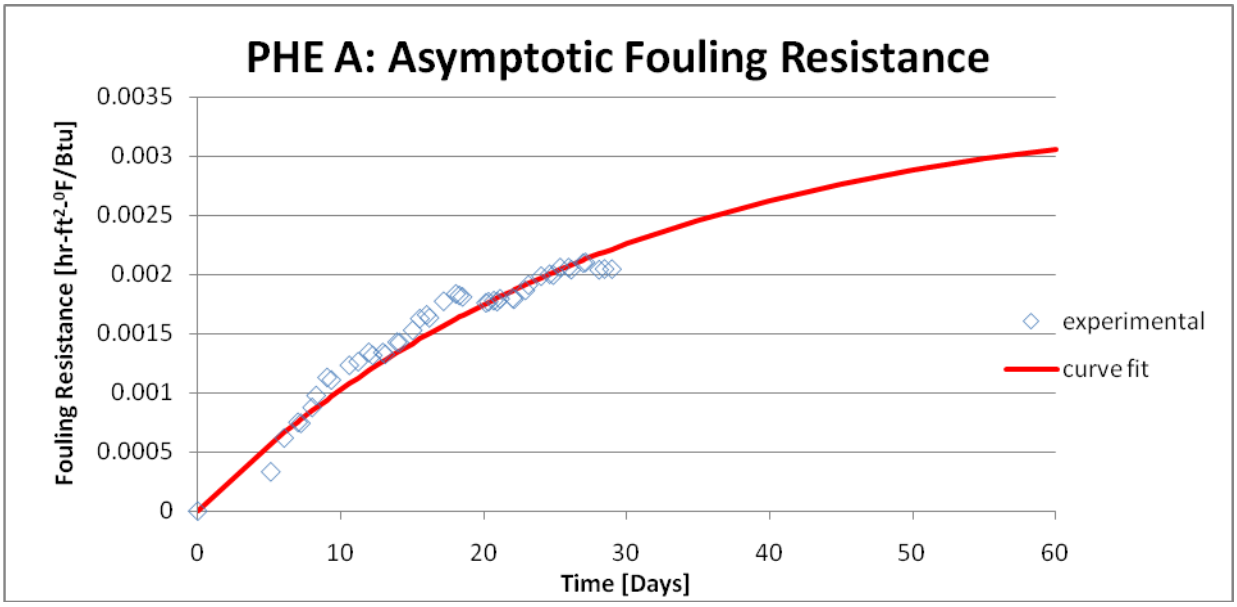

Figure 5-13. PHE A: Asymptotic fouling resistance

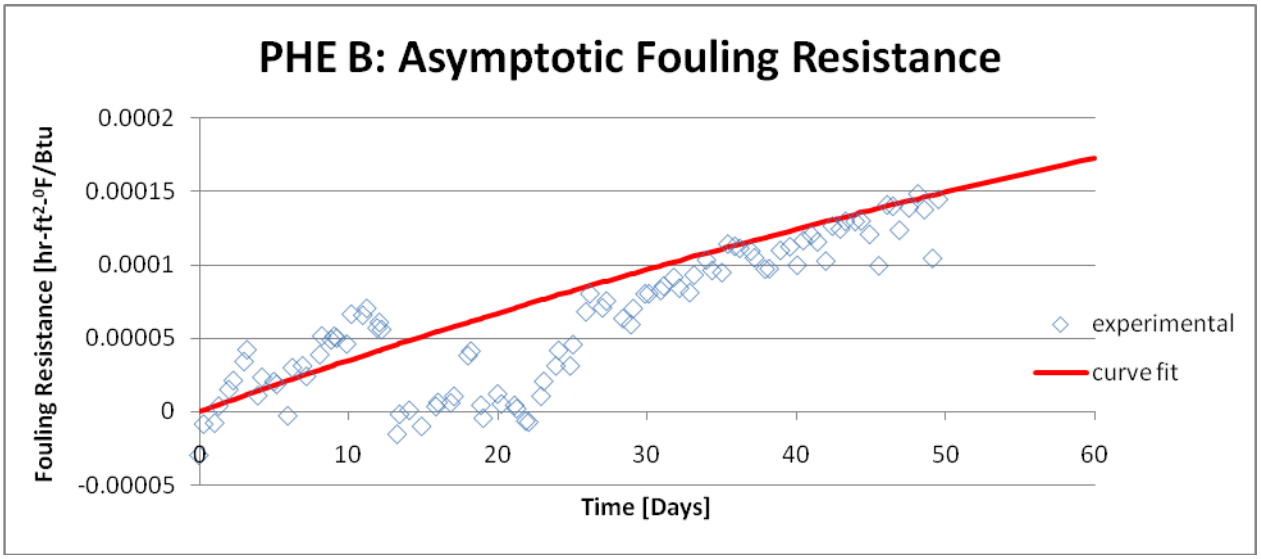

Figure 5-14. PHE B: Asymptotic fouling resistance

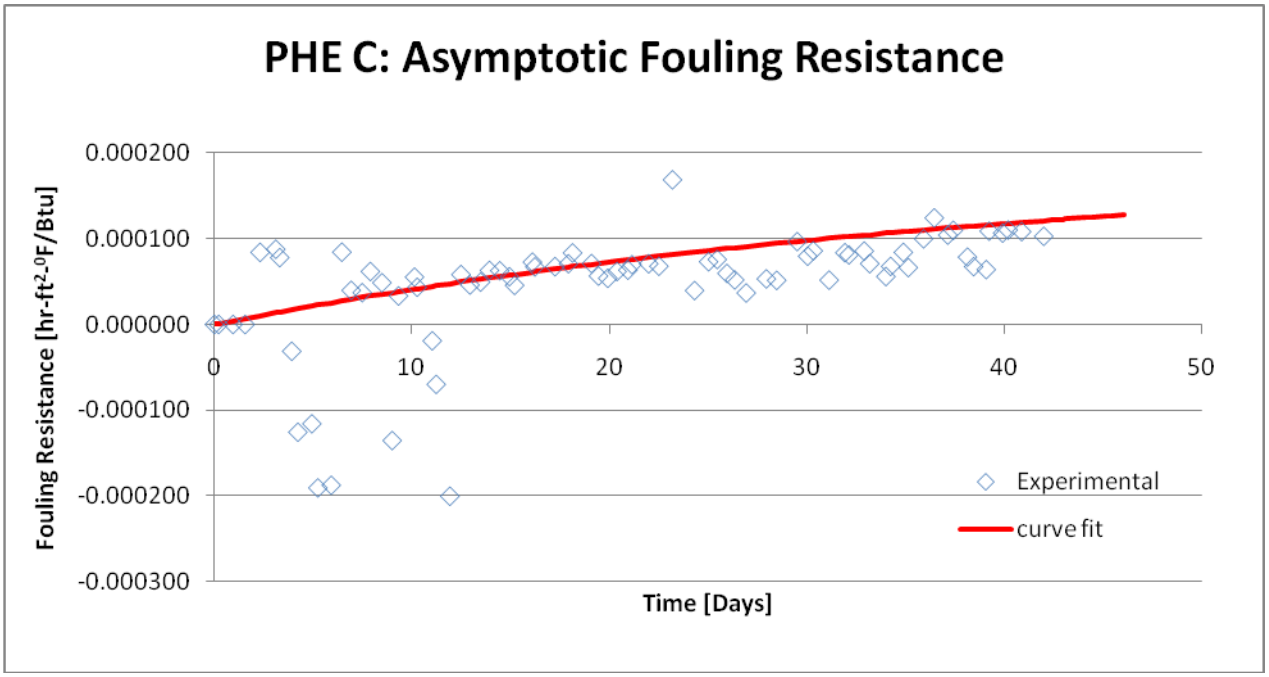

Figure 5-15. PHE C: Asymptotic Fouling Resistance

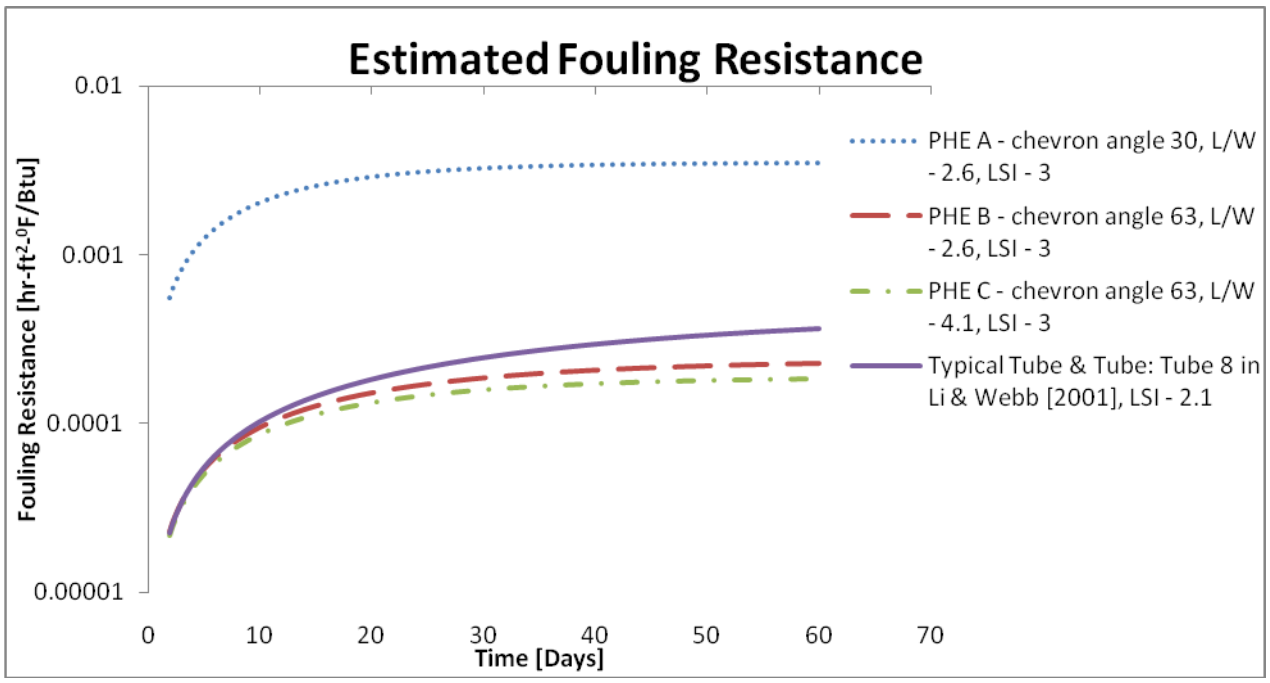

Figure 5-16. Comparison of Asymptotic Fouling Resistance

Even though for all three PHEs tested an asymptotic fouling resistance value is calculated using equation 5.1 as it was never actually reached, the fouling resistance was found to increase continuously during the period of the tests, but it is assumed an the fouling process follows equation 5.1 and an asymptotic fouling resistance will be reached when the rate of removal and deposition reach the same value. For PHE A which was tested for a period of 28 days the fouling resistance reached 57% of its asymptotic value while for PHE B it reached 62.5 % after 50 days and for PHE C it was found to be 63% after 42 days. However even if the asymptotic fouling resistance is reached the effect of the concentration of the minerals due to the cooling tower will lead to fouling in other parts of the loop, like auxiliary heat exchangers, in the pipes and flow control valves creating large pressure drops which may lead to damage of pumps which was the case in this project.

5.9 Discussion of the results

- Accelerated type fouling tests were conducted on 3 different brazed plate heat exchangers (PHEs A, B & C) operating as condensers. There were two unique factors differentiating the 3 heat exchangers, PHE A had a chevron angle of 30^0 while PHEs B & C had a chevron angle of 63^0. PHEs A and B had identical geometries and heat transfer area of 4.6 ft^2 resulting in a water side flow velocity of 0.63 ft/s (0.19 m/s) while PHE C had an area of 3.9 ft^2 resulting in a water side flow velocity of 1.09 ft/s (0.33 m/s).
- The overall heat transfer coefficient under clean conditions (UA_c) was found to be the highest for PHE C around 1220 Btu/hr-^{0}F, while that of PHE B was found to be 1200 Btu/hr-^{0}F. This slight difference is due to the flow velocities. Larger velocity in PHE C creates more turbulence resulting in better heat transfer. PHE A had the lowest UA_c approximately 0.75 times that of PHEs B and C around 900 Btu/hr-^{0}F which is due to the chevron pattern. The low chevron angle results in less mixing of the flow and generates less turbulence resulting in a reduced heat transfer.
- Under clean conditions PHE A was found to have the lowest pressure drop of around 1.1 psi while that of PHEs B and C was 1.3 and 3 psi respectively. This trend is in accordance with previously reviewed work. The low chevron angle associated with PHE A offers least impedance to the flow resulting in a low pressure drop across the heat exchanger, while PHE C had a much higher flow velocity than PHEs A and B resulting a pressure drop almost 3 times higher.
- Even though the focus of this research is on the fouling of brazed plate heat exchangers operating as condensers several crucial observations were made regarding the other constituents of the system. In theory fouling occurs only on the hottest part of the system which in this case is the condenser but that was not to be the case here. The condensers are changed after every test but the post cooler in the cooling tower water remained in the system for a period of 8 months, though it is not the hottest part of the system it was found to have fouled significantly (partially blocked) reducing its heat transfer capacity and creating a large pressure drop in the system and had to be replaced. In addition to the post cooler deposits were found sticking to the walls of the pipes and along the inlets of the flow control valves reducing the flow area. A closer inspection of the pipes and the

valves showed that the deposit was found to be slimy which is likely the result of particulate fouling, it is assumed that particulate fouling contributed almost entirely to the fouling of the post cooler. Also the heating elements of the 6 kW heater used to heat the cooling tower water was found to have a coating of calcium deposits on it, this is understandable since it can reach high temperatures resulting in the calcium precipitating on its surface which were cleaned using bleach at the end of each test.

5.10 Modified Correlation for Overall Heat Transfer Coefficient (UA)

The overall heat transfer coefficient is calculated according AHRI standard 450 [2007] using the following equations.

$$UA = \frac{Q}{LMTD} \tag{5.3}$$

$$Q = \dot{m}_w \times C_p \times \Delta T \tag{5.4}$$

$$LMTD = \frac{\Delta T_1 - \Delta T_2}{\ln(\frac{\Delta T_1}{\Delta T_2})} \tag{5.5}$$

$$\Delta T = T_{w_i} - T_{w_o} \tag{5.6}$$

$$\Delta T_1 = T_{sat} - T_{w_i} \tag{5.7}$$

$$\Delta T_2 = T_{sat} - T_{w_o} \tag{5.8}$$

Where,

UA – overall heat transfer coefficient	[Btu/hr-^{0}F]
Q – Water side heat transfer	[Btu/hr]
LMTD – Log mean temperature difference	[^{0}F]
T_{wi} – water inlet temperature	[^{0}F]
T_{wo} – water exit temperature	[^{0}F]
T_{sat} – Refrigerant saturation temperature	[^{0}F]

It can be seen that in the correlation for UA only the inlet and exit temperatures on the water side are considered while that on the refrigerant side are neglected, that is, only the refrigerant saturation temperature is taken into account in the LMDT definition (5.4). This definition assumes saturated refrigerant vapor and saturated refrigerant liquid at the inlet and outlet of the PHE, respectively. The condensation process is represented by the segment from the state point 2 to 3 in Figure 5-17. The heat transfer rates due to the portions 1-2 and 3-4, in which

the refrigerant is superheat vapor and subcooled liquid, are neglected.

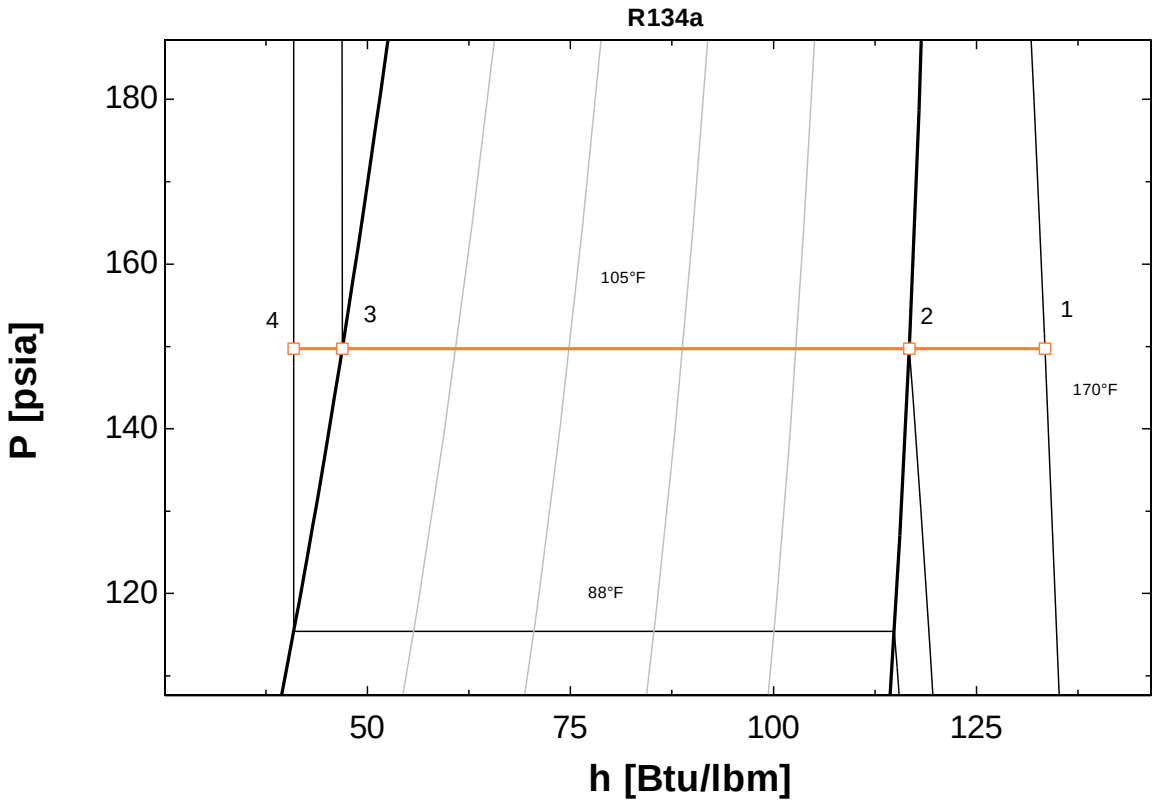

Figure 5-17. Refrigerant Condensation Process

In the case of the tests being conducted in this project the refrigerant saturation temperature is 105 ^{0}F, the degree of superheat is 65 ^{0}F resulting in a refrigerant inlet temperature of 170 ^{0}F as shown in state point 1 of Figure 5-17 . The refrigerant exit temperature depends on the heat transfer characteristics of the condenser being tested. For PHE's B and C the refrigerant exits in the subcooled region at a temperature around 88 ^{0}F while for PHE A is the saturation temperature of 105 ^{0}F since it is in the two phase region. Table 5-10 shows the heat transfer rates that occur in the superheated, 2-phase and subcooled region in percentage with respect to the total heat transfer rate. The values are estimated for the case of Figure 5-17, in which refrigerant R134a enter sat a temperature of 170 ^{0}F, exits at 88 ^{0}F, and has a saturation temperature of about 105 ^{0}F.

Table 5-10. Percentage Heat Transfer by Region

Region of the refrigerant in Figure 5-18	Heat Transfer Rate [% of total heat transfer)
Superheated (segment 1→2)	18
2-Phase (segment 2→3)	75.5
Subcooled (segment 3→4)	6.5

From Table 5-10 it can be seen that only 75% of the total heat transfer occurs in the 2-phase region. The LMTD method suggested by AHRI Standard 450 [2007] accounts for about 75% of the heat transfer capacity. This method might be accurate enough for predicting the UA values of the heat exchanger but to estimate the actual fouling resistance, which is differences in the UAs, the superheat and subcooling portions might need to be accounted for. The following modifications could be made to equations (5.6) and (5.7) to take into account the effect of superheat and subcooling.

$$\Delta T_1 = T_{r_i} - T_{w_o} \quad (5.9)$$

$$\Delta T_2 = T_{r_o} - T_{w_i} \quad (5.10)$$

Where,

T_{ri} – Refrigerant inlet temperature [^{0}F]

T_{ro} – Refrigerant exit temperature [^{0}F]

The temperature differences (5.8) and (5.9) are the actual temperature differences between refrigerant and water at the inlet and outlet sections of the PHE. They can substitute the expressions (5.6) and (5.7) in the LMDT definition (5.4) with the constraint that the refrigerant saturation temperature is around 105°F.

Figures 5-18, 5-19 and 5-20 show comparisons of the heat transfer coefficient (UA) calculated according to AHRI Standard 450 [2007], termed as "ARI Std UA", and the overall method suggested above, termed as "modified UA". The comparison is given first during the UA clean correction phase of the heat exchangers. In the case of PHE A since the refrigerant exits in the 2-Phase region its saturation temperature is taken as the exit temperature.

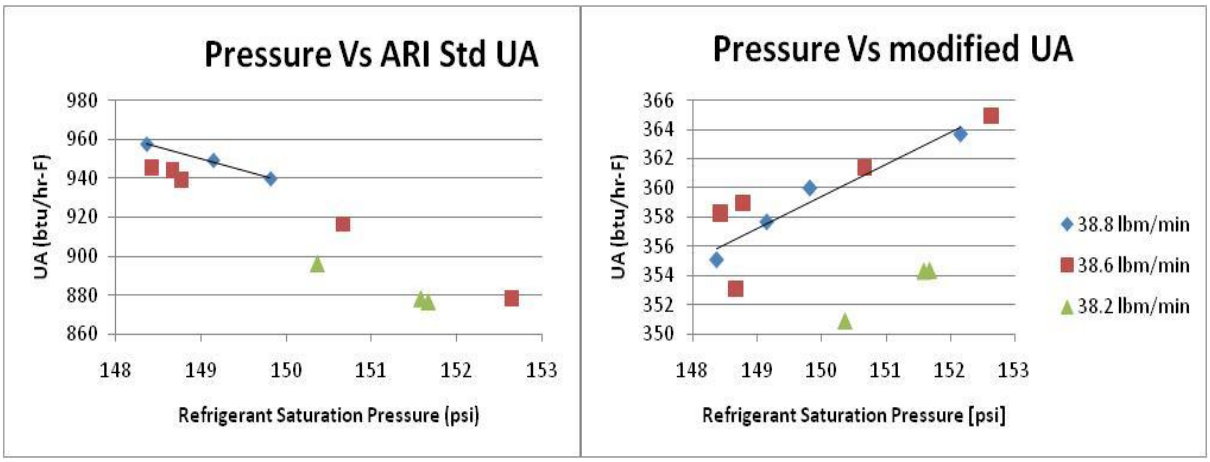

Fig 5-18. PHE A: Comparison of Overall Heat Transfer Coefficients

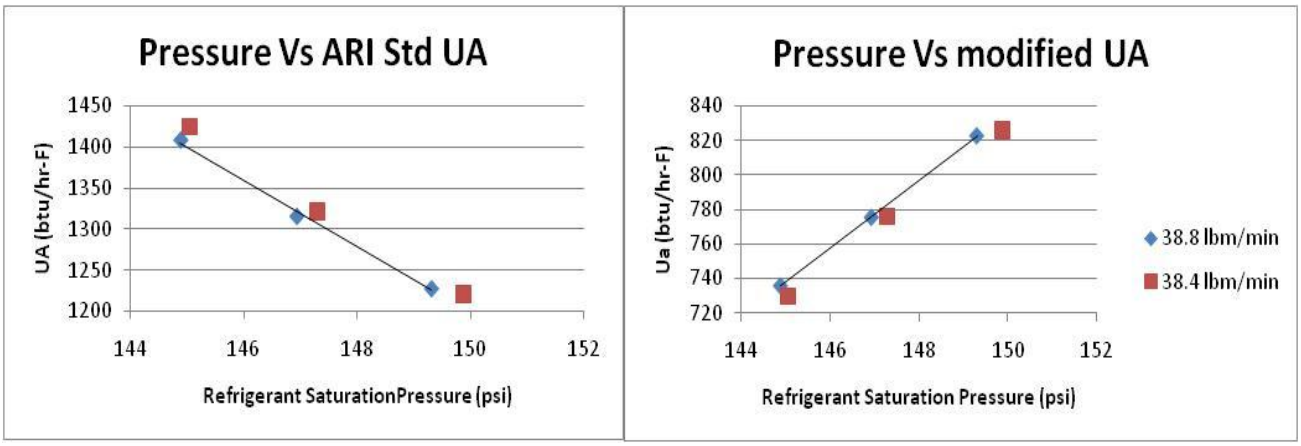

Fig 5-19. PHE B: Comparison of Overall Heat Transfer Coefficients

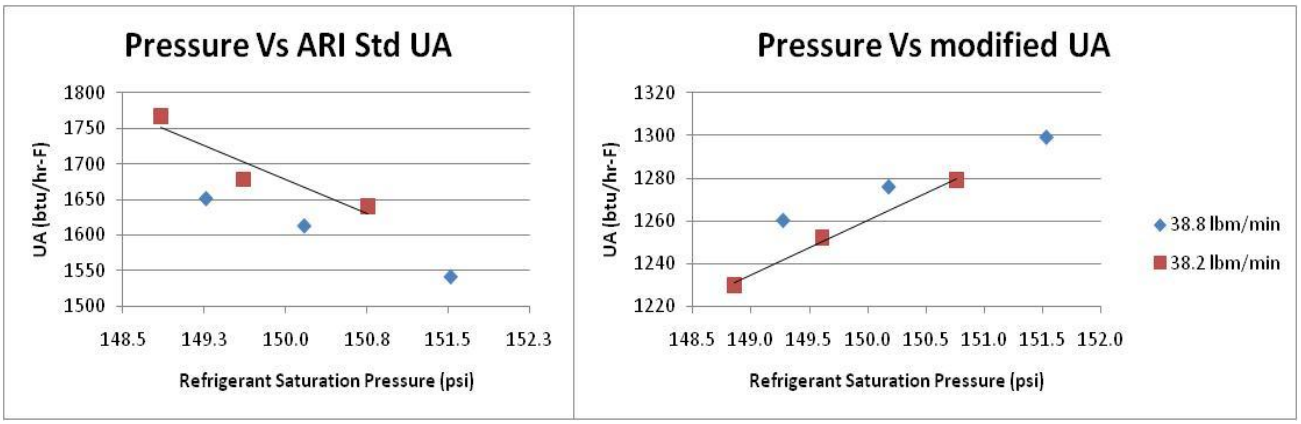

Fig 5-20. PHE C: Comparison of Overall Heat Transfer Coefficients

For all three PHEs it can be seen the "ARI Std UA" decreases with refrigerant pressure while the "modified UA" increases. For PHEs B and C it can also be observed that as the water flow rate increases the "ARI Std UA" decrease while the "modified UA" increases. This is not a physical phenomenon but rather an artifact hidden in the calculation of the ARI Std UA. The trends of the "modified UA" are more intuitive than those of the "ARI Std UA". Since higher refrigerant pressure and water flow rate should enhance the heat transfer rates the overall heat transfer coefficient UA is expected to also be higher. It can be observed that in all 3 cases the value of the "modified UA" is significantly less than that of the "ARI Std UA", approximately 62% less for PHE A, 45 % less for PHE B and 27 % less for PHE C. This is due to the increase

in the value of the LMTD since the degree of superheat is being taken into account for the "modified UA".

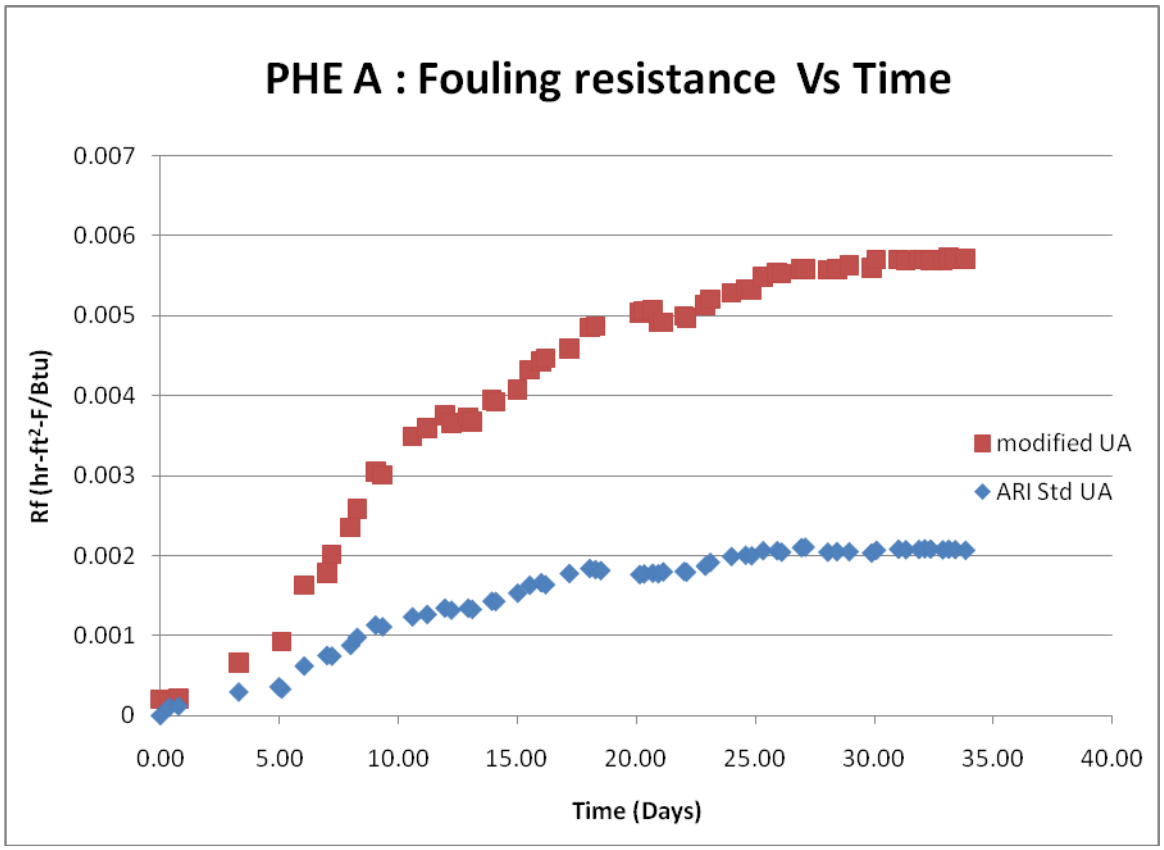

Fig 5-21. PHE A: Comparison of fouling resistance

Figures 5-21, 5-22 and 5-23 show the comparison of the fouling resistance calculated using the "ARI Std UA" and the "modified UA". In all cases it can be seen that the fouling resistance calculated using the "modified UA" is higher, for PHE A it is around 3 times higher at the conclusion of the test while for PHE B it is almost 4 times. In the case of PHE C it is slightly higher. For PHE A both fouling resistance curves follow the same trend while for PHE B they follow the same trend but the changes are much larger in the "modified UA" curve.

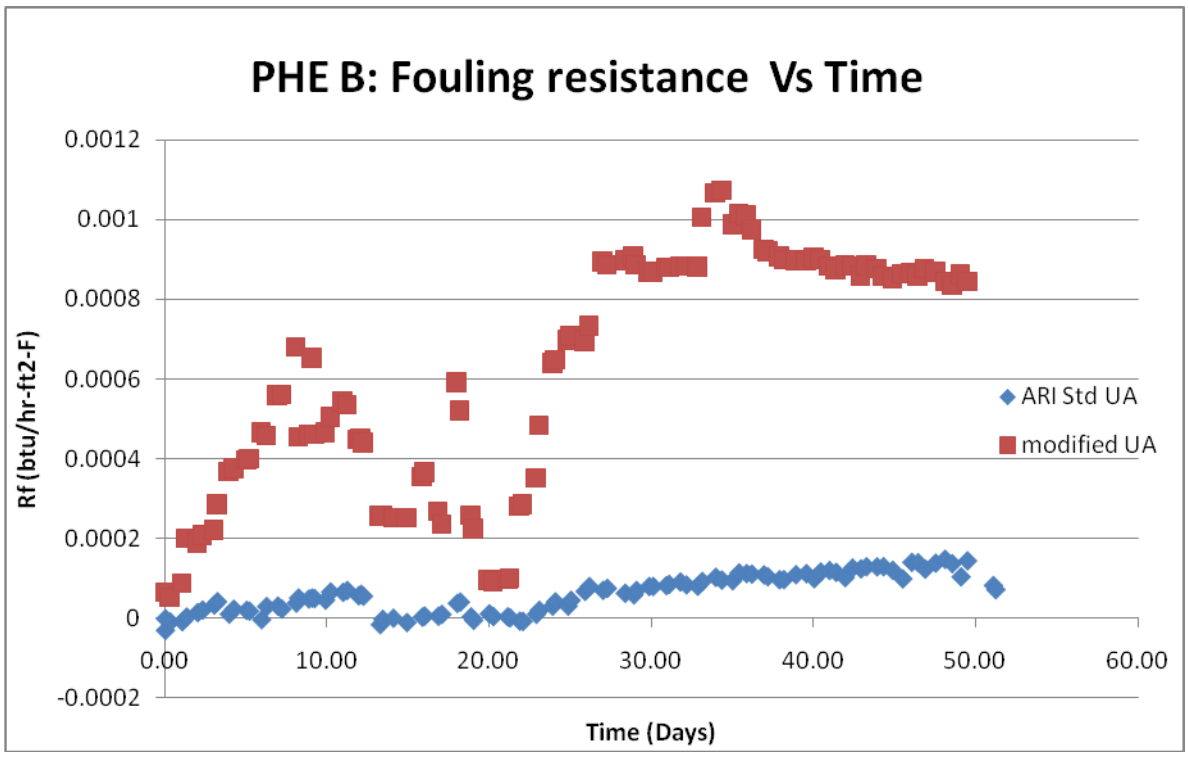

Fig 5-22. PHE B: Comparison of fouling resistance

The drawbacks of using this "modified UA" to compute the fouling resistance is that slight changes in amount of superheat, subcooling or both will cause a significant change in the "modified UA" even though the heat transfer in these regions is only a fourth of the total heat transfer, this can be observed in Figures 5-22 and 5-23 where the fouling resistance calculated using the "modified UA" rises and falls steeply.

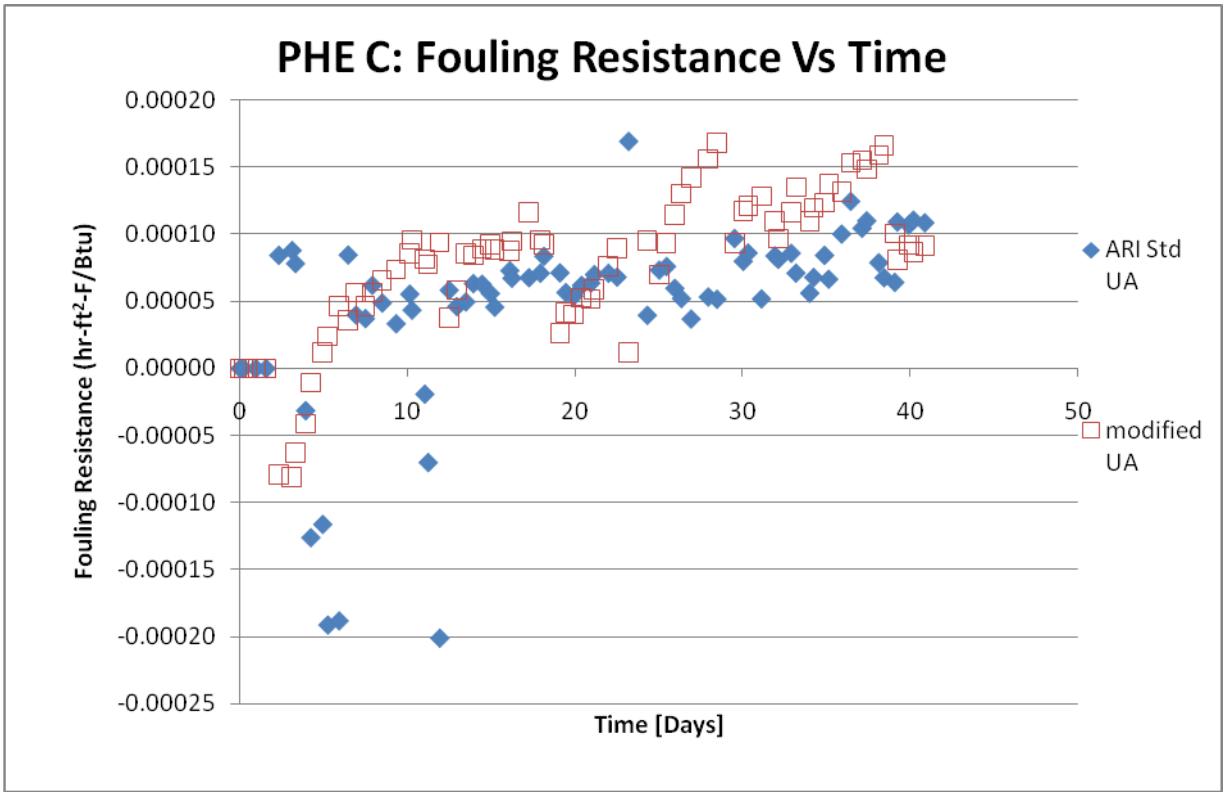

Fig 5-23. PHE C: Comparison of fouling resistance

CHAPTER VI

CONCLUSIONS AND RECOMMENDATIONS FOR FUTURE WORK

6.1 Conclusions

Enhanced heat transfer surfaces used in plate heat exchangers (PHEs) provide higher heat transfer coefficients than conventional plain tubes but their long term fouling characteristics were not sufficiently studied in the previous work available in the open domain. In particular, no data are available on fouling of PHEs operating as condensers. This thesis focuses on understanding the mineral precipitation and particulate fouling mechanisms of PHEs and develops an experimental methodology to measure the fouling resistance and pressure drop in this type of exchangers when they run at operating conditions similar to the ones in the actual cooling tower application. Since fouling is a very slow process accelerated-type tests were developed in laboratory. The accelerated tests progressively concentrate the water while running it through the PHE and a cooling tower. The water is maintained saturated in minerals at all time and becomes supersaturated near the boundaries of the plates of the PHEs. This mechanism is close to the real case scenario and seems to be the key factor controlling the fouling mechanism. Three PHEs have been tested to demonstrate the feasibility of the fouling resistance measurements. The specific conclusions are as follows:

1. An experimental facility was designed and constructed which was able to test the propensity for fouling of brazed plate type condensers used to condense refrigerant R134a at pressures up to 175 psi using cooling tower water. The cooling tower water is created by mixing chemicals in fixed ratios to demineralized water and the process can be easily replicated. The facility incorporates a small scale cooling tower to provide the concentration effect to the cooling tower water, creating an atmosphere which is similar to the actual operation of cooling towers used in practice.

2. A data acquisition and control system was designed using LabView Real time environment. Precise control of the cooling tower water temperatures, refrigerant inlet temperature and pressure was achieved using PID controls provided in the LabView software to control the heaters using SCR power pack controllers. The refrigerant flow

rate is controlled by varying the power supplied to the refrigerant pump using a VFD drive which can be manually adjusted using the LabView software and the cooling tower water flow rate is controlled using a number of metering valves provided in the system.

3. Accelerated type fouling tests up to 55 days were conducted on three different brazed plate heat exchangers operating as condensers. Two of the plate heat exchangers PHE A and PHE B had identical geometries (number of plates, aspect ratios, heat transfer area of 4.6 ft^2) but different chevron angles (30^0 & 63^0)and two other heat exchangers PHE B and C had the same chevron angle (63^0) but different aspect ratio (length/width) of the plates.

4. An analysis on the overall heat transfer coefficient (UA) under clean conditions was performed for all three PHE's that were tested. It was found that the PHE with the low chevron angle had a UA which was approximately 0.75 times that of the PHEs with the larger chevron angle. The UA was found to be extremely sensitive to the refrigerant saturation pressure and cooling tower water flow rate and the variation was linear. Hence a calibration of the UA was performed which yielded a linear equation used to compute the UA under clean conditions using the refrigerant pressure assuming all other operating conditions are constant.

5. The pressure drop across the PHEs was measured using a differential pressure transducer; it was found that the PHE C with chevron angle of 63 degree and 3.9 ft2 of heat transfer area had the largest pressure drop and around 3 times that of the PHE A, which has chevron angle of 30 degree and smallest pressure drop across it.

6. The chevron angle was found to be the most important factor affecting the fouling resistance. The PHE with chevron angle of 30 degrees was found to have a greater rate of fouling than the PHEs with the chevron angles of 63 degrees. The asymptotic value of the fouling resistance was calculated by curve fitting the experimental data; the PHE with the

low chevron angle had an asymptotic fouling resistance around15 to 20 times larger than that of the PHEs with the larger chevron angle.

7. A comprehensive uncertainty analysis was performed on the fouling resistance, it was found that the fouling resistance was most sensitive to the temperature of simulated cooling water exiting the condenser. This accounted for almost 99% of the total uncertainty. Hence after the first two PHEs were tested the RTD's were recalibrated again for improving their accuracy in a smaller range of operation. This resulted in the accuracy improving from 0.11 ^{0}F to 0.011 ^{0}F, which resulted in the uncertainty decreasing from 38 % to 18 % under similar operating conditions of 0.4°F temperature difference of the leaving water under clean and fouled conditions.

8. In addition to the condensers it was found that with long period of operation other heat exchangers in system are exposed to precipitation fouling. The post cooler which is used to cool the cooling tower water exiting the condenser was found to be partially blocked creating a large pressure drop. This damaged the water pump. Also deposits were found adhering the pipes and around the entrances of the flow control valves thereby reducing the flow area. Hence, along with replacing the condenser, the other heat exchangers in the system needed to be replaced. In this facility a post cooler was replaced after 3 condensers were tested, that is, about after 9 months of operating conditions with severe fouling potential water. Also the pipes and flow control valves needed to be cleaned over time; this can be done by brushing or by circulating a weak acid solution through the loop.

6.2 Recommendations for future work

1. In the current work an analysis is done to study the effect of refrigerant saturation pressure and water flow rate on the overall heat transfer coefficient under clean conditions of PHE. Future work can involve analyzing the effects of other parameters like degree of superheat on the refrigerant, refrigerant flow rate and water inlet temperature on the overall heat transfer coefficient under clean conditions.

2. At present accelerated fouling tests have been carried out on heat exchangers with 2 different chevron angles (30^0 and 63^0) and aspect ratios (2.6 and 4.1). PHE D which is an heat exchanger with an aspect ratio of 2.06 is scheduled to be tested next, analyzing its heat transfer characteristics under clean and fouled conditions will give a better understanding of the parameters that affect them.
3. The current accelerated fouling tests are carried out at a refrigerant saturation temperature of 105 ^{0}F, from the literature review it is understood that an increase in temperature of the heat transfer surface leads to increased fouling, hence an accelerated fouling test at a refrigerant saturation pressure of 110 or 115 ^{0}F can be carried out the study the effect of refrigerant pressure on the fouling process.
4. At present three of the four available PHEs have identical chevron angle but different aspect ratios and heat transfer areas resulting in different flow velocities, hence the current tests rather than analyzing the effect of the aspect ratio on the fouling resistance analyses the effect of flow velocity instead. To have a better understanding of the effect of the aspect ratio on the fouling it is necessary to test two heat exchanger having different aspect ratios but same water and refrigerant velocities.
5. The LSI of the cooling tower water used in these tests is maintained around 3, it depends largely on the water evaporation rate in the cooling tower and the pH, the water evaporation rate is currently around 22 gallons/day and the pH around 9.3, tests can be carried out at different evaporation rates and pH to analyze their effect on the fouling resistance.
6. During the course of tests it was found that auxiliary plate heat exchangers other than the condenser on the cooling tower loop were susceptible to fouling, also valves and pipes were found to have accumulated deposit over time. It is assumed that fouling on the auxiliary heat exchangers and pipes is particulate. Particulate fouling can be minimized using filter which removes particles with diameters greater than 5µm, hence connecting a filter in line with the cooling tower loop will help determine if the fouling in the auxiliary heat exchanger and other parts of the loop is particulate in nature. Also this will help in determining the individual contribution of particulate fouling and precipitation fouling to the total fouling of the condenser since the current accelerated fouling tests involves both particulate and precipitation fouling.

7. Lastly a tube and tube heat exchanger can be used instead of the plate heat exchanger as the condenser to be able to compare the fouling resistances under similar operating conditions.

REFERENCES

N.Andritsos, A.J.Karabelas. (2003). Calcium carbonate scaling in a plate heat exchanger In the presence of particles. *International Journal of Heat and Mass Transfer, 46, 4613-4627.*

AHRI standard 450. (2007). Performance rating of water-cooled refrigerant condensers, remote type. *Air-Conditioning, Heating and Refrigeration Institute, Airlington, VA 22201, USA.*

AHRI guideline E (1997). Fouling factors: A survey of their application in today's air-conditioning and refrigeration industry. . *Air-Conditioning and Refrigeration Institute, Airlington, VA 22201, USA.*

Z.H.Ayub. (2003). Plate heat exchanger literature survey and new heat transfer pressure drop correlations for refrigerant evaporators. *Heat Transfer Engineering, 24(5):3-16.*

B. Bansal, X.D. Chen, H. Muller-Steinhagen. (2007). Analysis of 'classical deposition law for crystallization fouling. *Chemical Engineering and Processing, 47, 1201-1210.*

B.Bansal. H.Muller-Steinhagen, X.D.Chen. (2000). Performance of plate heat exchangers during calcium sulfate fouling – investigation with an inline filter. *Chemical Engineering and Processing, 39, 507-519.*

L.Chamra. (2006). Water-side fouling inside smooth and augmented copper alloy condenser tubes in cooling tower water applications. *ASHRAE 1205 TRP, Final report.*

J.W.Cleaver, B.Yates. (1975). A sub-layer model for the deposition of particles from a turbulent flow. *Chemical Engineering Science, Vol 30, 983-992.*

J.W.Cleaver, B.Yates. (1976). The effect of particles re-entrainment on particle deposition. *Chemical Engineering Sciecne, Vol 31, 147-151.*

A.Cooper, J.W.Suitor, J.D.Usher. (1980). Cooling water fouling in Plate heat exchangers. *Heat Transfer Engineering, Vol 1, No 3, 50-65.*

W.W.Focke, J.Zachariades, I.Oliver. (1985). The effect of corrugation inclination angle on the thermo hydraulic performance of plate heat exchangers. *International Journal of Heat and Mass Transfer,Vol 28, No 8 , 1469-1479.*

J.Gentry. (2007). Simulation and validation of hybrid ground source and water-loop heat pump systems. *MS Thesis, Oklahoma State University.*

S.Grandgeorge, C.Jallut, B.Thonon. (1998). Particulate fouling of corrugated plate heat exchangers. Global Kinetics and equilibrium studies. *Chemical Engineering Science, Vol. 53, No 17, 3051-3071.*

S.I. Haider, R.LWebb, A.K.Meitz. (1992). An experimental study of tube side fouling resistance in flooded water chiller evaporators. *ASHRAE Transactions 98 (part 2), 86-103.*

D.Hasson. (1979). Precipitation Fouling. *Proceedings of the International Conference on the fouling of Heat Transfer Equipment, Rensselaer Polytechnic Institute.*

S.Kakac, H.Liu. (1998). Heat Exchangers: selection, rating and thermal design. *CRC Press LLC*

A.J.Karbelas, S.G.Yiantsios, B.Thonon, J.M.Grillot. (1997). Liquid side fouling of heat exchangers. An integrated R & D approach for conventional and novel designs. *Applied Thermal Engineering, Vol 17, No 8 , 727-737.*

D.Q.Kern, R.A.Seaton. (1959). A theoretical analysis of thermal surface fouling. *Brit*

Chem Engineering, 4(5), 258-262.

T.Kho, H.Muller-Steinhagen. (1999). An experimental and numerical investigation of heat transfer fouling and fluid flow in flat plate heat exchangers. *Trans IChemE, Vol 77, Part A.*

S. A. Klein. (2006). "Engineering Equation Solver," *V7.723-3D ed, Madison, WI, USA: F-Chart Software.*

G.A.Longo. (2008). Refrigerant R134a condensation heat transfer and pressure drop inside a small brazed plate heat exchanger. *International Journal of Refrigeration, Vol 31, 780-789.*

Lim [2010]. A preliminary investigation of fouling in brazed plate heat exchangers. *M.S Thesis, Oklahoma State University, Stillwater, OK.*

H. Muller-Steinhagen. (1999). Cooling-water fouling in heat exchanegrs. *Advances in Heat Transfer, Vol 33. 415-496.*

A.Mulley, R.M.Manglik. (1999). Experimental study of turbulent flow heat transfer in a Plate heat exchanger with Chevron plates. *Journal of Heat Transfer, vol 121, no 1, 110-117.*

R.Oliveira. (1997). Understanding Adhesion : A means for preventing Fouling. *Experimental Thermal and Fluid Sciences, 14:316-322.*

E.F.C.Sommerscales. (1979). Introduction and summary: The fouling of heat transfer equipment. *Proceedings of the International Conference on the fouling of Heat Transfer Equipment, Rensselaer Polytechnic Institute.*

R.A.Troupe, J.C.Morgon, J.Prifiti. (1960). The plate heater Versitile Chemical Engineering tool. *Chemical Engineering progress, vol 56, no 1, 124-128.*

A.S.Wanniarachchi, U.Ratnam, B.E.Tilton, K. Dutta-Roy. (1995). Approximate correlations for chevron-type plate heat exchangers. *HTD-Vol 34, 1995 National Heat Transfer Conference- Vol 12 ASME.*

W.Li and R.L.Webb. (2000). Fouling in enhanced tubes using cooling tower water: Part 1: long term fouling data. *International Journal of Heat and Mass Transfer 43 (19), 3579-3588.*

W.Li and R.L.Webb. (2000). Fouling in enhanced tubes using cooling tower water: Part 2: combined particulate and precipitation fouling. *International Journal of Heat and Mass Transfer 43 (19), 3579-3588.*

W.Li and R.L.Webb. (2002). Fouling characteristics of internal helical-rib roughness tubes using low velocity cooling tower water. *International Journal of Heat and Mass Transfer 45 (19), 1685-1691.*

Y.Y.Yan, H.Liao, T.Lin. (1998). Condensation heat transfer and pressure drop of refrigerant R-134a in a plate heat exchanger. *International Journal of Heat and Mass Transfer, 42, 993-1006.*

Q.Zhenhua, Y.Chen, C.Ma. (2008). Experimental study of fouling on heat transfer surface during forced convective heat transfer. *Chinese Journal of Chemical Engineering, 16(4), 535-540.*

APPENDIX A

TURN ON PROCEDURE FOR FACILITY

1. Fill the batch tank with 90 gallon of cooling tower water and the conical tank to maximum capacity with lab hot water.
2. Purge the chilled water loop with city water and the superheater loop with city water and a small amount of azole.
3. Turn on the TACO pumps on the fouling water loop and adjust the flow rate to 38.8 lbm/min using the metering valves provided.
4. The flow distribution to the cooling tower and post cooler is controlled by gate vales located at the exit of the flow meter; adjust the valves till a flow rate of 1 gpm through the cooling tower is observed. The flow rate to the cooling tower can be determined by closing the ball valve provided at the exit and timing the change in water level. After the desired flow rate is reached open the ball valve to allow flow from the cooling tower to the batch tank.
5. Turn on the 6KW heater located in the batch tank, set the EH 1 PID RANGE DC-output high to 10V, set point temperature to 84.97 and EH 1 cut of to 97 as shown in the figures A-1 and A4.

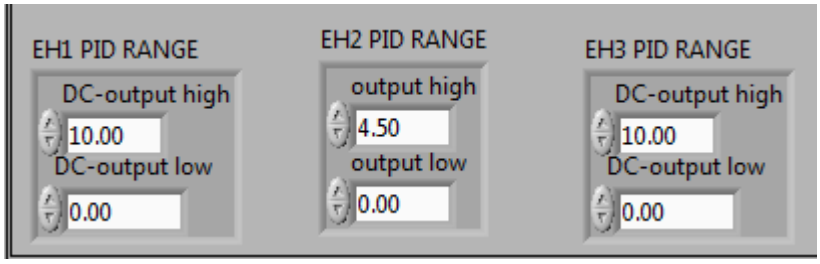

Figure A-1. Heater power output control

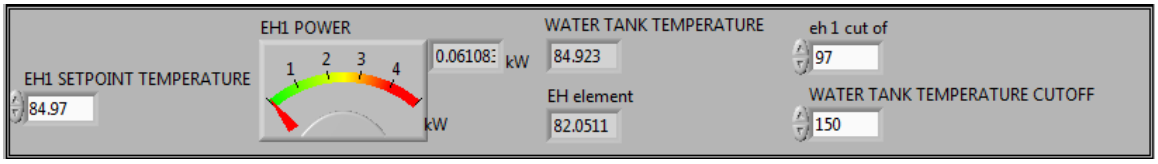

Figure A-2. Heater 1 control

6. Turn on the pumps located on the chilled water, evaporator and superheater loops.
7. Turn on the 24 KH heater located on the superheater loop, set the EH2 PID RANGE DC-power output to 4.5V as shown in Figure A-1, the set point temperature to 170.1, EH-2 water exit cutoff to 180 and EH-2 heating element cutoff to 200 as shown in Figure A-3.

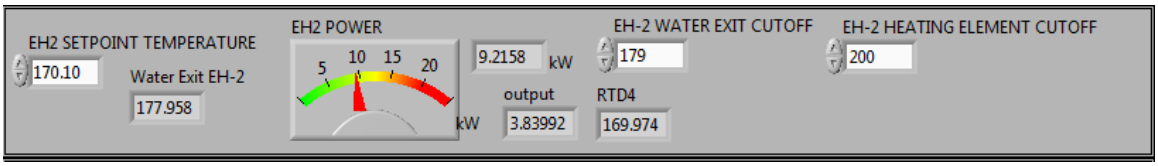

Figure A-3. Heater 2 control

8. Turn on the 3 KW heater located on the evaporator loop, set the EH# PID RANGE DC-power output to 10 V as shown in Figure A-1, EH3-set point temperature to 98 and EH3-cutoff temp to 150 as shown in Figure A-3.

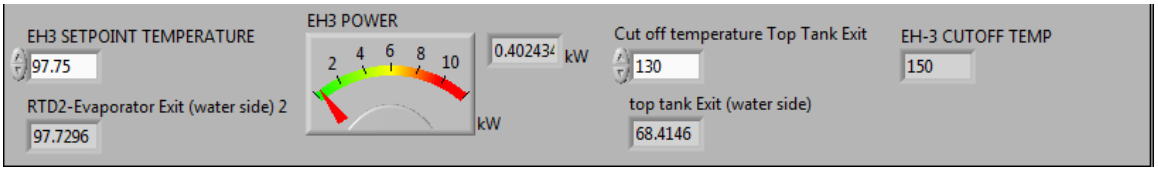

Figure A-4. Heater 3 control

9. Once the desired water temperatures are reached on all the evaporator and superheater loops start to charge refrigerant, charge the refrigerant till the pressure on system reaches 165 psi.
10. Turn on the refrigerant pump to 25 rpm and view the flow rate, if a positive flow rate is observed then start increasing the pump speed in 50 rpm intervals till the desired flow

rate of 3.5 lbm/min is observed. If a negative flow rate is observed then provide more subcooling to the refrigerant by adjusting the metering valves provided on the chilled water loop till around 15 – 20 degree of subcooling is observed. The saturation temperature is obtained from the measured pressure and the amount of subcooling is determined by subtracting the temperature measured at the pump inlet (thermocouple 23) from the saturation temperature.

11. If a negative flow rate is still observed then charge more refrigerant and repeat step 10.
12. The pressure is observed on the pressure (psig)2 plot shown in Figure A-4. If the observed pressure exceeds the desired pressure then decrease then slightly decrease the EH3-set point temperature shown in Figure A-3 and if the observed pressure is less than the desired pressure then increase the EH3- set point temperature.

APPENDIX B

OVERVIEW OF FOULING TESTS

Table 2-2 below provides a quick overview of the fouling tests reported in the literature and the main findings.

Table B-1. Overview of fouling tests

	Objective	Parameters	Results
Cooper et al. [1980]	Determine fouling resistance of plate heat exchangers condensing steam using cooling water obtained from different natural sources.	PHE: 7 plates each 1.14 m in length and 0.45 m width. Tests conducted at 2 flow velocities, 0.84 and 0.45 m/s. Water treated to prevent biological and corrosion fouling.	Asymptotic fouling resistance reached after 25-28 days of operation. Asymptotic fouling resistance at 0.85 m/s was half that at 0.45 m/s. Fouling occurred only on upper third of the plates which is the hottest part.
Karabelas et al. [1997]	Study the effect of chevron angle and flow velocity on particulate fouling of plate heat exchangers.	PHE's of 30^0 and 60^0 corrugation angles tested. Flow velocities ranging from 0.35 to 1.35 m/s. Mean particles size 5 µm	Asymptotic fouling resistance obtained between 4-13 days of testing. Fouling resistance (m^2K/W) a. for 30^0 plate: At 0.35 m/s is $13.5 * 10^{-5}$ At 1.35 m/s is

			$1.7 * 10^{-5}$ b. For 60^0 plate At 0.35 m/s is $4.2 * 10^{-5}$ At 1.35 m/s is $0.3 * 10^{-5}$
Grandgeorge et al. [1998]	Study the effect of chevron angle and flow velocity on particulate fouling of plate heat exchangers.	PHE's of 30^0 and 60^0 corrugation angles tested. Mean particles size 4-5 µm. Flow velocities ranging from0.02 – 1.4 m/s. Duration of tests is 800 hours.	Fouling resistance (m^2K/W) at velocity of 0.16 m/s a. For 30^0 plate is 0.00057 b. For 60^0 plate is 0.0001
Andritos and Karabelas [2003]	Study calcium carbonate scaling in plate heat exchangers in the presence of particles	PHE: 8 plates with flow area of 186 cm^2. Tested with different particles sizes of 15, 5.3 and 0.8 µm added to tap water with PH controlled. Tests conducted in different directions of flow. Duration of tests less than 5 hours.	An increase in concentration of larger particles caused a greater increase in pressure drop than smaller particles. An increase in flow velocity led to a decrease in the scale formation. The direction of flow had no effect on scale

			formation.
Bansal et al. [2000]	Analyze performance of plate heat exchangers during calcium sulfate fouling	Calcium sulfate solution used as foulant. PHE: 60^0 corrugation angle with length 0.43 m and width 0.12 m. Filter with size 1µm used to remove particles hence reducing particulate fouling.	Fouling resistance was found to: 1. Increase with increase in concentration of calcium sulfate. 2. Decrease with increase in flow velocity. 3. Increase significantly if the filter is removed. Deposit thickness was greatest at the hottest part.
Zhenhua et al. [2008]	Study the fouling of heat transfer surface under different operating parameters.	Foulant used is a mixture of sodium bicarbonate and calcium chloride solutions. Coaxial heat exchanger is used with hot water entering at 70^0C with average wall temperature varying from 50-60^0C.	Most cases fouling asymptotic fouling resistance was reached in 15-32 hours. The average wall temperature was found to increase slightly due to fouling. Crystals were found not only on the heat transfer surface but

			also in the foulant. An increase in asymptotic fouling resistance was observed with an increase in: 1. Foulant hardness 2. Foulant alkalinity 3. Foulant temperature 4. Heat transfer surface temperature However increase in foulant flow velocity resulted in a decrease in fouling resistance.
Chamra [2006]	Study the effect of water side fouling on copper condenser tubes using cooling tower water.	9 tubes with different inside fin geometries (no of starts, helix angles) tested. R134a condensing at a saturation temperature of 105^0C used to heat the cooling tower water.	Tubes with greater number of starts and larger helix angles fouled more. Asymptotic fouling resistance close to $1.76E^{-7}$ ^{0}C- m^2/W for tubes with 45 starts and helix angles 35^0 and 48^0.

		Duration of tests was 58 days.	
Webb and Li [1999 a & b]	Conduct long term fouling tests of condenser tubes using cooling tower water.	8 tubes with different inside geometries (helix angles, no of starts) were tested to condense R11 in a 250 ton refrigeration unit. Flow velocity was 1.07 m/s. Duration of tests was 100 days.	Tubes with greater number of starts and larger helix angles fouled more. Tube containing 45 starts and having a helix angle of 45^0 was found to have an asymptotic fouling resistance of 0.000144 m^2K/W. Analysis of deposit showed that 59% was due to precipitation fouling and the rest due to particulate fouling.

VITA

Annamalai Ramesh

Candidate for the Degree of

Master of Science

Thesis: AN EXPERIMENTAL FACILITY TO MEASURE FOULING RESISTANCE IN CONDENSERS

Major Field: Mechanical and Aerospace Engineering

Biographical:

Education:

Completed the requirements for the Master of Science in Mechanical Engineering at Oklahoma State University, Stillwater, Oklahoma in July, 2010.

Completed the requirements for the Bachelor of Engineering in Mechanical Engineering at Anna University, Chennai, Tamil Nadu/India in 2007

Name: Annamalai Ramesh Date of Degree: July, 2010

Institution: Oklahoma State University Location: Stillwater, Oklahoma

Title of Study: AN EXPERIMENTAL FACILITY TO MEASURE FOULING RESISTANCE IN CONDENSERS

Pages in Study: 135 Candidate for the Degree of Master of Science

Major Field: Mechanical and Aerospace Engineering

Scope and Method of Study:

Heat exchangers are employed to transfer thermal energy between two fluids. Fouling is defined as the accumulation of deposits on the heat transfer surface which provides a resistance to the heat transfer, thereby decreasing the heat transfer capacity of the surface. The air conditioning industry has been under pressure to improve the efficiency of systems adopting these heat exchangers. The current thesis involves the design and construction of an experimental facility to measure the thermal and hydraulic performances of three brazed plate heat exchangers (BPHEs) of different geometries (chevron angles and aspect ratios) operating under controlled fouling conditions.

Findings and Conclusions:

Fouling tests conducted on the three BPHEs revealed that the chevron angle of the plates had a significant impact on the overall heat transfer coefficient (UA) and fouling resistance, a BPHE with a chevron angle of 30^0 had a UA 0.75 times less and a fouling resistance 15 times larger than a BPHE with a chevron angle of 63^0 and identical aspect ratio. The aspect ratio was found to have a slight impact on the UA and fouling resistance, a BPHE with an aspect ratio 4.1 had a UA 2 % greater and a fouling resistance 17 % lower than a BPHE with an aspect ratio of 2.1 and identical chevron angle.